



UNIVERSITY OF THE
WITWATERSRAND,
JOHANNESBURG

Title of research

**Development of Castor Oil-based paints with anti-radiation
and antimicrobial properties**

Msc research dissertation

Prepared by Nekhavhambe Edza (543787)

Submitted to

School of Chemical and Metallurgical Engineering, Faculty of Engineering and the Built
Environment, University of the Witwatersrand, Johannesburg, South Africa

Supervisor: Prof Diakanua Nkazi

Co-supervisor: Dr Hembe Elie Mukaya

17 September 2021

Declaration

I hereby declare that this MSc Dissertation entitled “*Development of castor oil based paints with anti-radiation and antimicrobial properties*” was carried out by me.

The content and discussions put forth are based on my reading and understanding of the published documentations, and this report was not submitted for any degree or diploma before, either in this or in any other University. All documentation used are acknowledged at the respective place in the text.



Nekhavhambe Edza

(Student Number: 543787)

Abstract

Agricultural commodities are increasingly being utilized in the chemical industry as alternative raw materials to petrochemicals. In the polymer industry, vegetable oils are used to produce oleo-based polymers which find application in the paint and coatings industry as chief ingredients. Among the vegetable oils, castor oil has gained much interest because it is non-edible and constitute of ~90% ricinoleic acid which offers flexible modifications.

In this research, castor oil was used to synthesize a drying oil, polyurethanes and epoxy resins, and to achieve this objective, castor oil had to undergo certain chemical modifications, which include: epoxidation, ring opening, dehydration and polymerization. The synthesized paints were then blended with Ag and TiO_2 NPs to impart anti-radiation and antimicrobial properties. The synthesized paints were characterized by FTIR and 1H NMR to confirm the occurrence of the reactions and also to evaluate the reaction conversion. Rheology studies were done to determine the usability of the synthesized materials as coatings. A study was performed on the drying time of the drying oil, polyurethanes and epoxy resins paint formulations under atmospheric conditions. Further tests were done to test for the anti-radiation and antimicrobial properties. A 100% conversion was obtained for epoxidation reaction for the following reaction conditions: 35 °C temperature, 4wt% catalyst amount, 1:2 (castor oil: H_2O_2) ratio and 32 hrs reaction time. For the ring opening reaction a conversion of ~ 70% was obtained when the reaction was done with H_2O as the nucleophile and $HClO_4$ as catalyst. The temperature was 100°C with a mass ratio of 1:18:0.2 (ECO: H_2O : $HClO_4$) for 48 hrs. A conversion of 43% for DCO and 53% for RCO was attained at the following reaction conditions: 240 °C, 0.1 g $NaHSO_4$ and 120 min reaction time. The synthesized CO-based polyurethanes had a 6 hrs drying time when a 2k catalyst was added, while

the drying time for epoxy resins was 6 days. The lowest drying time for the drying oil was 2 days. It was found that *Streptococcus sp* growth inhibition can be obtained at a low concentration of Ag/AgTiO₂ NPs within the paints. For the anti-radiation properties, it was found that paint sample with NPs TiO₂++ showed no changes at all after UV irradiation for 90 minutes. With the chemical modifications and incorporation of the right additives, paints were obtained that can be used practically.

Acknowledgement

I would like to acknowledge DST and CSIR for affording the financial support for this research not forgetting the University of the Witwatersrand for the premises to undertake this research. To the lab technicians, I am thankful for landing a helping hand when it was needed.

I am forever indebted to my supervisor Prof Nkazi and co-supervisor Dr Mukaya for the all-inclusive support so that I may be able to complete this research. Thank you for the guidance and making the time to attend to any problems I encountered in this journey. I am truly thankful.

To my loving family: My parents (Ndidivhani Gladys Nekhavhambe and Tshilidzi Peter Nekhavhambe), my sister (Vhuthuhawe Nekhavhambe) and brother (Gudani Nekhavhambe), thank you for the constant motivation, kind words and support either emotionally or financially, I am truly thankful.

To my Starflower, Onicah Makgato, thank you for believing in me even when I didn't believe in myself, I never would have made it without your companionship, constant encouragement and kind words. I am forever grateful.

I would like to thank Mr Mutshinyalo Nwamadi for availing himself when I needed the help, I appreciate the support and contribution towards my research.

To my amazing research group (Oil & Gas research group) thank you for undergoing this journey with me and all the motivation and support you have offered. Special thanks to Jude Bonsu, thank you for being such a wonderful friend, I truly appreciate the support that you showed me.

God has truly been faithful.

Contents

Declaration	2
Abstract	3
Acknowledgement	5
List of Figures	9
List of Tables	13
List of abbreviations.....	14
Chapter 1: Background and Motivation	15
1.1. Introduction	15
1.2. Problem statement.....	18
1.3. Research aim and objectives	20
Chapter 2: Literature review	21
2.1. Paint	21
2.2. Vegetable oils	25
2.3. Castor Oil	31
2.4. The chemistry of castor oil.....	34
2.4.1. Dehydration of castor oil	34
2.4.2. Epoxidation	36
2.4.3. Ring Opening	40
2.4.4. Polymerization	42

2.5. Antiradiation and Antimicrobial Coatings	49
2.5.1. Antiradiation Coatings.....	50
2.5.2. Antimicrobial coatings	53
Chapter 3: Methodology.....	60
3.1. Materials.....	60
3.2. Chemo-enzymatic Epoxidation reaction	60
3.2. Ring opening reaction	61
3.3. Dehydration reaction.....	63
3.4. Polyurethane synthesis	64
3.5. Epoxy Synthesis	68
3.6. Addition of nanoparticles for Antiradiation and Antimicrobial	71
3.7. Characterization Technique of resins	72
3.7.1. Spectroscopic analysis	72
3.7.2. Rheology Studies	72
3.7.3. Tests for the anti-radiation and antimicrobial properties	73
Chapter 4: Results and discussion.....	74
4.1. Material synthesis	74
4.1.1. Epoxidation reaction.....	74
4.1.2. Ring opening	75
4.1.3. Dehydration reaction	76

4.1.4. Polyurethane synthesis	77
4.1.5. Epoxy synthesis.....	79
4.2. FTIR Analysis	81
4.2.1. FTIR analysis of CO and ECO	82
4.2.2. FTIR of RCO	83
4.2.3. FTIR for drying oil	84
4.2.4. Polyurethane synthesis	85
4.2.5. Epoxy synthesis.....	86
4.3. ¹ HNMR Analysis	90
4.3.1. ¹ HNMR analysis of CO and ECO	91
4.3.2. ¹ HNMR spectrums for RCO	96
4.3.3. ¹ HNMR spectrum for drying oil	99
4.4. Rheology studies.....	100
4.5. Drying time.....	107
4.5.1. Drying oil.....	108
4.5.2. Castor oil/RCO as polyol.....	110
4.5.3. Epoxy resins.....	115
Chapter 5: Antimicrobial properties of the paint	117
5.1. Antimicrobial properties	117
5.2. Anti-radiation properties of the paint.....	119

Conclusions and Recommendations	122
References	125
Appendix	147
Appendix A: Coatings based on drying oil, polyurethane and epoxy resins after being painted on a wall to cure under atmospheric conditions	147
Appendix B: FTIR Spectra	150
Appendix C: Pictures of reaction Set up and Equipment used	151

List of Figures

Figure 1: Representation of most common fatty acids with industrial importance	26
Figure 2: Oxidative film formation of unsaturated fatty acids	28
Figure 3: Structure of Castor oil	31
Figure 4: Dehydration of castor oil reaction scheme	36
Figure 5: Castor oil chemo-enzymatic epoxidation mechanism with CALB as catalyst, phase interaction.	39
Figure 6: Reaction scheme of epoxide ring opening reaction with H_2O	42
Figure 7: Epoxy application in different in sectors	47
Figure 8: Chemo-enzymatic epoxidation of castor oil with CALB as a catalyst	60
Figure 9: Schematic representation of ring opening reaction with H_2O	62
Figure 10: Successive reactions to obtain a drying oil.....	63
Figure 11: Synthesis of chain extended CO polyurethanes.....	65

Figure 12: Synthesis of RCO chain extended polyurethanes	66
Figure 13: Crosslinking mechanism of PA and Epoxy resin	70
Figure 14: Crosslinking mechanism of DDM with Epoxy resin	71
Figure 15: Picture of the CO (left) and synthesized ECO (right)	75
Figure 16: A picture of RCO (left) and ECO (right).....	76
Figure 17: A picture of DCO (left) and RCO (right)	77
Figure 18: Representative samples of the PUs obtained from CO and RCO (left to right respectively).....	78
Figure 19: Curing process with phthalic anhydride hardener.....	79
Figure 20: Pictures of the synthesized epoxy resins of both PA (left-first 3 samples) and DDM (right- last three samples) cured coatings.....	80
Figure 21: Stacked FTIR spectra for both CO and ECO.....	82
Figure 22: FTIR comparison spectrums of ECO and RCO.....	83
Figure 23: FTIR comparison spectrums of CO, ECO, RCO, DRCO and DCO.....	84
Figure 24:FTIR spectrum of CO and P17 as representative sample for the castor oil based polyurethanes before and after addition of 2k catalyst.	86
Figure 25: FTIR Spectrum for ECO, ER2 (PA based epoxy resin) and PA	88
Figure 26: FTIR Spectrums comparing ECO, ER6 (epoxy resin DDM) DDM as hardener	90
Figure 27: ¹ HNMR stacked spectrum of CO and ECO at two reaction times	92
Figure 28: Enzyme-catalyzed epoxidation of castor oil for a time at 35 °C and 45 °C, 4 wt% (related to castor oil) catalyst loading and 1:2 (Castor oil: H ₂ O) molar ratio.....	94
Figure 29: Enzyme- catalyzed epoxidation at 35 °C , 1:2 (castor oil: H ₂ O) molar ratio with different catalyst amount.	95

Figure 30: ¹HNMR spectrum of ECO and RCO with the mass ratio of the reactants of 1:18:0.2 (castor oil: H₂O: HClO₄).....97

Figure 31: Graph showing the effect of reaction time on conversion when the ratio is 1:18:0.2 for reactants and the temperature is 100 °C.98

Figure 32: Graph depicting the effect of the amount of HClO₄ as catalyst on the conversion when the reaction conditions are 100 °C temperature and for 48 hrs.98

Figure 33: Stacked ¹HNMR spectrums for CO, ECO, RCO, DCO and DRCO..... 100

Figure 34: The graph of shear rate vs shear stress for selected samples of the drying oil 102

Figure 35: Graph depicting the relationship between the shear rate and shear stress of the CO based polyurethanes. 103

Figure 36: Graph of shear rate with shear stress of polyurethanes based on RCO and MDI and the yield point 104

Figure 37: graph illustrating the relationship between increasing shear rate and shear stress of Epoxy resins with PA and DDM as hardener..... 105

Figure 38: Graph showing the relationship of shear stress and viscosity of CO based polyurethanes at different amounts of MDI. 106

Figure 39: Graph showing the relationship of viscosity with differing shear rate of polyurethane based on RCO with different amounts of MDI. 106

Figure 40: Graph showing the relationship between increasing shear rate with viscosity of Epoxy resin with PA and DDM as hardener. 107

Figure 41: Bar graph comparing the drying time for different paint samples after addition of beeswax, filler and pigment..... 109

Figure 42: Bar graph comparing the drying time of different polyurethanes when DBTL is used as catalyst.....	111
Figure 43: Bar graph comparing the drying time of different polyurethanes when 2k catalyst is used.	112
Figure 44: Graph of the drying time when different amount of 2k catalyst is added to a 1:1 ratio castor oil based polyurethane coatings.....	113
Figure 45: Bar graph comparing the drying time of different RCO based polyurethanes	114
Figure 46: Bar graph comparing the drying time of different ER based paints with PA/DDM as hardener.....	115
Figure 47: Agar plates before being placed into the incubation room (left) and agar plate spotted with PCO Ag against Escherichia coli (right).	117
Figure 48: Bar graph showing the inhibition zones for 5 different paint samples exposed to different bacteria.	118
Figure 49: UV irradiation box	120
Figure 50: Stereo Microscope Image (200µm) for Paint Sample PCO (left) before UV irradiation and (right) 90 minutes after UV irradiation.....	120
Figure 51: Stereo Microscope Image (200µm) for Paint Sample PCO TiO ₂ ++ (left) before UV irradiation and (right) 90 minutes after UV irradiation.....	121
Figure 52: Picture of different samples painted on a wall to test for the drying time under atmospheric conditions.....	147
Figure 53: Epoxy paints with DDM as the hardener after film formation	148
Figure 54: Polyurethanes based on CO and MDI without pigment after film formation	148

Figure 55: PUs based on CO with Bismuth oxide pigment (top left) and Iron oxide (top right and bottom middle) after film formation.	149
Figure 56: Epoxy resins with PA as hardener after film formation.....	150
Figure 57: Stacked FTIR spectrums of RCO and RCO based polyurethanes synthesized using different amounts of MDI.....	150
Figure 58: Epoxidation reaction set-up.....	151
Figure 59: Ring opening reaction set-up.....	151
Figure 60: The experimental setup for polyurethane synthesis.	152
Figure 61: Fourier Transform Infrared Spectroscopy (FTIR) equipment.....	152
Figure 62: Magnetic Nuclear Resonance equipment.....	153
Figure 63: Rheometer equipment.....	153

List of Tables

Table 1: Subdivision of paint variation according to different criteria.....	22
Table 2: Solvation effect on polar or nonpolar film forming agent of different solvents	23
Table 3: Additives according to different functions in different stages of paint formulation until film formation.....	25
Table 4: Chemical compositions and Iodine values of various vegetable oils	30
Table 5: Physical properties of castor oil	33
Table 6: Effect of polyol functionality with its molecular weight on the resulting type of polyurethane.	44
Table 7: Physical and Chemical properties of pure MDI.....	67

Table 8: Proportions for the synthesis of polyurethane coatings	68
Table 9: Physical and Chemical properties of PA/DDM	69
Table 10: Proportions for the Epoxy resin synthesis	69

List of abbreviations

CALB – Lipase B Candida Antarctica

FFA – Free Fatty Acid

DBTL - dibutyltin dilaurate

PU's – Polyurethanes

CO- Castor Oil

ECO - Epoxidized castor oil

RCO - Ring-opened castor oil

PA - Phthalic anhydride

DDM- 4,4'- diaminodiphenyl methane

NP- Nanoparticles

DO- Drying oil

ER- Epoxy resin

DRCO- Dehydrated ring opened castor oil

Chapter 1: Background and Motivation

1.1. Introduction

Since the 1920's agricultural commodities were used in the chemical industry mostly for fuel and other products that can be used by consumers (Wool & Sun, 2005). The use of vegetable oils in paints and coatings dates even way back to the time of cave paintings (40,000 years ago) (Jones, et al., 2017). The function of the vegetable oil was as a drying oil, meaning that the oil formed a film when exposed to atmospheric oxygen. The use of agricultural commodities came to be replaced by chemicals derived from petroleum mainly because of the lower costs and the durability of the petro-based products. With new technologies emerging, the bio-based products can be improved to compete with petro-based products both in terms of cost and performance (durability).

There is an urgent need to reduce the degree on which we rely on fossil fuels (oil, coal and natural gas) so that we can reduce emissions of greenhouse gases that are contributing to climate change; as we are continually experiencing the increase in temperatures of the planet and as a result endangering the lives of species on earth (Popp, et al., 2014; Shahzad, 2015; Tondi & Schnabel, 2020; Huang & Zhai, 2021). It is in the direct use of fossil fuels that concern lies, although there are still reserves being harvested and also other ones being found, the accessibility of such reserves is still a concern, thus it still stands that they are finite resources as they cannot be replenished (Hernandez, et al., 2020). Even a much greater concern is the detrimental effects that they pose on the environment. As the world is determined to move towards the direction of a low carbon future, renewable resources are a key factor in achieving this (Huang & Zhai, 2021; Ayanlade, et al., 2020). We cannot escape from the fluctuating prices of fossil fuels since it is a monopoly of Middle East countries since they have the greatest reserves thus any political or social unrest or discord leads to price fluctuations worldwide (Abdullah & Muhammed, 2021). This factor

becomes another motivator to shift dependency from fossil fuels to renewables since they can be obtained locally and are plentiful. The fact that plants use sunlight and carbon sources in the atmosphere such as CO_2 for photosynthesis confirms the fact that bio-based products are environmentally friendly as CO_2 is one of the gases that is leading to global warming (Wool & Sun, 2005). Currently there has been an increasing interest in using vegetable oils to produce industrial raw materials/products (Dyer, et al., 2008; Wool & Sun, 2005). As nature's renewable resources, vegetable oils contribute to sustainable development and green chemistry (Lee, et al., 2021; Nekhavhambe, et al., 2019).

The main constituents of vegetable oils are triglycerides which are formed as a result of the esterification of glycerol and three fatty acids with chain lengths mainly ranging between C8-C24 (Zhang, et al., 2017; Dyer, et al., 2008; Del Rio, et al., 2011; Madbouly, et al., 2016). Depending on the crop along with the growth conditions, including the extraction method used during the recovery of the oil, the fatty acid distribution or composition of each oil varies (Sanyang & Jawaid, 2019; Jones, et al., 2017). The variation also includes fatty acid chain length, the degree of unsaturation, stereochemistry of double bonds, and other present functional groups. This variation determines the properties of the vegetable oil, physically and chemically; and these properties thus affect the end use of the oil (Dyer, et al., 2008; Zhang, et al., 2017; Nekhavhambe, et al., 2019). For example, linolenic and linoleic are the most prominent fatty acids in linseed oil and have a high degree of unsaturation and find application as paint binders (Tammekivi, et al., 2021). Castor oil is classified as a natural polyol, as it contains a high quantity of ricinoleic acid as such it has been used extensively in the synthesis of polyurethanes (Paraskar, et al., 2021). Oils such as coconut oil and palm kernel have a rich amount of lauric acid, which is a saturated fatty acid and these oils find application as surfactants for producing soaps and detergents (Dyer, et al., 2008;

Meier, et al., 2007, Lafarga, et al., 2021). Sunflower, soybean, and rapeseed oil find application in polymer and lubricant synthesis as they consist mainly of unsaturated fatty acids (Karmakar, et al., 2021).

The polymer industry uses vegetable oils or fatty acids to a great extent. Polymers are essential as almost all the products that we are in contact with daily are constituents of polymers (Moreno, et al., 2018; Nekhavhambe, et al., 2019). For oleo-based polymers to be able to compete with petro-based polymers in terms of performance the vegetable oils undergo several modifications/functionalization (Nekhavhambe, et al., 2019; Hernandez, et al., 2020).

Some oleo chemically- derived products are already found in the market as a replacement of Petro-based products. For example, linseed oil as a drying oil, epoxidized Soybean oil is used as a plasticizer, cocomonoglyceride sulfate that is obtained from coconut oil find application as a surfactant, dicarboxylic acids such as sebacic acids are also in use and in the market (Xu, et al., 2020; Tesser, et al., 2020, Nekhavhambe, et al., 2019). Polyurethanes which are derived from renewable resources find application as coatings, adhesives, sealants, elastomers and also as foams. Due to the viscosity, low vitality, high flash point, and inertness; vegetable oils find application in lubricants (Karmakar, et al., 2021; Nekhavhambe, et al., 2019).

Castor oil as a renewable raw material continues to gain interest in the chemical and polymer industries (Severino, et al., 2012; Nekhavhambe, et al., 2019). Besides the fact that it is non-edible; it has a high oil content (~50%) and can grow in areas subject to drought. The ester linkage, double bond present in ricinoleic acid as well as the hydroxyl group make castor oil a suitable raw material allowing for versatile chemical modifications for the chemical industry (Mubofu, 2016; Nekhavhambe, et al., 2019). Reactions such as esterification, hydrolysis, and alcoholysis can occur on the ester linkage; while epoxidation, hydrogenation, and halogenation can occur on the

unsaturation site. The hydroxyl functional group allows for dehydration and poly-addition reactions. Castor oil is suitable for the production of resins for paint production, the resins can vary from drying oils, polyurethanes, epoxies, and alkyds (Nekhavambe, et al., 2019).

1.2. Problem statement

In the paint and coatings industry, polymers are chief ingredients as resins. Paint is under much scrutiny as it is considered to be a hazardous material because there are several significant environmental concerns posed by the entire process of producing paint starting from the extraction of raw materials to the disposal of the paint after use. Volatile organic compounds (VOCs) are also a major concern for paint manufacturers and users as they contribute to global warming and even physical problems to those who inhale them (Cunningham, et al., 2019). Consumers are demanding greener products thus there is a need to focus on reducing VOCs and the carbon (CO_2) impact (Jenkin, et al., 2016). The idea in paint production is the substitution of resins derived from petrochemicals and substituting with oleo-based resins from renewables. Although the most important function of coatings is surface protection there is still a vast range of requirements that coatings can meet such as flame retardancy, insulation, conduction, and antibacterial properties. In almost all industries (civil engineering sector, metal processing, machinery production, etc.) (Goldschmidt & Streitberger, 2007). Coatings can be functionalized to possess different properties of which in this research it is anti-radiation and antimicrobial properties.

Protection of materials from Ultraviolet (UV) rays which lead to photo-destruction is essential and of high practical interest (Mahltig, et al., 2005; Xing, et al., 2021). UV rays similar to visible light has a wavelength ranging from 100 to 400 nm in the electromagnetic spectrum. Architectural coatings are used to enhance the durability of wood in outdoor environment. The wood may be used for construction or decorative purposes (Cristea, et al., 2010; Jirous-Rajkovic & Miklečić,

2021). Exposure to light can lead to discoloration, loss of gloss and embrittlement thus there is a need to protect the wood substrate. UV absorbers are used for this purpose which may be organic or inorganic. The UV absorbers increase polymer stability and thus are used in coating formulations. Clear finishes on substrates perform very badly thus incorporation of UV absorbers is a necessity. The most frequently used inorganic UV absorbers include ZnO and TiO_2 nanoparticles (Aloui, et al., 2007; Cirule, et al., 2021).

Industries such as construction, shipping, and marine face the problem of microorganisms causing biofouling, moulding, and mildews (Palanichamy & Subramanian, 2017). There is a great need to develop antimicrobial coatings in industries where a high standard of hygiene is required such as hospitals, nursing homes, daycare, and medical applications (Hochmannova & Vytrasova, 2010). One of the greatest health threats is antibiotic resistance thus there is the need to produce metal-based antimicrobial agents to fight against antibiotic-resistant bacteria (Zheng, et al., 2018).

These are just two aspects of the greater problems that coatings can solve since they can be tailor-made to meet the requirements that a consumer desires to fulfill. Different vegetable oils are used to produce resins which are polymers, but castor oil is in the limelight because it is unique in that it is the only oil that contains ~90% of ricinoleic acid which is a natural polyol. This fatty acid is very valuable in industrial applications.

1.3. Research aim and objectives

The aim of this research is to develop castor oil-based paints with anti-radiation and antimicrobial properties. The objectives are outlined below:

- To modify castor oil into a drying oil with conjugated double bonds to be used in paint production.
- To produce polyurethanes and epoxy resin from castor oil as precursors for paint production.
- To study the drying time of the different paint formulations under atmospheric conditions
- To decrease the drying time for the different paint formulations
- To determine the radiation attenuation properties of the produced paints blended with TiO_2 NPs
- To produce a paint with antimicrobial properties by blending the paint formulations with TiO_2 and Ag NPs.

Chapter 2: Literature review

2.1. Paint

The first materials to be used in paint production were natural resins (shellac, carbohydrates, and starch). These types of coatings took time to dry (cure) which led to solvent borne coatings coming into play. But with the emergence of the solvent-borne coatings (~80% of solvent) gave rise to environmental concerns. As a result of the environmental concerns and also improvement of a technical nature, coatings that are more environmentally compatible are in use such as: water-based paints, powder coatings, high solids coatings, UV curable coatings, and radiation induced cured coatings (Mannari & Patel, 2015).

The primary functions of coatings are surface protection and decoration. But due to the versatility of coatings there are numerous specifications that coatings can meet besides protection and decoration. These specifications include flame-retardant coatings, antibacterial coatings, insulating coatings, etc. All these requirements can be attributed to different industries such as electrical engineering, civil engineering, and machinery production. Coatings contribute a great deal in the economy as many commodities require to be coated so that the value can be retained and even prolong the usefulness of a commodity/product (Goldschmidt & Streitberger, 2007).

The area of coatings is vast and paint forms just a part of this large class. Paint is said to be a liquid, a powder or a paste that transforms into an opaque film when applied on a surface for the purpose of protection or decoration (Goldschmidt & Streitberger, 2007; Van De Mark & Sandefur, 2005; Muller & Poth, 2011). Paint can be classified into different classes according to Table 1:

Table 1: Subdivision of paint variation according to different criteria (Goldschmidt & Streitberger, 2007; Winklaar, 2009; Mannari & Patel, 2015)

Classification	Function of coating	Layer on the coating system	Purpose of paint	Environmental compatibility	Processing conditions	Film forming agent chemistry
Different types of paints	Clearcoat	Primer	Car paint	Water-based	Baking enamel	Alkyd resin
	Metallic paint	Primer surfacer	Decorative	High-Solids	Oxidatively curable	Acrylic resin
	Solid paint	Topcoat	Industrial	Radiation curable Powder		Cellulose nitrate lacquer

The major constituents of paint include the film forming agent (resin), solvent, pigment, and additives (Winklaar, 2009). Among the mentioned constituents, the resin is an indispensable component in formulating a paint solution. The resin can be categorized based on different criteria one of which is based on natural resins (cyclorubber or chlorinated rubber, cellulose esters) and synthetic resins. Regardless of the source of the resin the same requirements of wetting substrate, adhesion, and solidification must be met. Resins can be macromolecular substances (carbohydrates) or polymeric substances (Goldschmidt & Streitberger, 2007; Mannari & Patel, 2015). The formation of a continuous smooth film occurs via physical drying and chemical curing. Chemical curing takes pre-eminence when the film forming agent is constituted of reactive functional groups. Physical drying occurs when the solvent evaporates from the paint solution, in this way the molecular chains/components come together thus molecular interaction increases the viscosity resulting in a physical hardening (Mannari & Patel, 2015). With chemical curing the reactive substances undergo cross linking which increases the average molecular weight of the

film and subsequent solidification of the film. These two film forming processes affect the physical/mechanical strength and chemical resistance of the formed film. The cross-linking in chemical curing occur by poly-addition, poly-condensation or polymerization reactions (Mischke, 2010).

There are certain material properties such as viscosity and surface tension, that must be regulated in paint formulation and processing. The primary function of the solvent is to regulate viscosity, but the solvent can also aid in the ability of the resin to wet the substrate especially when it has a lower surface tension than the substrate (Goldschmidt & Streitberger, 2007). Some solvents act as thinners in coating formulation as they react with the resin and thus remain within the formulation. In application, solvents are frequently used as combinations or mixtures and the combination is dependent on the film forming agent and evaporation rate of the solvent. The most commonly used solvents are aromatic (e.g. xylene) and aliphatic (mineral spirit, ethyl acetate, alcohols, etc.) hydrocarbons (Goldschmidt & Streitberger, 2007). Solvents can be further divided according to their solvation effect on polar or nonpolar film forming agents; Table 2 is a summary of the classification.

Table 2: Solvation effect on polar or nonpolar film forming agent of different solvents (Goldschmidt & Streitberger, 2007)

Types of solvents	Film forming agent (polar/non-polar)
Lower ketones	Polar
Higher ketones	Less polar
Aliphatic hydrocarbons (gasolines, benzines or paraffin)	Polar to nonpolar
Aromatic hydrocarbons (Toluene, xylene)	Alkyd resins
Glycol ethers	Polar and Semi-polar

Pigments function to give colour, tinting strength and hiding power to the formed film. Further functionalities of pigments are the ability to impart anticorrosive properties to the film, even antibacterial properties. Films degrade from outdoor exposure to sunlight but pigments have the ability to absorb the UV rays thus protecting the film (Goldschmidt & Streitberger, 2007; Muller, 2010). Pigments can be organic, inorganic, or metallic. Iron oxides and TiO_2 are common among the inorganic pigments as they possess excellent hiding power and superb chemical resistance, respectively (Muller, 2010).

Additives are added into the paint in very small quantities, but they play a significant role of optimizing paint manufacturing, processing, and film formation. Some of the roles played by additives include suppressing sedimentation of pigments, enhancement of flow of the paint formulation, acceleration of curing and increasing resistance to UV radiation (Goldschmidt & Streitberger, 2007). Table 3 summarises various additives according to different functions.

Table 3: Additives according to different functions in different stages of paint formulation until film formation (Goldschmidt & Streitberger, 2007; Mannari & Patel, 2015)

Different stages in paint manufacture and applications	Coating manufacture and storage stability	Optimization of Processing properties	Optimization/influence of Film formation and film properties
Different additives	Tensides	Wetting agents	Catalysts - Initiators - Photo initiators - Siccatives
	Defoaming agents	Flow control additives	
	Deaerators		
	Inhibitors - Pigment sedimentation - Premature crosslinking		

2.2. Vegetable oils

Agricultural commodities used in paint manufacturing include carbohydrates (cellulose, starch) and natural oils. The application of carbohydrates as film forming agents still find application in the furniture, woodworking, and the automotive sector as cellulose nitrate and cellulose acetobutyrate. Despite the application of carbohydrate-based resins in the mentioned sectors, natural oils take precedence as natural raw materials in film forming agents. They transform into a high viscosity liquid thus solidifying into a hard film by interaction with atmospheric oxygen. Figure 1 is an illustration of the most common fatty acids that are useful in industry.

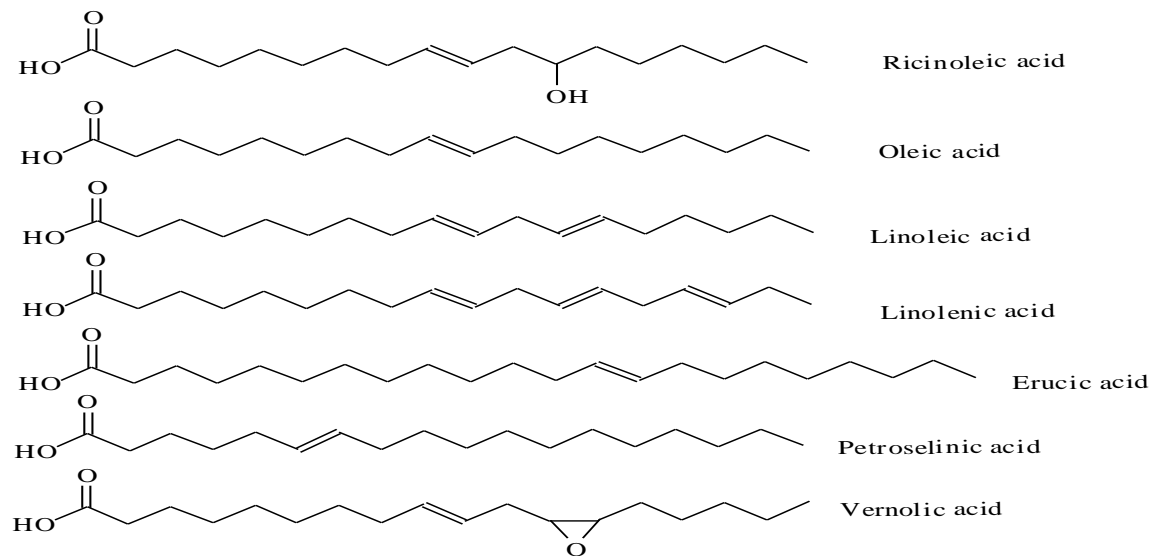


Figure 1: Representation of most common fatty acids with industrial importance (Zhang & Kessler, 2016; Madbouly, et al., 2016).

Iodine value is a variable that is used to measure the degree of unsaturation of vegetable oils and is vastly used to group vegetable oils into three classes. This value is defined as the amount of iodine in grams absorbed by a 100g of oil. Various methods are used for calculating the iodine value; but the commonly used are the Wijs and Hanus methods. The similarity in all the methods is the assumption that a double bond will take up two atoms of iodine under the specified test conditions (Nekhavambe, et al., 2019). An excess of a solution of iodine monochloride (ICl) in acetic acid and cyclohexane is added to the fatty acid in the Wijs method (Chong, 2012; Nekhavhambe, et al., 2019). The amount of iodine consumed is indirectly measured by reacting the excess unreacted ICl with potassium iodide to liberate I_2 which is then titrated with sodium thiosulphate (Chong, 2012; Patterson, 2011; He & Liu, 2019; Meier, et al., 2007; Nekhavhambe, et al., 2019). An iodine value that exceeds 170 show a drying oil, semi-drying oils have iodine values between 100 and 170 while an iodine value < 100 refer to non-drying oils. Oils classified as drying oils cross-link when exposed to atmospheric oxygen to form a three-dimensional network

through autoxidation, which follows the free radical polymerization mechanism (Mischke, 2010; Tumosa & Mecklenburg, 2012; Nekhavhambe, et al., 2019). Free radical polymerization consists of a series of reactions that involve free radicals and these are: initiation, propagation, and termination. The drying process of drying oils is more complex than what is described by the free radical polymerization as several side reactions occur, but it does give insight to a certain degree. In the beginning of the drying process, antioxidants are consumed followed by a rapid uptake of oxygen forming hydroperoxides, and as the hydroperoxides are consumed a cross-linked film is formed (Mischke, 2010; Matyjaszewski & Davis, 2002; Nekhavhambe, et al., 2019). Figure 2 present the drying process of unsaturated fatty acids.

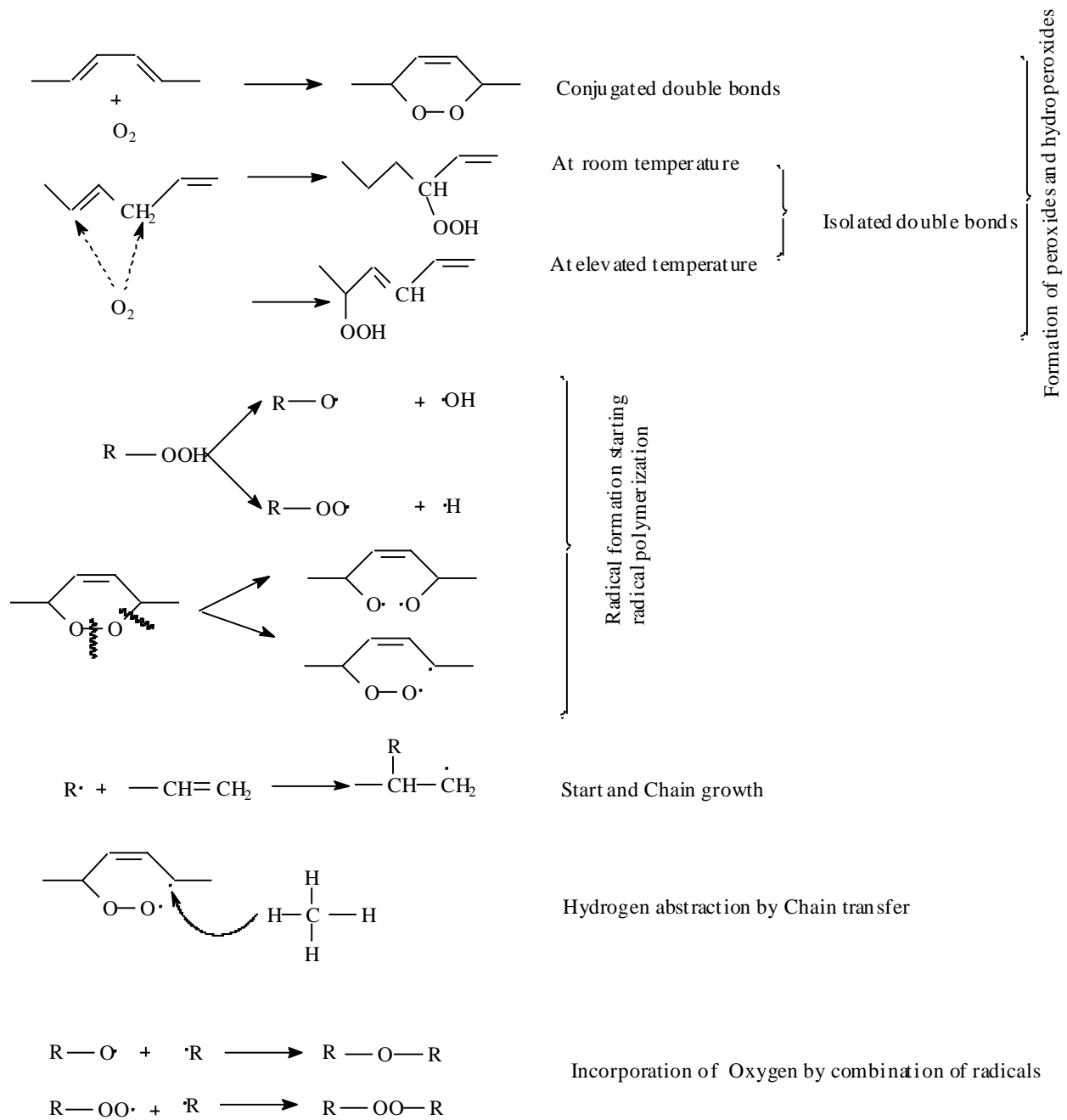


Figure 2: Oxidative film formation of unsaturated fatty acids (Goldschmidt & Streitberger, 2007; Tumosa & Mecklenburg, 2012; Nekhavhambe, et al., 2019)

From Table 4, linseed has an iodine value of 171.9 confirming that it is a drying oil, finding application mostly in coatings as it has good drying properties. This is due to the fact that linseed oil contains 54.59 wt% of linolenic acid which is a polyunsaturated oil. Canola, cottonseed, sunflower and soybean are classified as semi-drying oil based on their iodine values. These oils have the highest amount of linolenic acid with 53.33 wt% soybean, 54.83 wt% cottonseed and 67.58 wt% sunflower. Table 4 give the iodine values of castor and olive oil, of 85.3 and 88.2 respectively as such they are classified as non-drying oils and can only be used as coatings after chemical modification is done to introduce functional groups that enhance drying.

Table 4: Chemical compositions and Iodine values of various vegetable oils (Giakoumis, 2018; Kirk-Othmer, 2004; Gunstone, 2002; Erhan, 2005; Belgacem & Gandini, 2008; Nekhavhambe, et al., 2019)

Vegetable oils	Fatty acid composition (w/w %)															Average iodine value (mg/100g)
	C12:0	C14:0	C16:0	C16:1	C17:0	C18:0	C18:1	C18:1 OH	C18:2	C18:3	C20:0	C20:1	C22:0	C22:1	C24:0	
	Lauric	Myristic	Palmitic	Palmitoleic	Margaric	Stearic	Oleic	Ricinoleic	Linoleic	Linolenic	Arachidic	Gondoic	Behenic	Erucic	Lignoceric	
Canola		0.1	4.1	0.3	0.1	1.8	60.9		21.0	8.8	0.7	1.0	0.3	0.7	0.2	109.3
Castor			1.0			1.0	3.0	89.5	4.2	0.3	0.3	0.7				85.3
Cottonseed		0.7	21.6	0.6		2.6	18.6		54.4	0.7	0.3		0.2			119.1
Jatropha	0.1	0.27	14.39	0.69	0.08	5.83	42.05		35.90	0.23	0.09	0.10	0.14		1.47	100.2
Linseed	0.71			6.0		3.0	17.0		14.0	60.0						171.9
Olive		0.08	11.26	0.88	0.07	2.79	74.52		9.82	0.51	0.49	0.29	0.16	0.04	0.17	88.2
Rapeseed			4.0			2.0	56.0		26.0	10.0						110.5
Soybean		0.1	11.0	0.1		4.0	23.4		53.2	7.8	0.3		0.1			128.2
Sunflower	0.5	0.2	6.8	0.1		4.7	18.6		68.2	0.5	0.4					128

2.3. Castor Oil

The *Ricinus communis* L. is believed to have its origin in various areas including Africa, Asia, India and China and from the seeds of this plant, castor oil is obtained (Mubofu, 2016; Mensah, et al., 2018; Kunduru, et al., 2015; Nekhavhambe, et al., 2019). It has been used as a purgative since the oldest time. Properties of castor oil such as high viscosity, high lubricity, stability at a range of temperatures and insolubility in aliphatic petroleum solvents and fuels; make it usable as a lubricant for equipment (Mutlu & Meier, 2010; Nekhavhambe, et al., 2019). Castor oil is unique among other oils because it contains ~ 90% of unsaturated fatty acid ricinoleic acid (Zhang, et al., 2017; Kunduru, et al., 2015). It is an inedible oil and has been used extensively for synthesis of industrial products (biodegradable polymers, paints, coatings and biofuel) and for pharmaceutical application (Mensah & Brien, 2018;Nekhavhambe, et al., 2019). The use of castor oil as a renewable raw material in the chemical and polymer industries continues to grow (Severino, et al., 2012; Nekhavhambe, et al., 2019). Figure 3 below shows the structure of castor oil.

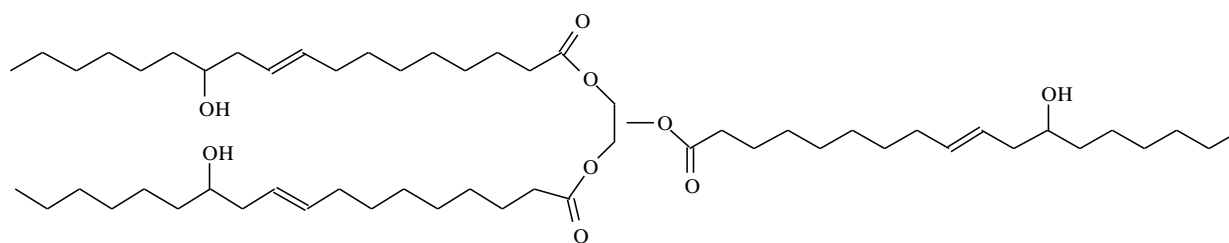


Figure 3: Structure of Castor oil

Castor plant is a crop that can easily grow in harsh environments (drought, saline soil) and does not require a lot of attention when cultivated, and in tropical regions it yields a high content of oil. Local farmers can be able to establish small scale farming structures, thus it a promising crop (Scholz & da Silva, 2008; Nekhavhambe, et al., 2019). There is a continual steady increase in the

impact of castor oil in the world economy (Mubofu, 2016). The world's leading country in the production of castor oil is India (Nekhavambe, et al., 2019).

Castor oil has been used extensively in the chemical industry to produce bio-based polyurethanes, which were traditionally produced from petroleum resources as such the demand for this oil is high. The extensive use of edible oils such as soybean, sunflower, and corn in the chemical industry results in a competition with the food industry. Thus there is a need for non-edible oils that can be used exclusively for industrial applications and castor oil fits this criteria (Metzger, 2009; Nekhavhambe, et al., 2019).

Castor oil has a yellow or yellow-brown colour and it is highly viscous because of the hydroxyl group in the ricinoleic fatty acid (Scholz & da Silva, 2008). The values of specific gravity, viscosity, and hydroxyl number are high for castor oil as compared to other vegetable oils. In comparison with other oils; castor oil has a long shelf life being soluble in alcohol but insoluble to aliphatic petrochemical fuels and solvents. It has a high calorific value, cetane number and does not contain phosphorus or carbon residues thus it used for biodiesel production (Scholz & da Silva, 2008). The presence of the hydroxyl group greatly affects properties such as viscosity, the heat of fusion and solubility (Mensah, et.al., 2018). The density of castor oil is high; 952.5 kg/m^3 on average compared to oils such as canola, linseed, olive, and soybean with density of 915.6, 912.8, 928.2 and 912.6 kg/m^3 respectively.

Viscosity can be reported as kinematic viscosity or dynamic viscosity. Viscosity can be defined as the resistance to flow /shear due to internal friction, whereas for kinematic viscosity is due to gravity (Boda, et al., 2015; Diamante & Lan, 2014; Gunstone, 2004). The presence of the hydroxyl group on the castor oil increases intermolecular or inter-chain hydrogen bonding that restricts the

flow of the molecules leading to the higher viscosity of the oil (Gilbert, 1941). On average, the kinematic viscosity of castor oil is $239.7 \text{ mm}^2/\text{s}$, and it is very high when compared to other oils: canola (34.7), linseed (26.2), olive (32.7) and soybean (32.7) (Giakoumis, 2018). This property makes castor oil good for lubrication (Nekhavhambe, et al., 2019). Table 5 gives the values of some properties of castor oil.

Table 5: Physical properties of castor oil (Mensah & Brien, 2018; Kirk-Othmer, 2004; Belgacem & Gandini, 2008; Nekhavhambe, et al., 2019)

Variable	Units	Value
Oil content (in seeds)	%	43.3-56.2
Density	kgm^{-3}	946-961
Specific gravity @ 20°C	-	0.951
Iodine value	mgg^{-1}	84.5-85.5
Acid value	mg KOHg^{-1}	0.03-4.9
Free FA	%	0.06-3.4
Hydroxyl value	mg KOHg^{-1}	164.5
Melting point	°C	-20 to -10
Saponification value	mgg^{-1}	182.9
Unsaponifiable matter		3.4
Kinematic viscosity	mm^2/s (= cSt)	239.7
Refractive index @ 20°C	-	1.47

2.4. The chemistry of castor oil

Ricinoleic acid as the major constituent of castor oil allows for versatility in chemical industry applications (Salimon, et al., 2012). The three functional groups on ricinoleic acid (ester linkage, double bond and hydroxyl group) allow for numerous chemical modifications of castor oil into assorted products depending on the end use (Mutlu & Meier, 2010; Mubofu, 2016; Nekhavhambe, et al., 2019).

2.4.1. Dehydration of castor oil

castor oil is a non-drying oil because it has a low iodine number but through the process of catalytic dehydration, castor oil can possess drying or semi-drying properties. The dehydration reaction is carried out at elevated temperatures (250 -300 °C), which is the optimum temperature range, as too much heat leads to polymerization and gelation of the oil (Ding, et al., 2018; Nekhavhambe, et al., 2019). This reaction is usually carried out in an inert atmosphere/vacuum to avoid oxidative polymerization, side reactions and moisture on the dehydrated product (Mutlu & Meier, 2010; Mubofu, 2016; Nezihe, et al., 2011; Nekhavhambe, et al., 2019). The reaction scheme is given in Figure 4. During the dehydration process, the carbonium ions are formed by an electrophilic attack on the unpaired electrons on the hydroxyl oxygen atom, thus forming a hydroxonium ion, which is followed by the loss of water (Nezihe, et al., 2011; Mamudu, et al., 2019; Ding, et al., 2018; Nekhavhambe, et al., 2019). The hydroxyl group on the 12th carbon can be removed along with the hydrogen in the 11th or 13th carbon resulting in either conjugated or non-conjugated double bonds (Ding, et al., 2018).

Various catalysts have been used in the dehydration of castor oil which include: salts, resins, clays, and mineral acids. With the most commonly used catalyst being sodium bisulfate ($NaHSO_4$)

(Mamudu, et al., 2019; Nekhavhambe, et al., 2019). There have been drawbacks with the use of this catalyst in that it is easily mixed with the reactants becoming difficult to separate from the product. Because of this, $NaHSO_4$ can be loaded on silica or alumina and molecular sieves to improve its catalytic properties. In a research done by Jian-Fei, et al. (2018) a mesoporous material (MCM-41) was used as a support for $NaHSO_4$ to improve its performance. The catalyst was prepared using supercritical impregnation. The mesoporous structure of the catalyst reduces resistance to mass transfer as a result facilitating the access of reactants to active sites and the diffusion of products (Nekhavhambe, et al., 2019).

Mamudu, et al., (2019) studied the effect of $NaHSO_4$ catalyst on a batch process. Sodium bisulfate ($NaHSO_3$) was chosen as the anti-polymerization agent. The change in the physiochemical properties in relation to hydroxyl value, viscosity and iodine value with respect to reaction time and temperature were considered. The reaction was carried out at 250 °C with 1% $NaHSO_4$ and 1% $NaHSO_3$ with samples drawn after 30, 45, 60, 90 and 120 min. When a catalyst was used the reaction time in which maximum conversion was reached was 60 min while the reaction time was 180 min when the catalyst was not used. The longer reaction time resulted in a darker oil being obtained.

The product and reaction conditions depend on the catalyst thus the choice of catalyst for dehydration is very critical. Two products, conjugated double bonds or non-conjugated double bonds can be obtained after dehydration in varying proportions. These products affect the drying process of the drying oil as their reactivity is different. During the drying process hydrogen abstraction by free radicals occurs preferentially at the allylic position as the energy is low. Conjugated double bonds are double allylic making them more reactive leading to a more rapid

drying of the oil. Because of the high reactivity of conjugated double bonds, the drying oil formed is prone to undergo polymerization thus it is important to add an anti-polymerization agent along with the catalyst. Dehydrated castor oil is waterproof, flexible, dries rapidly and has good colour retention properties and find application in the coatings industry (Jian-Fei, et al., 2018; Nekhavhambe, et al., 2019).

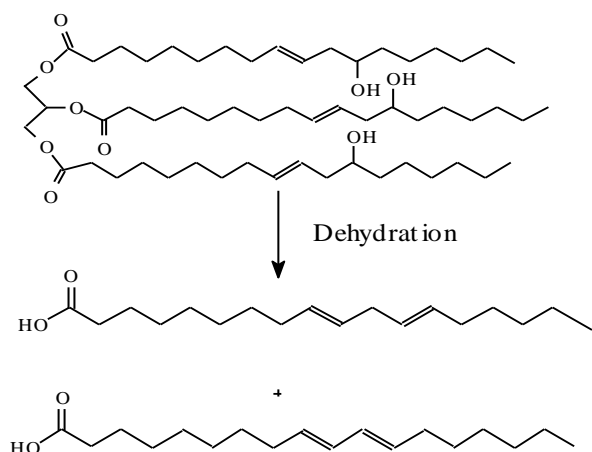


Figure 4: Dehydration of castor oil reaction scheme

2.4.2. Epoxidation

Epoxidation involves the addition of oxygen into a C=C unsaturation site present in vegetable oils. Vegetable oils such as linseed, soybean, corn, olive, and rapeseed (just to mention a few) are used industrially to synthesize epoxidized vegetable oils by the *prelzhaev* method (Bajwa, et al., 2016). The *prelzhaev* method for epoxidation although being the conventional way of performing epoxidation has a number of setbacks as strong acids are used as catalysts such as sulphuric (H_2SO_4) and phosphoric (H_3PO_4) acid for the *in situ* generation of peracids. The presence of a strong acid affects reaction selectivity as ring opening of the epoxide ring also occurs thus reducing

the C=C conversion resulting in undesirable byproducts . To counter these challenges, acid ion exchange resins and lipases are used as catalysts to increase the reaction selectivity and thus increasing reactants conversion (Zhang, et al., 2018).

Klaas and Warwel first studied the chemo-enzymatic epoxidation of plant oils in 1999. They studied the complete or partial 'self ' epoxidation of rapeseed, sunflower, soybean and linseed oil and found the selectivity and conversion to be 90%. In the 'self ' epoxidation of plant oils, the carboxylic acid needed to form peroxy acids is provided by FFA in the oil. The lipase is able to hydrolyze the oil triglycerides to get FFA. With this in view the product after epoxidation is a mixture of epoxidized triglycerides, epoxidized FFA, epoxidized monoglycerides and diglycerides. The epoxidized monoglycerides and diglycerides are difficult to remove from the product, thus to eliminate this they added 5.0wt% of FFA as part of the reactants and found that it was sufficient to suppress the hydrolysis of triglycerides. Vlcek & Petrovic, (2006) underwent a similar study as Klass and Warwel and found that hydrolysis occurred either way, whether FFA were added or not but when 8.0wt% of FFA were added the highest yield attained was 95%. Zhang, et al., (2018) confirmed this, that hydrolysis occurs whether FFA are added or not, yet the extent to which hydrolysis occurred was not the same. They analyzed the extent of triglyceride hydrolysis at 35°C with 8.0wt% oleic acid and 8.0wt% stearic acid and when no FFA was added. It was found that initially FFA are formed to a greater extent when there is no addition of FFA at the initial reaction yet the amount is lower in the final product. When FFA were initially added, there was still an additional 5.0 wt% that was formed by hydrolysis during the epoxidation. Thus hydrolysis occurred in either case. Zhang and colleagues (2018) also investigated the effect of adding toluene in chemo-enzymatic epoxidation on the conversion. They found that at low temperature (35%) the conversion was ~ 100% whether toluene was added or not. Yet when the temperature was raised to

50°C the addition of toluene increased the conversion. This was due to the fact that toluene lessens direct contact of enzyme and hydrogen peroxide (H_2O_2) which leads to enzyme deactivation especially when the temperatures are high. Thus it was concluded that the addition of FFA and toluene did not have much effect on the yield but temperature was the main variable to consider when performing chemo-enzymatic epoxidation. A study by Tomvall, et al., (2007) investigated the deactivation of the enzyme by incubating Novozym 435 in the presence of toluene, water, H_2O_2 , oleic acid, perpalmitic acid and epoxystearic acid at temperatures between 20 and 60 °C. The enzyme activity was measured after 48 h or 16 h depending on the reaction conditions. Epoxystearic acid was found to inactivate the enzyme slightly at a temperature of 50 °C while oleic and perpalmitic acid did not inactivate the catalyst. Within 48 h at temperatures between 20-60 °C when the lipase incubation was in water/toluene, no deactivation of the enzyme was observed. The concentration of H_2O_2 between 6-12 M at 20 °C did not affect the stability of the enzyme but when temperature was raised to 60 °C the enzyme lost activity quite rapidly and the rate of deactivation increased with increasing H_2O_2 concentration. Thus it was concluded that temperature and H_2O_2 concentration are the main parameters to consider in chemo-enzymatic epoxidation.

Novozyme 435 is a commercial lipase that has been used extensively in research for epoxidation reaction (Tomvall, et al., 2007), and it is prepared by immobilization of *Candida antarctica* Lipase B (CALB) on acrylic resin. The mentioned studies were done using this catalyst with soybean oil. In a study by Bajwa, et al., (2016) three commercially available immobilized lipase enzymes were investigated which include: fungal lipase (TRC091006), yeast lipase (TRC091012) and Novoenzyme 435. As a result of the study it was found that Novoenzyme 435 was the best for chemo-enzymatic epoxidation of karanja oil. The conversion was found to be 80% in 8-9 h reaction time at 30°C. The conversion was better compared with methods that are carried out in 6h at 80 °C.

The enzymatic method was found to be more efficient in relation to energy consumption and selectivity.

Candida antarctica Lipase B (CALB) is a lipase that is isolated from the *Candida antarctica* species, it is distinctive from other lipases because it has a hydrophobic surface. It has an open and closed structure that may affect its catalytic activity as well as interfacial activation. This enzyme has been used extensively in biocatalysis because it has good thermal stability, stable in organic solvents and its enantioselectivity. For the efficient use of lipases they are immobilized in different supports/carriers (Duleba, et al., 2019). Figure 5 shows the chemo-enzymatic epoxidation of castor oil with a lipase. The diagram shows the process of the formation of peroxy acid which in this case is per-ricinoleic acid, which in turn epoxidises the double bonds of the oil triglycerides to form epoxidized castor oil.

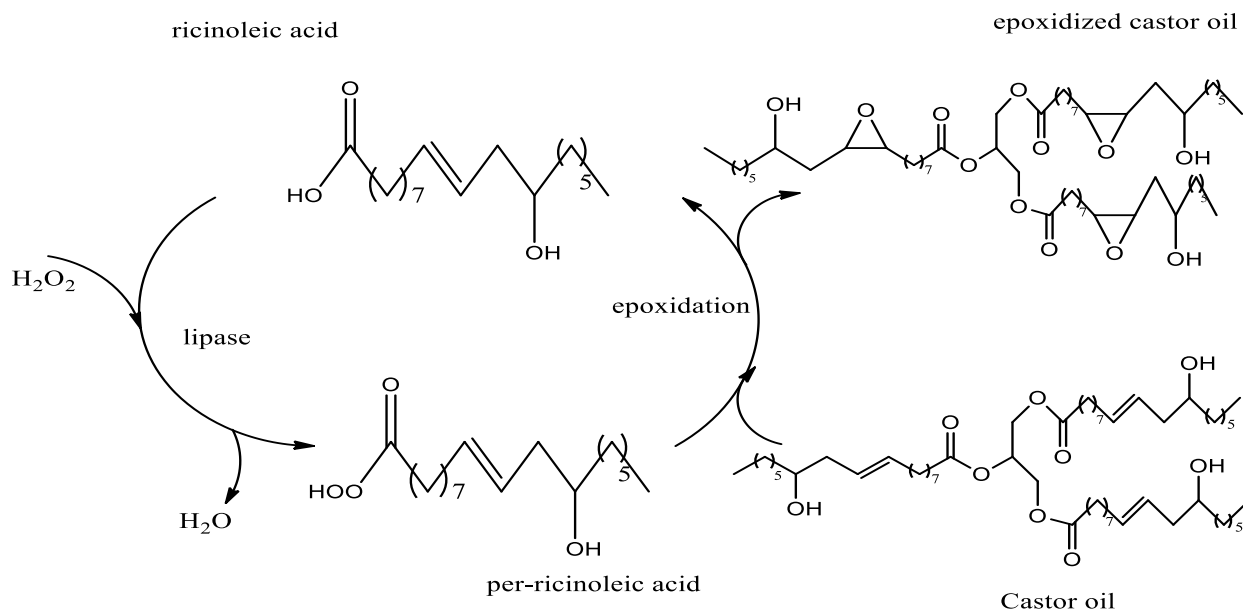


Figure 5: Castor oil chemo-enzymatic epoxidation mechanism with CALB as catalyst, phase interaction.

2.4.3. Ring Opening

The unsaturated fatty acids of vegetable oils can be functionalized with hydroxyl groups via different paths which include epoxidation followed by ring opening, hydroformylation, hydrogenation and ozonolysis (de Souza, et al., 2012; Desroches, et al., 2012). There are a number of nucleophilic reagents that are used in opening the oxirane ring and depending on the nucleophile used various products can be obtained. The reaction can be performed using water as a nucleophile in the presence of a strong acid such as H_2SO_4 . Alcohols can also be used as nucleophiles to open an epoxide ring resulting in the formation of secondary alcohols. The most frequently used alcohols include methanol and 2-ethyl-1-hexanol in the presence of H_2SO_4 or p-toluenesulfonic acid. Alcohols can be replaced with thiol nucleophiles such as butane-1-thiol for epoxide ring opening. The use of secondary amines for ring opening is not as efficient since there might be a competing reaction between esters present in the triglycerides with the amine. A number of carboxylic acids can also be used as nucleophiles to open the ring, an example of these include: acetic acid, fatty acids, lactic acid, propionic, hexanoic or octanoic acid. Diols such as diethanolamine or triethanol amine can open the epoxide ring resulting in both primary and secondary hydroxyl functions (Desroches, et al., 2012).

Sankaranarayanan & Srinivasan, (2015) synthesized functionalized castor oil derivatives namely: ring opened glyceryl ricinoleates, epoxy alkyl ricinoleates and ring opened alkyl ricinoleates. The products were obtained through ring opening and transesterification with epoxidized castor oil (ECO). A number of acid catalysts were studied and among these Amberlyst 15 was the most active with a conversion of 82% with methanol as nucleophile. The reaction conditions are as follows: 105 °C temperature, 4 hrs reaction time, ~180:1 molar ratio (methanol:ECO) with 10wt% catalyst with respect to ECO. The study was expounded further to study different nucleophiles

with similar reaction conditions to study the conversion. With the increase in the chain lengths of alcohol the conversion decreased. When water was used there was a 49% conversion and the product formed was a white gel. Acetic anhydride gave 69% conversion and acetone gave 39% conversion with formation of ketals while diethyl amine gave a 24% conversion. The lowest conversion was found for sodium azide with water which gave only 4% conversion.

The selection of a proper catalyst for the ring opening reaction is important as some catalysts can favor hydrolysis over the ring opening reaction. Catalysts such as H_2SO_4 and HCl serve as examples. Perchloric acid ($HClO_4$) is a better catalyst because it favors ring opening over hydrolysis of the ester linkage of the triglycerides (Sharma, et al., 2006).

Sharma, et al., (2006) synthesized biodegradable biolubricant from soybean oil. The soybean oil had to undergo a series of structural modifications using anhydrides of different chain lengths. The first reaction in this series of structural modifications was ring opening of the epoxidized soybean oil (ESBO). The reaction was done using water as a nucleophile and $HClO_4$ as a catalyst. The extent of the reaction was monitored by IR spectroscopy and it was observed that the bands at 823 and 843 cm^{-1} which correspond to the epoxy group disappeared as the reaction progressed and there was an increase in the band intensity at 3700-3100 cm^{-1} which correspond to the OH stretching vibrations of alcohols. The completion of the reaction was also confirmed with 1H -NMR. The peaks at 3.2-2.8 ppm which correspond to CH protons of the epoxy ring completely disappeared while peaks at 4.1-3.5 ppm appeared which correspond to protons attached to the carbon of the CHOH group. Other peaks on the 1H NMR spectrum were identified which were located at 3.5-3.0 ppm which are the protons attached to the oxygen of the CHOH group. The reaction time and temperature were selected for the ring opening step to ensure that the reaction

goes to completion or nearly 90%. Figure 6 is a generic representation of epoxide ring opening using water as a nucleophile.

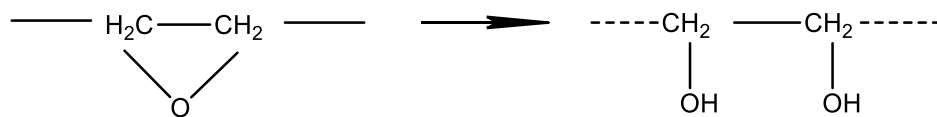


Figure 6: Reaction scheme of epoxide ring opening reaction with H₂O

2.4.4. Polymerization

Polyurethanes, polyesters, polyethers, polyamides, and polysulfides can be synthesized by step-growth polymerization (Sharma & Kundu, 2008; Nekhavhambe, et al., 2019). The two main reactions of step growth polymerization include poly-condensation and poly-addition. During poly-condensation two functional groups which may be of the same or different monomers, oligomers or short-chain polymers react to form a polymer that has a higher molecular weight. The most common by-product of the poly-condensation reaction is water but this is also dependant on the monomer (Douka, et al., 2018). The variety of monomers and the difference of reaction schemes have an effect in the reaction dynamics (Yokozawa & Yokoyama, 2007). With the polyaddition reaction, there is no loss of a small molecule during the reaction thus the repeating unit of the resulting monomer has the same composition as the monomer (O dian, 2004; Nekhavhambe, et al., 2019).

2.4.4.1. Polyurethanes

The original synthesis of polyurethanes is credited to Oto Bayer in the 1930's, the main application was in aerospace and for military purposes (Silva & Bordado, 2004). Industrially, polyurethanes are synthesized normally by the polyaddition reaction of isocyanates and polyols. As a natural polyol castor oil has been used to synthesize polyurethanes. The most commonly used catalyst in

polyurethane synthesis is dibutyltin dilaurate (DBTL). This organometallic catalyst has remarkable catalytic activity in the urethane formation reaction (Silva & Bordado, 2004). In addition to excellent properties, polyurethanes are versatile and have numerous technological applications such as the use as biomaterials (medical devices), adhesives, for construction (building insulation), and fibers (Hablott, et al., 2008; Liang, et al., 2018; Thakur & Karak, 2013; Zhang, et al., 2017). They are generally prepared by polymerization of polyols with diisocyanates or polyisocyanates. The reaction between the isocyanate and polyol is an exothermic reaction and produces a urethane group (Ionescu, 2005; Nekhavhambe, et al., 2019). In terms of their structure PU's consist of alternating hard segments (isocyanate) which give the polymer its stability, resistance to heat and physical cross-linking properties while the soft segment (polyether or polyester polyols) provides the elasticity in the PU's chain (Wang, et al., 2019;). The techniques utilised in polyurethane synthesis include: one-shot, prepolymer and quasiprepolymer synthesis. The one-shot technique is used commonly, where in all the raw materials are mixed together in one step with efficient mixing to obtain the polyurethane. With the prepolymer technique, the 1:1 or higher NCO/OH ratio is used thus ending up with NCO terminated polyurethanes. This prepolymer is then reacted with a chain-extender or a crosslinker to obtain high molecular weight polyurethane. The quasiprepolymer method is similar to the prepolymer technique, the difference is in the fact that the NCO is in substantial excess (Ionescu, 2005). The polyaddition reaction between the hydroxyl group and isocyanate results in numerous polyurethane systems such as foams, coatings, adhesives, sealants and biomedical implants (Sharma, et al., 2016).

Isocyanates may be classified either as aliphatic or aromatic and thus possess different reactivities. Aromatic isocyanates are more reactive than aliphatic and this is because of the electron withdrawing effect that the aromatic ring has. The most commonly used aromatic isocyanates

include toluene diisocyanate (TDI) and methylene diphenyl diisocyanate (MDI) whereas the aliphatic isocyanate include hexamethylene diisocyanate (HDI), isophorone diisocyanate (IPDI) and 4,4' dicyclohexyl diisocyanate (HMDI). The NCO/OH ratio in polyurethane synthesis has an effect on the resulting polyurethane. If the isocyanate is used in higher quantity the resulting polyurethane is rigid and can be used in foam application. Whereas if the quantity of isocyanate used is less compared to the polyol then the resulting polyurethane is more flexible and find application in coatings (Ionescu, 2005). Table 6 summarises the effect of polyol functionality with its molecular weight has on the resulting polyurethane type when reacted with a diisocyanate.

Table 6: Effect of polyol functionality with its molecular weight on the resulting type of polyurethane (Ionescu, 2005).

Polyol functionality (hydroxyl groups/mol)	Polyol Molecular weight (daltons)	Type of polyurethane
		Elastic
2-3	2000-10000	
3-8	300-1000	Rigid-crosslinked
2	2000-4000	Elastic linear
2-3	3000-6500	Crosslinked-flexible
3-8	150-1000	Rigid

For coatings application high molecular weight polyols with a functionality in the range of 2-3 hydroxyl groups/mol are used as this leads to a low degree of crosslinking. Low-branched oligo-polyols also find application in the development of coatings. Low molecular weight polyols with a high functionality of 3-8 hydroxyl groups/mol lead to rigid polyurethanes (Ionescu, 2005).

The physico-chemical properties of polyurethanes can be affected by the isocyanates that are used during polyurethane synthesis and also the same properties can be affected when chain extenders are used during synthesis. The physico-chemical properties that are of general interest in polyurethane synthesis are tensile strength, elongation at break, tensile modulus, surface hardness and density. These properties aid in studying the performance of the synthesized polyurethane. Many authors have undergone in the studies relating to these properties.

With a study done by (Swamy, et al., 2003) physico-chemical properties (density, tensile strength, percentage elongation at break, tensile modulus and surface hardness) of chain extended PUs were investigated. The PUs were synthesized with castor oil, isocyanates (MDI, TDI and HMDI) and chain extenders (1,4 butane diol and 1,6 hexane diol). Chain extended polyurethanes have better mechanical performance. Interms of density and tensile strength; 1,6-hexane diol with MDI/TDI PUs and 1,4 butane diol with MDI/TDI had the highest values respectively. 1,6-hexane diol chain extended PUs had higher surface hardness whereas 1,4-butane diol (with TDI) had the best tensile modulus. HMDI + 1,6-hexane diol based PUs had the lowest value for percentage elongation at break due to the presence of the methylene groups in the chain leading to poor mechanical performance. In a study by Hablot, et al. (2008) polyurethanes from TDI had the highest tensile strength yet IPDI had the highest elongation at break value. The focus was on thermoset polyurethanes based on castor oil with three different isocyanates namely: TDI, IPDI, and HDI. The study investigated the reaction homogeneity and effect of ratio of isocyanate and hydroxyl group. It was also found that TDI is more reactive because of its electron withdrawing effect compared to HDI and IPDI.

Tayde, et al. (2017) synthesized polyurethanes using castor oil as a bio-polyol and TDI. In their study the reactions were carried using DBTL as catalyst and also in the absence of catalyst. The coatings were tested for mechanical strength in relation to scratch and chemical resistance, hardness, and pot life. It was found that the PU with catalyst had minimum pot life while having better hardness and adhesion when the NCO/OH ratio was 1:1. The PU with higher hydroxyl content led to a higher crosslinking density thus higher film strength and higher chemical resistance. Lower hydroxyl content led to better film elasticity at NCO/OH ratio > 1 with lower chemical resistance. The effects on the coating was found to be based on the polyol and less on the type of isocyanate.

The polyol structure has an effect on the resulting polyurethane coating. In order to compare the structure effect of modified castor oil branched polyols and unmodified castor oil; Shaik, et al. (2019) undertook such a study. To produce the modified castor oil branched polyol (COBP), castor oil was reacted with succinic anhydride, petrochemical-based pentaerythritol/trimethylolpropane and biobased glycerol. The COBP was then reacted with IPDI to produce the polyurethane-urea coatings. The COBP had higher hydroxy values thus decreasing the drying time as a higher hydroxyl value increases the crosslink density. The COBP polyurethane-urea coatings showed a better thermo-viscoelastic and mechanical properties, and this in comparison with unmodified castor oil polyurethanes. This type of coating was found to be fit in moist environments as a protective coating.

2.4.4.2. Epoxy

Both the pre-polymers and cured resins (in this context referring to the coating) are referred to as epoxy resins. These type of resins have been available commercially for over 45 years and the first synthesis was in 1891. The commercial marketing of these resins began in the 1940 after the work of Pierie Castan and Sylvan Greenlee. The earliest epoxy resins were derivatives of Bisphenol-A and epichlorohydrin (Bryan, 1993).

Epoxy resins are classified as thermosetting polymers, and find application in adhesives, coatings and composites mainly due to the fact that they are low viscosity formulations, good insulation and good chemical and thermal resistance. They are also very chemically compatible with many materials tending to wet surfaces easily thus make good binders and also this account for the routine use as coatings and adhesives (Pradhan, et al., 2016).

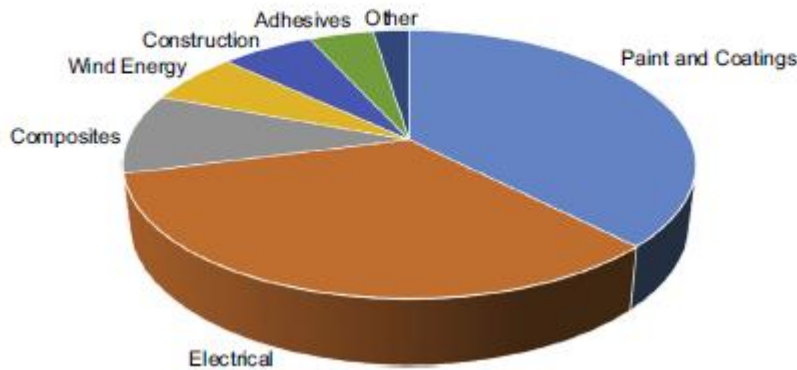


Figure 7: Epoxy application in different in sectors (Gibson, 2017)

The resin can be formed by either homo-polymerisation or chemical reaction between two monomers with differing functional groups. In either crosslinking path the common entity is the epoxy monomer which is characterized by an oxirane ring which is a three-member ring between

two carbons and an oxygen (Gibson, 2017). The electrophilic nature of the carbon atom allows ring opening to occur through a nucleophilic attack of the ring. Epoxy resins can be classified as glycidyl or non-glycidyl. Depending on the process (application) and properties required different curing agents can be used. The curing agents commonly used include: di/polyamines, anhydrides, polyamides and di/polyphenols. Diamines are very reactive and this reactivity is attributed to the high nucleophilicity nitrogen atom of the amine group (Gonzalez, et al., 2012).

Similar to conventional epoxy resins, vegetable oil based epoxy resins can fall under the two classes: glycidyl and non-glycidyl class. They find application mostly as plasticizers for PVC and diluents to produce high solid-low VOC epoxies. Despite their applications, vegetable oil based epoxy resins can still function in the same way as petroleum based ones thus used in producing coatings, adhesives and composites.

Pin & Sbirrazzuoli, (2015) synthesized biobased materials with toughened mechanical properties based on epoxidized linseed oil with MHHPA and BTDA through anionic copolymerization mechanism. The obtained highly cross-linked networks performed well in relation to good impact strengths, high glass transition temperatures, and thermal stability, as such there is a possibility for these materials to be used for industrial applications. The structural evolution during cross-linking was investigated by FTIR spectroscopy. The comparison was done between the initial monomers, the resin mixtures and the resin after curing. The main bands that confirmed the structural evolution of the Epoxy/MHHPA were: 1732 cm^{-1} corresponding to the a strong carbonyl stretch for triglyceride esters, ester stretching vibrations from copolymerization at 1160 cm^{-1} , and the disappearance of the C=O anhydride functionality of MHHPA at 1860 and 1780 cm^{-1} . The Epoxy/BTDA cured resin had similar characteristic band as MHHPA at 1732 cm^{-1} . The biorenewable ratio was increased by over 60% for ELO/MHHPA to 70% for the ELO/BTDA

systems which make these resins good biosourced alternatives. This study also allowed for the deeper understanding of the Epoxy/anhydride mechanism and the relationship between the structure and properties of the resultant resin. The synthesized bioresins were semiductile networks with good impact strength.

Epoxy GY systems crosslinked with Aliphatic and Cycloaliphatic EH polyamine adducts were investigated by Nikolic, et al., (2010). Fast FTIR spectroscopy was used as a method to estimate change in the kinetics of epoxy resin with the polyamine adducts. The crosslinking reactions of the different stoichiometric mixtures of the unmodified GY250 epoxy resin with the aliphatic EH606 and the cycloaliphatic EH637 polyamine adducts were studied. As the crosslinking proceeded, the primary amine groups of the polyamine adduct were converted to secondary and tertiary amines. There was a decrease in the band intensity of epoxy groups at about 915 cm^{-1} , as well as at about 3056 cm^{-1} during the process. The presence of the tertiary amine has a catalytic effect and causes the epoxide group to self-polymerize forming a polyether and the characteristic band at 1175 cm^{-1} for C-N stretching vibrations was seen. Thus the absence of epoxy, the presence of OH and C-N group confirmed the conversion of epoxy group into the corresponding polymer.

2.5. Antiradiation and Antimicrobial Coatings

Nanoparticles (NPs) find application in the surface coatings industry for the purpose of improving gloss, impact resistance, scratch and pencil hardness and antimicrobial properties. When particles have a size $<100\text{ nm}$ they are classified as NPs and the addition of these NPs into the polymer matrix acts as a reinforcement yet without disturbing the transparency and other properties of the coatings. The size of the NPs has a tremendous effect on the antimicrobial property of the coating. The appropriate size can provide a dominant attack on the microorganisms (Shaik, et al., 2015).

The small size of NPs gives them a high surface to volume ratio thus allowing for good interaction with microbes.

2.5.1. Antiradiation Coatings

In developing polymer composites different polymers are mixed with nano-fillers to give radiation attenuation property to the polymer. It is advantageous to use a polymer with aromatic groups on the backbone as aromatic rings give the polymer increased radiation resistance (O'Donnel, 1989). Other functional groups that improves radiation attenuation of polymers include, double or conjugated bonds and heterocyclic fragments (Wozniak, et al., 2017). The different proportions of the polymer and nano-filler give different mass attenuation of radiation.

Ultraviolet (UV) rays, similar to visible light has a wavelength ranging from 100 to 400 nm in the electromagnetic spectrum and can be subdivided into three bands: UVA (315 to 400 nm), UVB (290 to 315 nm) and UVC (100 to 290 nm). UV blockers can be divided between organic (UV absorbers) and inorganic. TiO_2 , ZnO , SiO_2 and Al_2O_3 are semiconductor oxides categorized as inorganic UV blockers. The inorganic UV blockers are preferred in practical applications because of nontoxicity, chemical stability at high temperatures and UV exposure (Yang, et al., 2004).

TiO_2 is a metal oxide (transition) that has found application in developing photocatalysts, semiconductors in solar cells, antimicrobial coatings and for protection of materials against UV radiation (Godnjavec, et al., 2012). It can be found in four mineral forms: rutile, anatase, brookite and TiO_2 (B) (Diez-Pascual ., 2018). TiO_2 has the natural property of UV absorption which can be attributed to this material having a large band gap that exists between its low energy valence band and its high energy conduction band. The band gaps of both rutile and anatase are 3.0 and 3.2 eV corresponding to 413 and 388 nm absorption edges respectively (Yang, et al., 2004). Rutile-form

TiO₂ is more suitable for UV protection because it has a lower photocatalytic activity which destroys the organic surrounding matrix if it is high (Godnjavec et al., 2010). TiO₂ possesses good UV blocking power and is also very advantageous for use in several practical applications as it is nontoxic, chemically stable at high temperature and has permanent stability under UV exposure (Yang, et al., 2004).

The mechanisms of TiO₂ as a UV blocking additive were studied by Yang, et al., (2004). The study was done for both films and fabrics. Only the results for the TiO₂ /binder composites films will be reported here. Four composite films were used for the tests and the transmittance, absorption and reflectance were studied. It was found that within the UV band, all the studied films showed a significant decrease in the transmittance of UV rays as compared to the pure binder, thus TiO₂ improves the films UV-blocking property. In the band of 290 to 350 nm the TiO₂ composite films had a strong absorption similar to the band of 350 to 400 nm yet in this latter band composite films also had strong scattering power which also play a role in reducing transmittance. The excellent UV-blocking power of TiO₂ is attributed to its UV-absorption capacity and some scattering/reflection effects in the long wavelength band of weak UV absorption or there may be no absorption at all. All the TiO₂ composite films had a high forward strong scattering.

Agglomeration of NPs within the binder dispersion is a challenge that is faced during coating formulation. These NPs tend to agglomerate because of the size ratios and this can affect the efficiency of the NPs in the formulation. Coupling agents are utilized in order to address this challenge. The use of trialkoxy silanes is recommended for surface treatment of NPs. The use of the coupling agent aid in achieving a proper dispersion of the NPs within the polymer matrix and also yields a better compatibility between the NPS and the polymeric material (Sabzi, et al., 2009).

Sabzi, et al., (2009) investigated TiO_2 as an additive in a clear polyurethane coat. The surface of the NPs were modified with amino propyl trimethoxy silane (APS) to improve the NPs dispersion and also increase possible interactions between NPs and polymer matrix. The results from this study showed that surface treatment of TiO_2 NPs with APS improved the dispersion, mechanical properties and UV protection of the polyurethane clear coat. A UV-vis spectrophotometer was used to evaluate the absorbance and transmittance of the nanocomposite coatings in the wavelength range of 230-700 nm. The study showed that the increase in TiO_2 NPs (1wt% till 3wt%) lead to a notable increase in the absorption percentage in UV the wavelength region. This observation agrees with literature since TiO_2 NPs inherently have the property of UV absorption and have a higher probability for light scattering. The increase in UV absorption with the increase in TiO_2 NPs make the polyurethane nanocomposite coatings suitable for outdoor weather resistant coatings.

For the purpose of preparing stable dispersions of TiO_2 within a clear coat, different surfactants (polyether modified dimethylpolysiloxane copolymer(Byk 333) and ethylene glycol octanol- 2) and percentage (0.6 to 1 wt%) of TiO_2 were used by Godnjavec et al., (2010) . The prepared samples were studied to determine the photostabilization efficiency of TiO_2 in a clear coat as UV absorber. The NPs were synthesized by the co-precipitation method and the size was found to be 50 nm from TEM analysis. The samples were coated on wood and the colour changes of the painted wood with different UV absorbers was used as an indication of the effectiveness of the coat during artificial weathering. The colour change or discolouration was used to assess wood degradation. The results indicated that the clearcoating with 0.6 and 1 wt% of rutile TiO_2 NPs stabilized by Bry 333 had the best photostabilization performance as a UV protection clearcoat. Another observation was that the UV absorption efficiency did not increase with an increase in the concentration of the NPs and this was assumed to occur as a result of agglomeration.

In a work done by Godnjavec, et al., (2012) surface treatment of TiO_2 with 3-glycidyloxypropyl trimethoxysilane was investigated in order to achieve a high UV absorbing efficiency and improved dispersion within the polymer matrix (acrylic clearcoat). TiO_2 was added at a 0.6 wt% of the coating and the GLYMO: TiO_2 ratios used were 0:1, 0.1:1, 1:1, and 2:1. The samples were placed in a QUV chamber for six weeks and the change in gloss was monitored under accelerated weathering. The change in gloss in accelerated weathering conditions strongly correlate to surface degradation level of the coating. It was observed before placing the samples in the chamber that the addition of GLYMO the gloss 60° of the coating. After placing the samples in the chamber the gloss change after six weeks of exposure was the smallest at a 1:1 ratio of GLMO: TiO_2 .

2.5.2. Antimicrobial coatings

The challenge of bacterial adhesion followed by biofilm formation has led to the use of antimicrobial coatings extensively in different industries. The effects of the aforementioned affect society both in an economic level and also from the health perspective. The coatings thus being formulated usually have the dual function of preventing microbes (bacteria, fungi, algae or virus) from adhering onto surfaces and also killing microbes either before or after coming into contact with surfaces.

It has been known since ancient times that metals can kill or protect against microorganisms. They can potentially inhibit the growth of microbes or destroy them completely thus they can be added into coatings as pigments or as additives. The coatings can be applied onto different substrates imparting the antimicrobial property onto that particular substrate. Metals in the nano size possess high antimicrobial properties. Among the metals silver (Ag), copper (Cu) and zinc (Zn) have been used more extensively. The metals impart antimicrobial properties onto the coating by the release

of the metal ions into the coating which will in turn come into contact with the microbes leading to the destruction of the microbes. The release of the ions and the influence on the rate of release are parameters that can decrease or increase the antimicrobial effect. Each metal has a specific antimicrobial property which is dependant on the microbe (Mahltig, 2018).

Ag has been found to be more advantageous because of low human toxicity and high wash fastness properties. The effectiveness of Ag⁺ has been found against the following bacteria: *Pseudomonas aeruginosa*, *Escherichia coli*, *Staphylococcus aureus* and *Staphylococcus epidermidis*. The Ag⁺ ions interfere with the bacterial cellular metabolism and membrane permeability while also contributing to the formation of reactive oxygen species that damage the cells of the bacteria (Singh, et al., 2018). A paper written by Fakhruddin, et al., (2020) stated that the bacterial effect of AgNPs were highest when the particle size range was 1-10 nm because of the highly reactive surface interactions. AgNPs have the ability to kill both gram-negative and gram-positive pathogens, and the multifaceted antimicrobial mechanism of Ag increases its effectiveness as it is difficult for bacteria to develop resistance against it (Vasilev, 2019; Swaminathan & Sharma, 2018). Swaminathan & Sharma, (2018) reported findings from an unpublished work that the bacterial effect of AgNPs decreased as the size of the of the NPs increased and the shape of the particles also had an effect on the antimicrobial properties. Further discussion brought into light the fact that although in most studies spherical particles were utilized, actually truncated triangular shaped particles are reported to have a greater bactericidal effect compared to spherical and rod-shaped. Modified AgNPs shows the highest growth inhibitors towards microbes. AgTiO₂ as a modified metal oxide have effect on both Gram-positive and Gram-negative bacteria (Swaminathan & Sharma, 2018).

Ag based antimicrobial coatings are also available in the market. *SilverSan* from PPG, is a formulation that incorporates Ag into epoxy, polyester, or hybrid powder coatings. The paint formulations are said to function via a slow release of the Ag⁺ ions through an ion exchange mechanism in the presence of atmospheric moisture, allowing interaction with Na⁺ within the microbes resulting in neutralization. Agion technologies have also produced an Ag⁺ based antimicrobial coating, *Alista* powder coating where in the Ag is bonded to a biocompatible zeolite. The mechanism of the interaction of Ag⁺ ions with the microbes is through the release of Ag⁺ from an inorganic aluminosilicate in a unique absorption and exchange mechanism. The coating is able to have prolonged functionality to protect against microbes because atmospheric moisture facilitates the slow release of the Ag⁺ ions. Other available coatings include the *Microban* antimicrobial coatings. The Microban technology is a Sherwin-Williams and Lintech partnership. The formulation involves the use of polyvinylidene difluoride coating as a matrix and the Ag is incorporated into this matrix as the active ingredient. The Ag⁺ NPs when coming into contact with the microbes attack the cell wall and membrane of the microbe thus disrupting the metabolism thus killing the microbe. The presence of the Ag⁺ NPs also inhibit the reproduction of the microbes by interfering the conversion of nutrients into energy (Tiwari & Chaturvedi, 2018).

The antimicrobial activity of AgNPs was investigated against *E.coli* by Sondi & Salopek-Sondi, (2004) as a model for Gram-negative bacteria. The tests were performed in a Luria-Bertani (LB) medium on solid agar plates and on a liquid system which was supplemented with varying concentrations of AgNPs. The size of the AgNPs were verified with TEM to be 12 nm. At a bacterial colony of 10⁵ CFU applied on the plates, the bacterial inhibition was 70% when the concentration of AgNPs was 10 μg cm⁻³. At a concentration of 20 μg cm⁻³ the colonies were reduced significantly and only seen at the edges of the plates while a concentration of 50-60

μgcm^{-3} , had a 100% reduction of colonies. The AgNPs on LB plates could inhibit the growth of *E.coli* (concentration dependant as well as colony) while the AgNPs in liquid medium only caused a delay in the growth of *E.coli* even when the NPs concentration was high. The gradual reduction in concentration of NPs caused growth of bacterial cells to resume.

Kim, et al., (2007) investigated the antimicrobial activity of Ag nanoparticles against yeast, *Escherichia coli*, and *Staphylococcus aureus*. The size of the AgNPs were 13.5 nm and varying concentrations of AgNPs were supplemented into the liquid systems and Agar Muller Hinton plates were used. It was observed that at low concentrations of AgNPs yeast and *E.coli* were inhibited while the inhibition for *S. aureus* was mild. These results were associated with the difference in the characteristics of bacteria in relation to the membrane structure and thus made the point that the mildness of inhibition of AgNPs against *S. aureus* could be associated to the difference in the membrane structure.

In a study by Zielecka, et al., (2011) a silicone acrylic architectural paint and impregnates were incorporated with silica nanospheres containing immobilized silver or copper nanoparticles to impart antimicrobial and antifungi properties. These nano fillers were tested against *Escherichia coli*, *Staphylococcus aureus* as well as *Aspergillus niger*, *Paecilomyces varioti*, *Penicillium funiculosum*, *Chaetomium globosum*. The results were compared with pure silver nanospheres and it was found that this new group of nanofillers is more effective.

Gram-negative bacteria (*Shigella sp.*, *Escherichia coli*, *Pseudomonas areuginosa* and *Klebsiella sp.*) and Gram-positive bacteria (*Streptococcus sp.*, *Bacillus sp.*, *Staphylococcus sp.*) including one fungus *Candida sp* were tested against AgNPs that were biosynthesized by *Rhodotorula sp.* Strain ATL72. The size of the NPs were found to be 8.8 to 21.4 nm, and were found to be effective

against the aforementioned microbes. It was confirmed that the shape of the AgNPs has a substantial effect on the antimicrobial properties of the particles. The shape of NPs were monitored (spherical, rod-like and triangular) and it was found that the triangular-shaped nanoparticles were the most effective (Soliman, et al., 2018).

The research performed by Bechtold, et al., (2020) evaluated the biocidal effect of Ag NPs on a water soluble polyurethane paint composition. The paint formulations were tested against two bacteria: *Escherichia coli* and *Staphylococcus aureus* and two fungi strains: *Aspergillus niger* and *Penicillium funiculosum*. The size of the synthesized NPs were predominantly 40 nm. From the results, the effectiveness of the Ag NPs was confirmed at all the concentrations that were tested. The standard method used considers that a tested sample must have an antimicrobial activity ≥ 2 to be considered effective. The antimicrobial activity of *Staphylococcus aureus* was found to be very close to 2 thus showing that the concentration of Ag NPs is close to the minimum inhibitory concentration. For the fungi, the results showed that the concentration of the Ag NPs were not sufficient to inhibit fungi growth. The conclusion was drawn based on literature which shows that Ag NPs are effective towards the tested fungi strains thus the results were attributed to the insufficient concentration of the Ag NPs within the coating film.

Titanium dioxide (TiO_2) nanoparticles possess antimicrobial properties against a variety of microorganisms. These NPs have attracted attention because of their less volatile nature (Shaik, et al., 2015). Bacteria that has been found to be susceptible to TiO_2 include: *Lactobacillus acidophillus* and *E.coli*. The TiO_2 mechanism for antibacterial activity involves firstly damage to the cell wall and then membrane disorganization. The disorder in the cell membrane is caused by the accumulation of the NPs on the membrane and while the internal accumulation leads to the

death of the cell. TiO_2 NPs have a vast number of applications which include: paint, UV protection, electrochromics, and photocatalysis (Diez-Pascual, 2018).

Shaik, et al., (2015) synthesized a castor oil based coating (CPEA) using terephthalic acid and then further modified by toluene-2,4-diisocyanate to obtain the poly(urethane-esteramide) nanocomposite. TiO_2 was added with a varied concentration of 0.1 till 0.5 wt%. The tested microorganisms tested include three bacteria (*Staphylococcus aureus*, *Escherichia coli*, and *Bacillus Pasteurii*) and three fungal strains (*Furasium Solani*, *Penicillium notatum*, and *Aspergillus niger*). For the antimicrobial test only UCPEA-13 sample was tested for antimicrobial effect based on the disk-diffusion method. The sample that contained 0.4 wt% was chosen because at this concentration there was good dispersion within the polymer matrix. After the test the zones of inhibition for the bacterial strains were as follows: *Staphylococcus aureus* (14 mm), *Escherichia coli* (25 mm), and *Bacillus Pasteurii* (16 mm). For the antifungal effect, the inhibition zones for UCPEA-13 were as follows: *Furasium Solani* (26mm), *Penicillium notatum* (24mm), and *Aspergillus niger* (21mm). These results showed that the UCPEA coatings exhibit good antimicrobial properties.

Diez-Pascual , (2018) prepared and characterized a novel acrylated epoxidized linseed oil (AELO) based biocomposites. The biocomposites were reinforced with anatase TiO_2 nanoparticles to be used as coatings with antimicrobial properties. Two tests were performed to evaluate the antimicrobial properties of the biocomposites. The first one was according to the ISO 22, 196:2007 standard, and in accordance to this standard the tested samples must have a value higher than 2 to be considered to have antibacterial effectiveness and these tests were done both under UV light (365 nm) and dark conditions. The second test was the agar diffusion test. Four nanocomposites

were prepared with varying concentrations of TiO_2 : 1.0, 2.5, 5.0, and 7.5 wt%. The size of the NPs was 40 nm. The coatings were tested against Gram-negative bacteria *E.coli* and Gram-positive bacteria *S.aureus*. Under both the tested conditions (light and dark conditions), it was observed that the antimicrobial action improved with an increasing content of NPs that were in contact with the bacterial membranes. It was observed that the better the dispersion of the NPs within the polymer matrix the higher the bacterial action and this observation explains the reasons why the nanocomposite with 7.5 wt% and 5.0 wt% NPs had a similar activity. The growth of *E.coli* was restrained when TiO_2 loading was ≥ 5.0 wt% while at NPs loading of ≥ 2.5 wt% the growth of *S.aureus* was held back. These variances in growth inhibition were connected to the structural and chemical differences in the cell surfaces of the bacteria. The outer membrane of Gram-negative bacteria offers resistance to a number of substances including small hydrophilic molecules thus reducing the harm that can be caused by ROS generated by the NPs. Based on the agar diffusion test it was found that at 2.5 wt% NPs content growth inhibition of both *E.coli* (13.9 mm) and *S.aureus* (16.0 mm) was observed. At the highest loading of 7.5 wt% the growth inhibition was 18.6 mm (*E.coli*) and 20.3 mm (*S.aureus*).

Chapter 3: Methodology

3.1. Materials

Cold pressed castor oil was obtained locally from SSD (Selokong Sa Dimelana) Pty (Ltd); 30% Hydrogen Peroxide (H_2O_2), Diethyl Ether, and Lipase B Candida Antarctica immobilized on Immobead 150, recombinant from *Aspergillus Oryzae* (CALB), TDI, MDI, HMDI, Phthalic anhydride (ReagentPlus, 99%) [PA; molecular weight (MW) = 148.12 g/mol, melting point = 131-134°C, boiling point = 284 °C, vapor pressure: < 0.01 mmHg (20 °C), assay : 99%] and 4,4'- Diaminodiphenylmethane \geq 97.0% (GC) [DDM; melting point = 88-92 °C, freezing point = 230 °C] were supplied by Sigma Aldrich, South Africa

3.2. Chemo-enzymatic Epoxidation reaction

Figure 8 below is the schematic representation of the epoxidation reaction of castor oil using CALB as a catalyst.

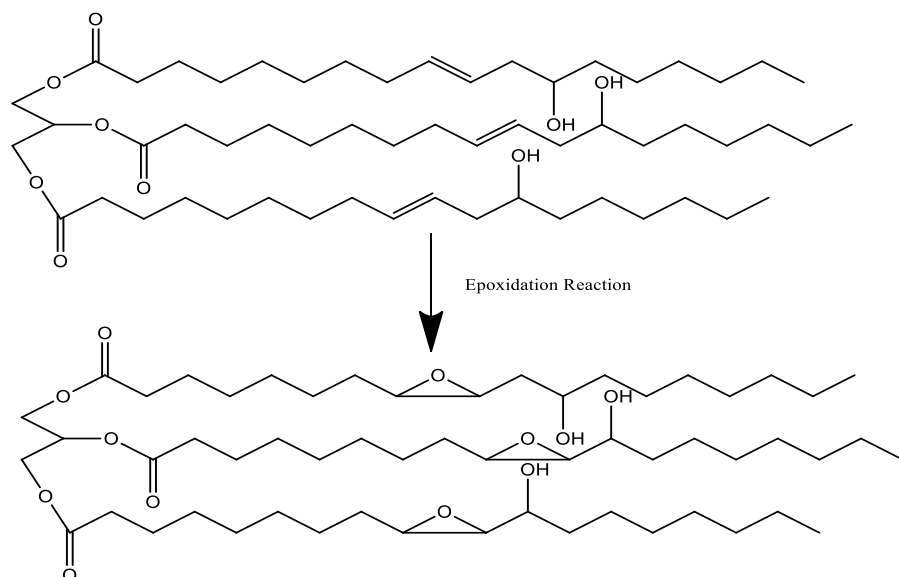


Figure 8: Chemo-enzymatic epoxidation of castor oil with CALB as a catalyst

Epoxidation of castor oil (Chemo enzymatic epoxidation) reaction specifics:

- a) The reaction was carried out in a 250 ml three necked round bottom flask reactor placed in a water bath on top of a magnetic stirring hotplate
- b) The reactor was fed with 50 g of castor oil with 2 g of CALB and stirred with a speed of 400 rpm with a magnetic stirrer
- c) 52 g of H_2O_2 was added stepwise using a dropping funnel within 20 min
- d) The reaction was carried out for 32 hrs at 35 °C
- e) After the reaction was complete the reaction mixture was allowed to cool and then placed in a separating funnel
- f) The organic layer (top part) was removed by the addition of 100 ml of diethyl ether and any excess moisture was removed by the addition of magnesium sulphate.
- g) Then concentrated under low pressure in a rotary evaporator

Figure 58 in appendix C is the picture for the epoxidation reaction set-up.

3.2. Ring opening reaction

The ring opening reaction was carried out using water in the presence of perchloric acid ($HClO_4$)

The mass ratio of the reactants was 1:18:0.2 (Epoxidized castor oil: H_2O : $HClO_4$). Figure 9 is the schematic representation of the reaction and Figure 59 in appendix C is a picture of the ring opening reaction set-up.

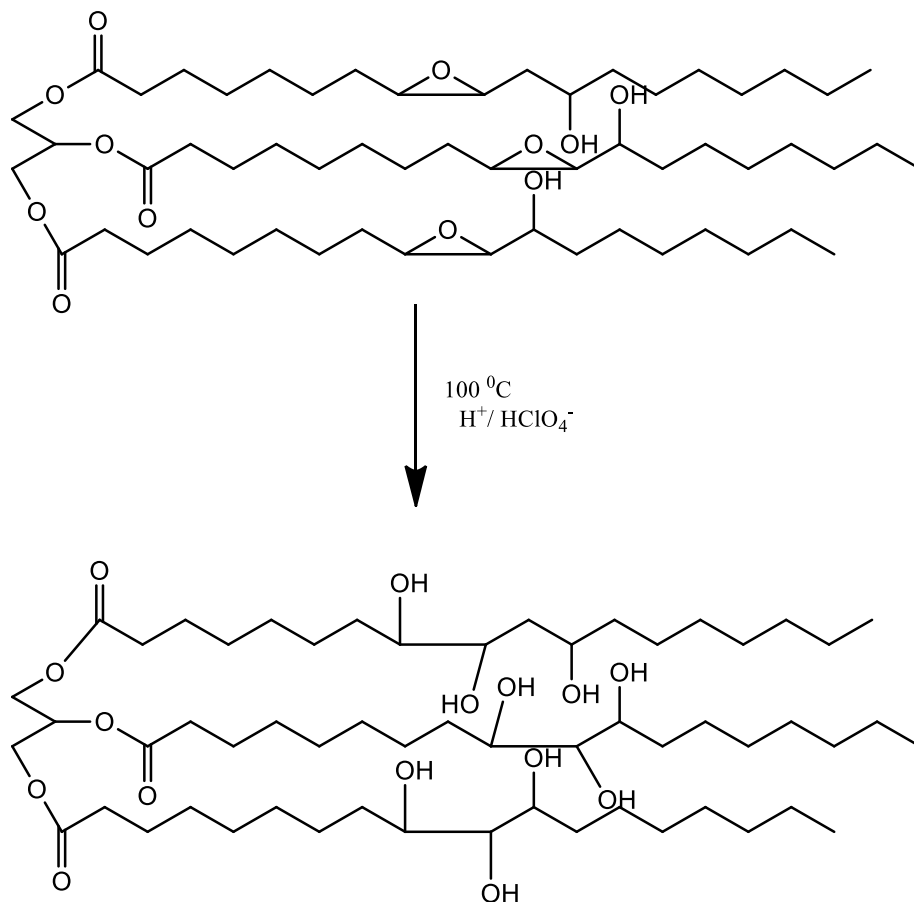


Figure 9: Schematic representation of ring opening reaction with H_2O

The procedure is detailed as follows:

- a) An oil bath was heated to a temperature of $100\text{ }^{\circ}\text{C}$
- b) Then 100g of epoxidized castor oil (ECO) and 1800 ml of water was added to the 1000 ml flask and allowed to heat up to the same temperature as the oil bath.
- c) After a temperature equilibrium was reached within the flask, 20 g of HClO_4 was added dropwise using a dropping funnel
- d) The reaction was allowed to continue for 48h
- e) After the reaction was complete, it was allowed to cool to room temperature, the aqueous phase (H_2O) was then separated from the organic phase (ring opened castor oil)

f) The product was then placed in an air tight container for characterization and further application

3.3. Dehydration reaction

Figure 10 below is a representation of successive reactions done to obtain a drying oil.

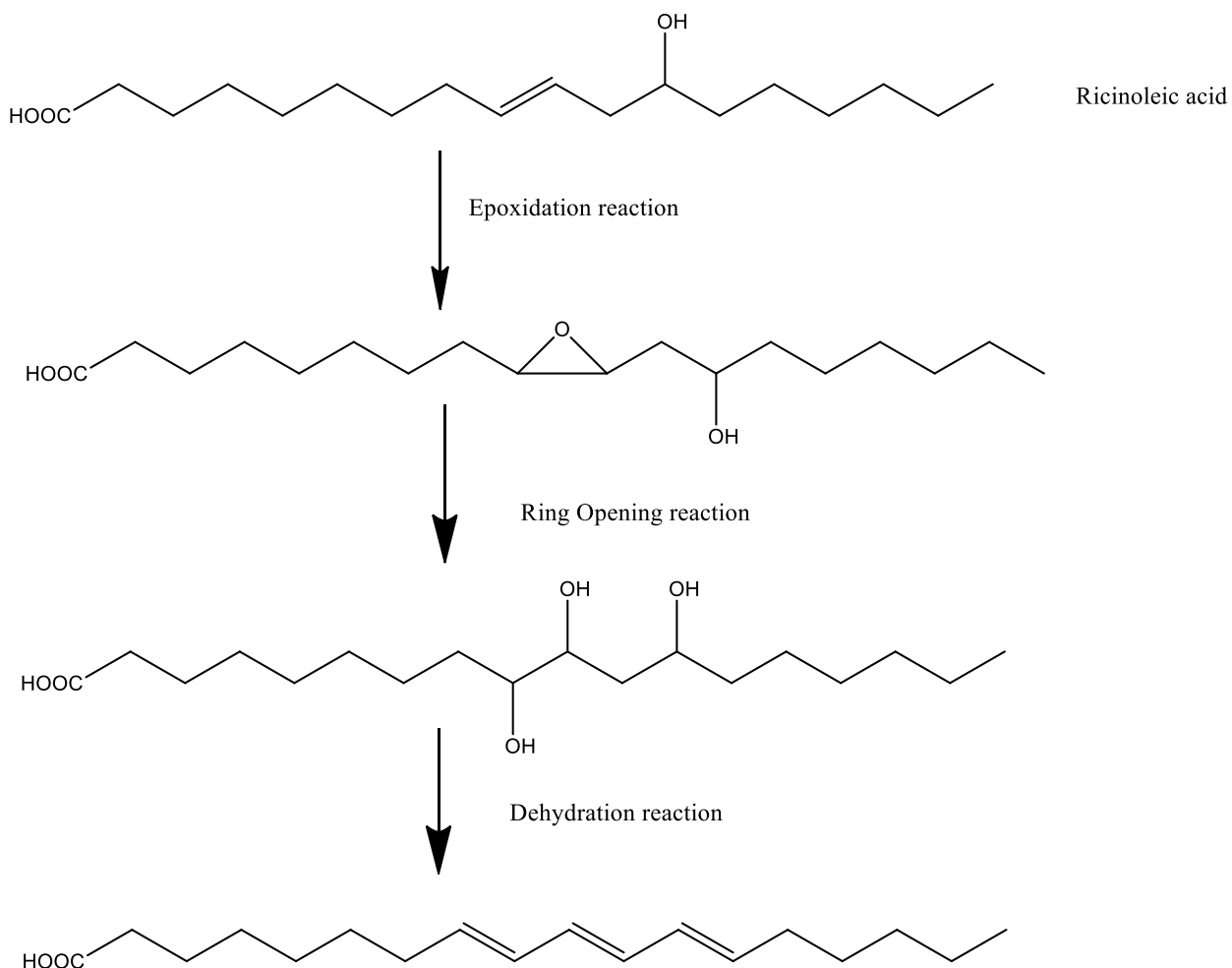


Figure 10: Successive reactions to obtain a drying oil

The procedure below outlines how the dehydration reaction was carried out:

- a) The reaction was carried out in a round bottom flask reactor

- b) 50 g of ring opened castor oil was added into the flask and heated up to a temperature the desired temperature while connected to a vacuum pump
- c) The vacuum was disconnected very fast and 0.1 g of NaHSO₄ was added very fast
- d) The vacuum was restored and temperature maintained for 30 min
- e) After this the vacuum was disconnected again and 1.0340 g of CaO was added
- f) Then heating was stopped, vacuum reconnected and oil left to cool to room temperature
- g) The drying oil was stored in an air tight container for characterization and paint application/synthesis

3.4. Polyurethane synthesis

Figure 11 is a representation of the poly-addition reaction with the reaction conditions and Figure 60 in appendix C is a picture of the polyurethane synthesis reaction set-up.

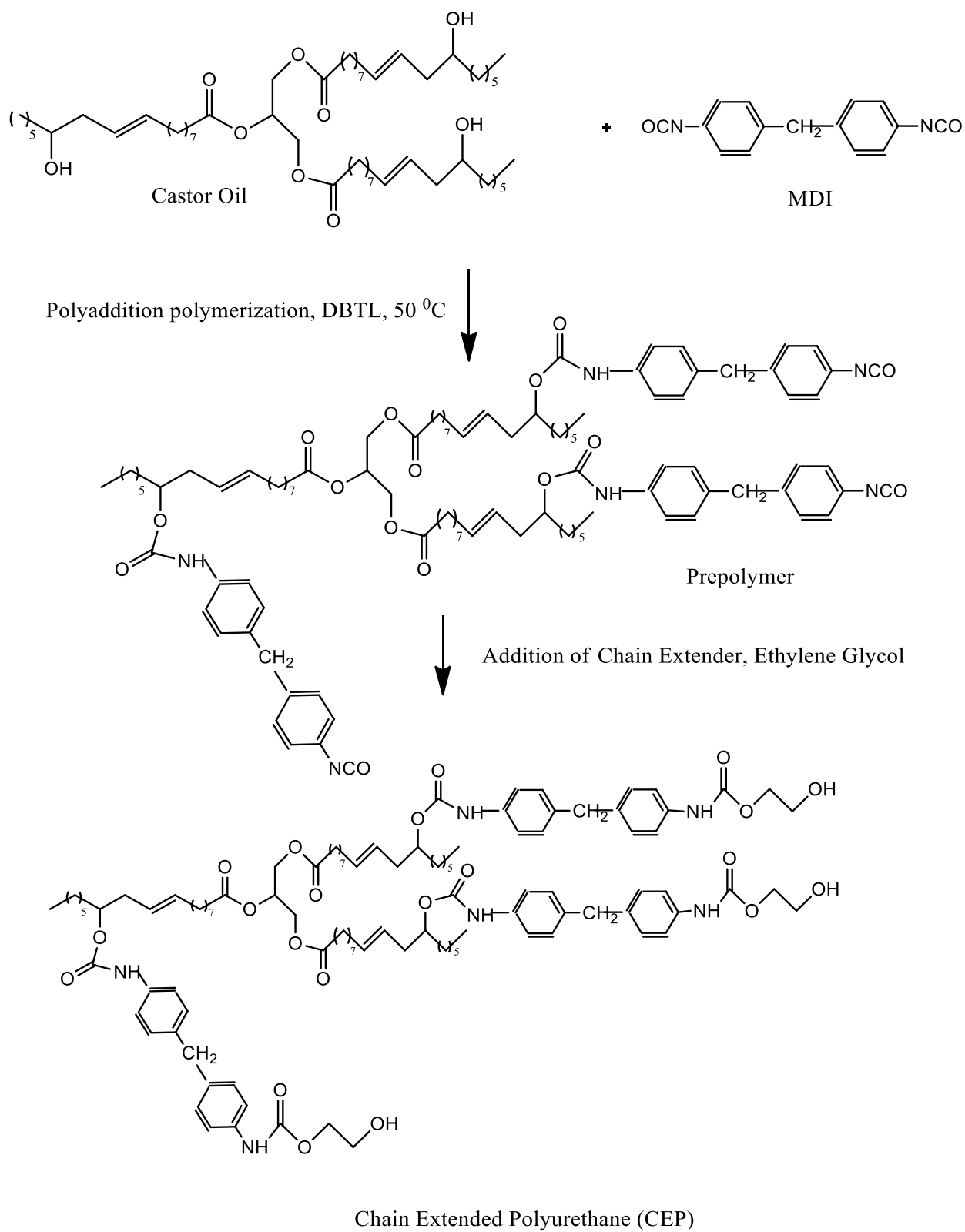


Figure 11: Synthesis of chain extended CO polyurethanes

Figure 12 is a further illustration of the polyurethane synthesis when ring-opened castor oil (RCO) is used, which affect the rate of crosslinking thus directly affecting the paint drying time and mechanical properties of the resultant film.

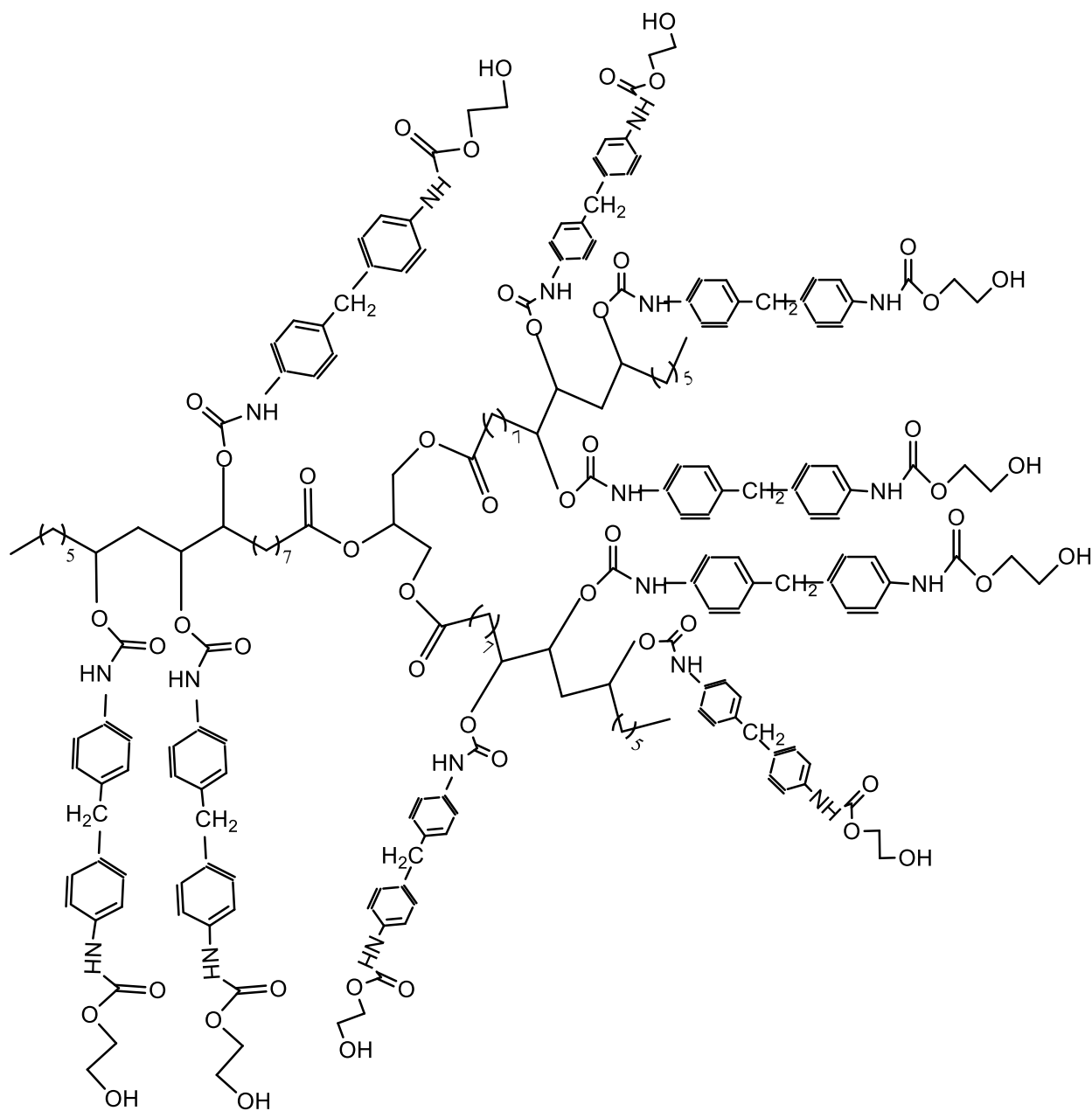


Figure 12: Synthesis of RCO chain extended polyurethanes

Table 7 details the characteristics of MDI as the isocyanate of choice for this study

Table 7: Physical and Chemical properties of pure MDI

Physical and Chemical properties of pure MDI	
Form	White Solid
Molecular weight, g/mol	250.25
Functionality, -NCO groups/mol	2
Boiling point, °C	200

For the synthesis of the polyurethane, castor oil or modified castor oil polyol and isocyanate will undergo a poly-addition polymerization with methyl ethyl ketone as solvent as detailed below:

- a) The reaction was carried out in a one-necked flask reactor and equipped with a mechanical stirrer
- b) The reactor was heated in a water bath at a temperature of 50 °C
- c) Modified castor oil/ castor oil and DBTDL were added into the reactor, stirred continuously at maximum speed.
- d) After reaching temperature equilibrium then a calculated amount of MDI was added into the reactor and the reaction was left to continue for 1 hour
- e) The reaction in which the chain extender was used after 1 hour of reaction; a calculated amount of ethylene glycol was added and reaction left to continue for another 1 hour under vigorous stirring

- f) After the reaction was completed the mixture was poured into an air tight container
- g) The ratio of isocyanate to castor oil was varied from 0.6 to 1.2.

Table 8 give the proportions that were used in the synthesis of the polyurethane coatings.

Table 8: Proportions for the synthesis of polyurethane coatings

Amount of castor oil (g)	Amount of Isocyanate (g)	Amount of solvent (MEK) (ml)	Amount of chain extender (Ethylene glycol) (wt%)	Amount of catalyst (%)
10	4	30	10	0.05
10	2.4	15	No extender	0.05
10	3.2	15	No extender	0.05
10	4.85	30	10	0.05

For the synthesis of the polyurethanes based on RCO the ratio was varied from 0.1 till 1.2. A chain extender was added at 1wt% of the RCO.

3.5. Epoxy Synthesis

The ECO was cured with phthalic anhydride (PA) and 4,4'- diaminodiphenyl methane (DDM) to obtain epoxy resins.

Epoxy resin synthesis:

- a) The reaction was carried out in a glass flask that has a magnetic stirrer
- b) PA/DDM (0.05, 0.075 or 0.10 mol) and castor oil (0.05 mol) was placed in the flask
- c) The glass flask was placed in a water bath at the desired temperature 155 °C for PA and a temperature of 90 °C for DDM
- d) The mixture was mixed thoroughly by a magnetic stirrer at a speed of 500 rpm

e) The reaction time was 30 min

Table 9 and 10 show the physical and chemical properties of PA/DDM and the proportions in which the monomers were added to synthesize the epoxy resins.

Table 9: Physical and Chemical properties of PA/DDM

Physical and Chemical properties of monomer	PA	DDM
Form	Solid	Solid
Molecular weight, g/mol	148,2	198,26
Melting point, °C	131	88-92

Table 10: Proportions for the Epoxy resin synthesis

Molar ratio of ECO/(PA/DDM)	Amount of ECO (mol)	Amount of PA/DDM	Solvent amount (ml) (MEK)- control viscosity and flow properties after reaction
1:1	0.05	0.05	10
1:1.5	0.05	0.075	10
1:2	0.05	0.1	10

Figure 13 and 14 shows the crosslinking of the epoxy monomer with PA and DDM respectively.

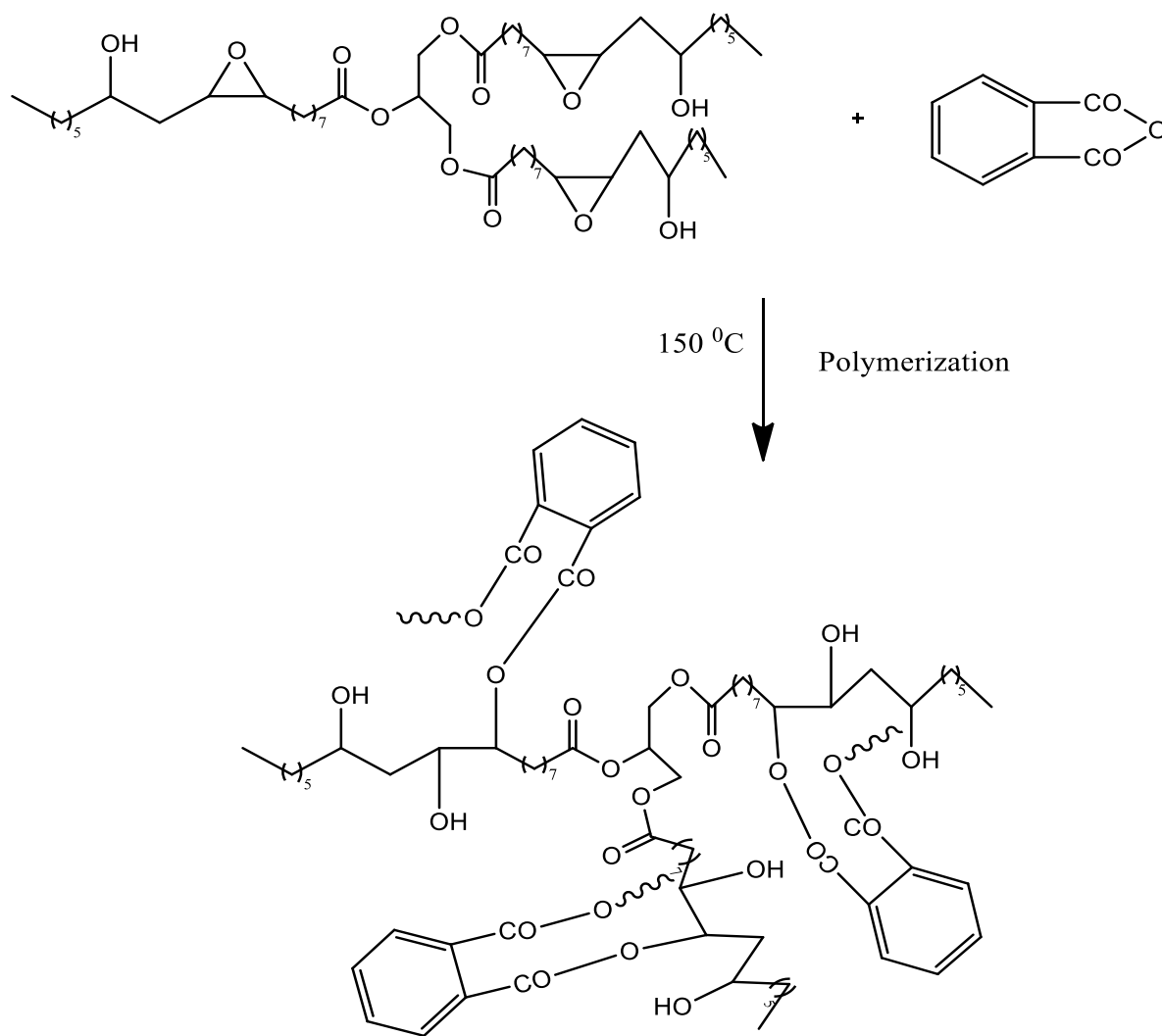


Figure 13: Crosslinking mechanism of PA and Epoxy resin

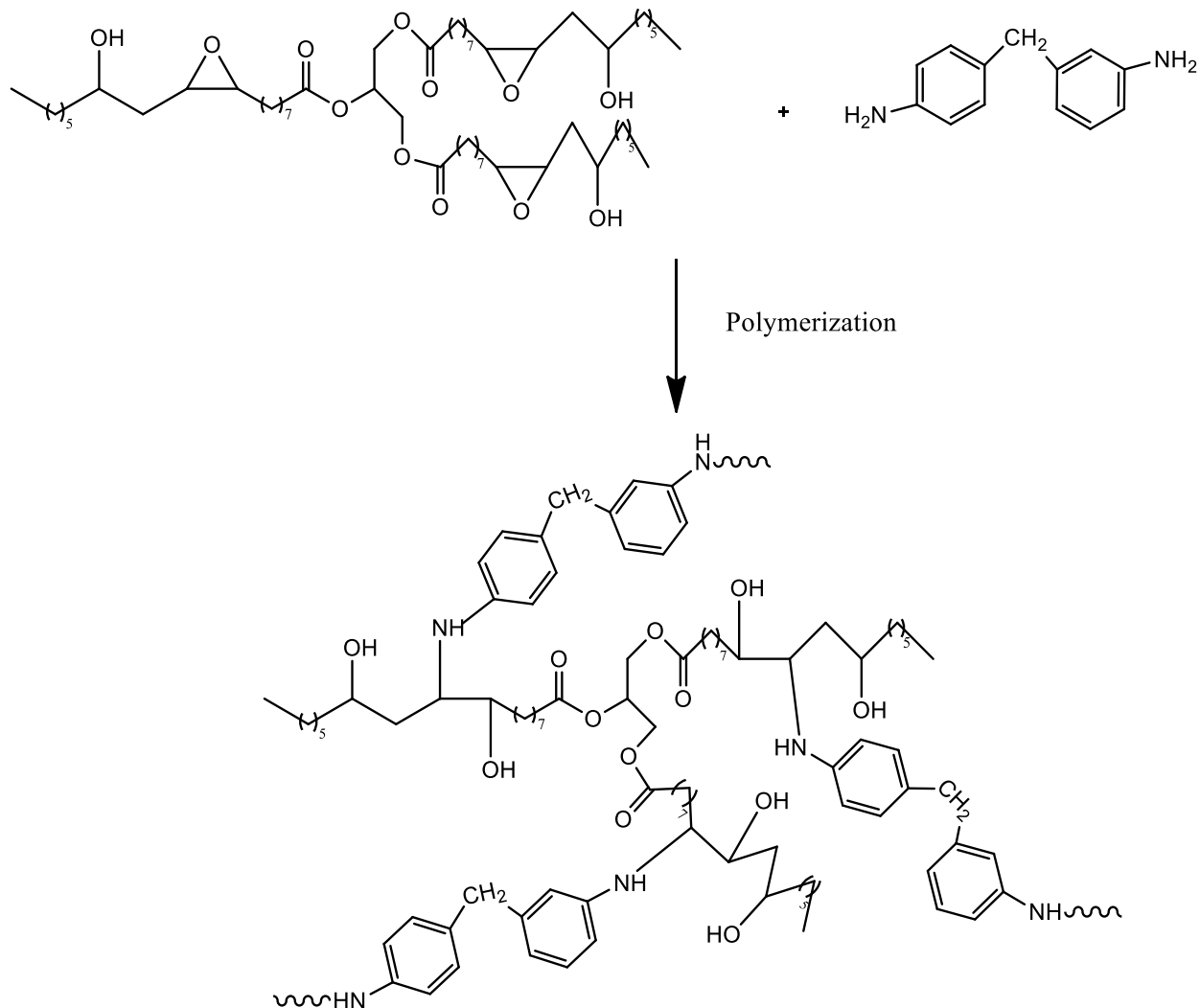


Figure 14: Crosslinking mechanism of DDM with Epoxy resin

3.6. Addition of nanoparticles for Antiradiation and Antimicrobial

The NP will be dissolved in MEK and mixed with the drying oil, polyurethane and epoxy resin in a glass cylinder. The nano-filler that was incorporated for anti-radiation properties TiO_2 , and for the antimicrobial properties the nano-filler include TiO_2 and Ag . The paints will be applied on appropriate surfaces to test for antimicrobial and anti-radiation properties. The NP were mixed with the paint through sonication.

3.7. Characterization Technique of resins

3.7.1. Spectroscopic analysis

With the spectroscopic methods electromagnetic radiation interacts with matter and based on the changes or response from the molecules one is able to identify the functional groups and the position of the functional groups.

3.7.1.1. Fourier Transform Infrared Spectroscopy (FTIR)

FTIR was used as a qualitative analysis to identify the presence of functional groups in synthesised polyols (OH groups), PU's (urethane linkage), epoxy resins (epoxy ring) and DO (the double bonds). The absorption peaks on the spectrum gave information on the molecular composition, molecular configuration and functional groups. Figure 61 in appendix C is a picture of the FTIR equipment that was used.

3.7.1.2. Magnetic Nuclear Resonance ($^1\text{H NMR}$)

$^1\text{H NMR}$ allows for the determination of the molecular structures of samples. This method was used for quantitative evaluation of samples. It was possible to identify the functional groups by assigning to which functional group they belong. $^1\text{H NMR}$ spectra were recorded using an Avance DRX 400 (Bruker, Germany) device at room temperature with CDCl_3 as solvent and tetramethylsilane (TMS) as internal standard. Figure 62 in appendix C is a picture of the equipment for the AvanceDRX device for $^1\text{H NMR}$ analysis.

3.7.2. Rheology Studies

This physical property of paints plays an important role in the flow properties of coatings. This the internal friction within the molecules that constitute the film forming agent or other monomers

present as part of the coating (polymer solution). Viscosity is measured by actually measuring the shear stress at a specified shear rate. The viscosity profile was measured using a RheolabQC SN897839; FW1.31 rheometer, at 20 °C and shear rate of 1-500 1/s.

3.7.3. Tests for the anti-radiation and antimicrobial properties

The test for the antimicrobial property of the paint was done according to the Disk-diffusion test (Kirby-Bauer test). The bacteria that were evaluated are: *Escherichia coli*, *Pseudomonas aeruginosa*, *Staphylococcus aureus* and *Streptococcus sp.* A standardized bacterial isolate was spread on an agar plate the paper disks containing the paint were placed and incubated at 37 °C for 24 hours. The zone of inhibition was measured using a ruler (mm) for the different samples and results read from the Kirby-Bauer chart.

For anti-radiation testing a UV irradiation box was fitted with UV lamps used to expose paint samples to UV radiation. The paint was placed on microscopic slides and placed inside the box for timed intervals.

Chapter 4: Results and discussion

4.1. Material synthesis

The section serves as a description of the synthesis of epoxidized castor oil (ECO), ring opened castor oil (RCO), dehydrated castor oil/ drying oil (DCO), polyurethanes and epoxy resins. Castor oil is a non-drying oil, thus for application in coatings there is a need to functionalize to confer the property of drying and thus forming a film when applied to a substrate. The chemical processes described serve this purpose. The main functional groups within castor oil that were of interest for modification include the C=C and OH group. Epoxidation modified the C=C double bonds into an epoxy for further application in polyol synthesis through ring opening and also epoxy resin synthesis. The OH group allowed for, dehydration and polyurethane synthesis.

4.1.1. Epoxidation reaction

Epoxidation involves the addition of oxygen into double bonds thus forming an oxirane ring, and this reaction is used to functionalise C=C within castor oil. The functionality of castor oil with the reactivity was increased by chemo-enzymatic epoxidation as a more environmentally friendly approach compared to the conventional Prilezhaev epoxidation process. The Prilezhaev process uses a strong acid as a catalyst (sulphuric acid) which not only catalyses the epoxidation but also the ring opening reaction as a result decreasing the conversion of C=C to an oxirane ring. To establish the optimum conditions for the chemo-enzymatic epoxidation of castor oil, three variables were investigated which include; temperature, reaction time and catalyst amount. The variables mentioned were investigated in the following ranges respectively: 30-55 °C, 12-32 hrs and 1-5 wt%. Figure 15 shows the ECO which has a lighter colour as compared to the castor oil (CO), as it can be seen in the contrasting pictures.



Figure 15: Picture of the CO (left) and synthesized ECO (right)

4.1.2. Ring opening

ECO (~ 3 epoxide groups per triglyceride) obtained from the laboratory after the epoxidation reaction described was used to synthesize a polyol. This method is simple and inexpensive and can increase the castor oil hydroxyl functionality to 9 OH/mol of oil.

The reaction was carried out in a 1000ml three necked flask, fitted with a reflux condenser, dropping funnel and thermometer. The mass ratio of the reactants was 1:18:0.2 (castor oil: H_2O : $HClO_4$). A calculated amount of castor oil was added together with H_2O into the flask and the contents were allowed to heat up to a temperature of 100 °C and then $HClO_4$ was added dropwise in 10 min. Samples were withdrawn from the flask after 12, 18, 24, 30, 36 and 48 hrs. The amount of $HClO_4$ was also varied from 1:0.1 till 1:0.3 (ECO: $HClO_4$). Reaction progress was followed by analysing the samples with FTIR. Figure 16 shows a sample of RCO in contrast with ECO.

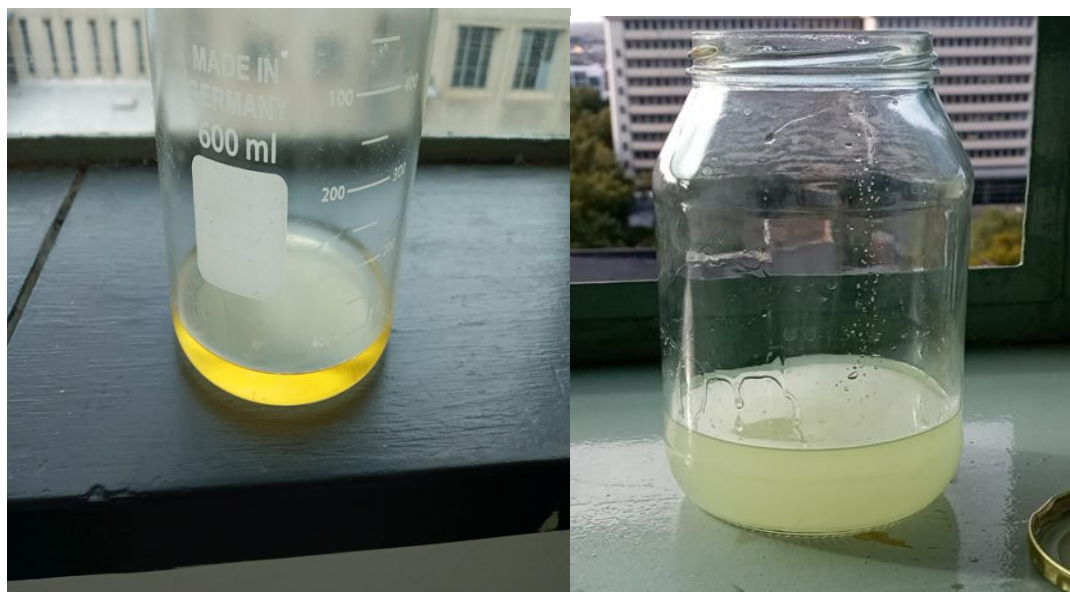


Figure 16: A picture of RCO (left) and ECO (right)

4.1.3. Dehydration reaction

Dehydration of CO and RCO was carried out with NaHSO_4 in the presence of concentrated H_2SO_4 under vacuum. Under these conditions of dehydration, the hydroxyl group and adjacent hydrogen atom from the C-11 or C-13 position of the ricinoleic acid portion of the molecule is removed as water. The parameters that were investigated are temperature and the reaction time. The temperature was varied from 180 till 240 °C and the reaction time was varied from 30 min till 120 min. After the study it was concluded that the optimum conditions were: 240°C temperature, 0.11 g catalyst amount and 120 min reaction time as confirmed by FTIR and ^1H NMR. Figure 17 shows selective samples of the drying oil (DO) obtained after the reaction in comparison with the RCO.



Figure 17: A picture of DCO (left) and RCO (right)

4.1.4. Polyurethane synthesis

Polyurethane synthesis was done using castor oil before any modification and also by using RCO castor oil with a higher functionality (OH value). MDI was used in the synthesis as the second monomer and DBTL was used as a catalyst. The NCO/OH ratio was varied between 0.6 and 1.2. During the synthesis, ethylene glycol was added as a chain extender and it also served to terminate the reaction after 1 hour of reaction time by inactivating the NCO group remaining in the polyurethane. The reaction was carried out at a temperature of 50°C. FTIR and ^1H NMR and rheology studies were used to characterize the synthesized polyurethanes and confirm the synthesis of the polyurethane. The paint formulation included the addition of resin, thinner, solvent and drying agent. In a second formulation, a 2k fast catalyst was added to further enhance the drying properties of the paint produced with castor oil as the polyol. The 2k catalyst was added

during application of the paint by thoroughly stirring and mixing in a proportion of 2 parts base (clear coat) to 1-part catalyst by volume. The paint was allowed to dry under atmospheric conditions.

The polyurethanes obtained ranged from a light yellow to cream white appearance as illustrated by the pictures in Figure 18. The samples on the left are representative samples obtained when castor oil was used and the samples on the right are representative of the polyurethanes obtained from ring opened castor oil.



Figure 18: Representative samples of the PUs obtained from CO and RCO (left to right respectively)

4.1.5. Epoxy synthesis

Curing with anhydride was done at elevated temperatures. The resulting resins have the advantage of having high tensile strength and thermal stability. ECO is a yellow viscous liquid at room temperature and PA was obtained in a solid form with a melting point of 131 °C. To obtain a homogenous mixture of the two reactants, the reaction was performed at a temperature of 150 °C for reaction with PA and 100 °C for the reaction with DDM. DDM is a tertiary amine and functions as a catalytic hardener during epoxy synthesis. A multiple number of reactions occur during the epoxy synthesis using anhydride as a hardener as depicted by Figure 19. This figure shows detailed a detailed representation of how the epoxy resin is synthesized with PA.

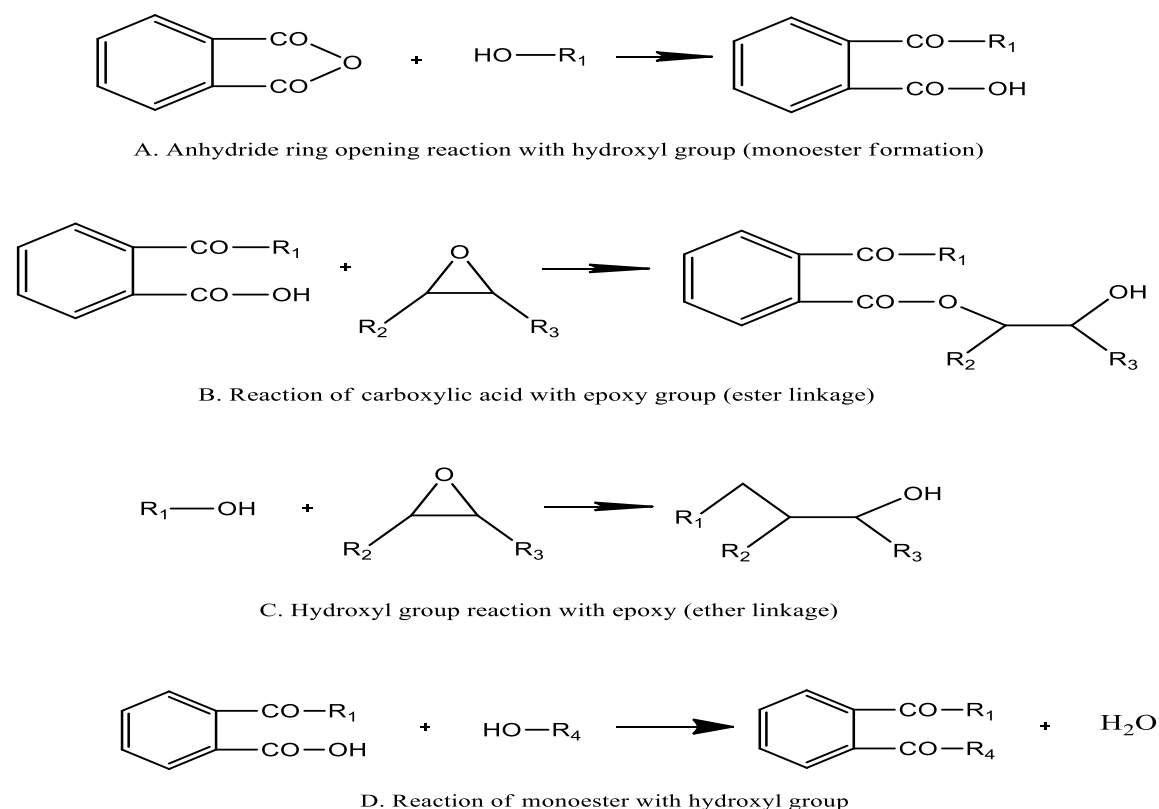


Figure 19: Curing process with phthalic anhydride hardener (Gibson, 2017)

As depicted in Figure 19, during the epoxy curing with PA hardener the first reaction that occurs is the ring opening of the PA, forming a monoester. In practical applications, reaction B and D are the most important successive reactions after the formation of the monoester.

Figure 20 shows pictures of the synthesized epoxy resin (ER) of both PA and DDM cured coatings respectively.

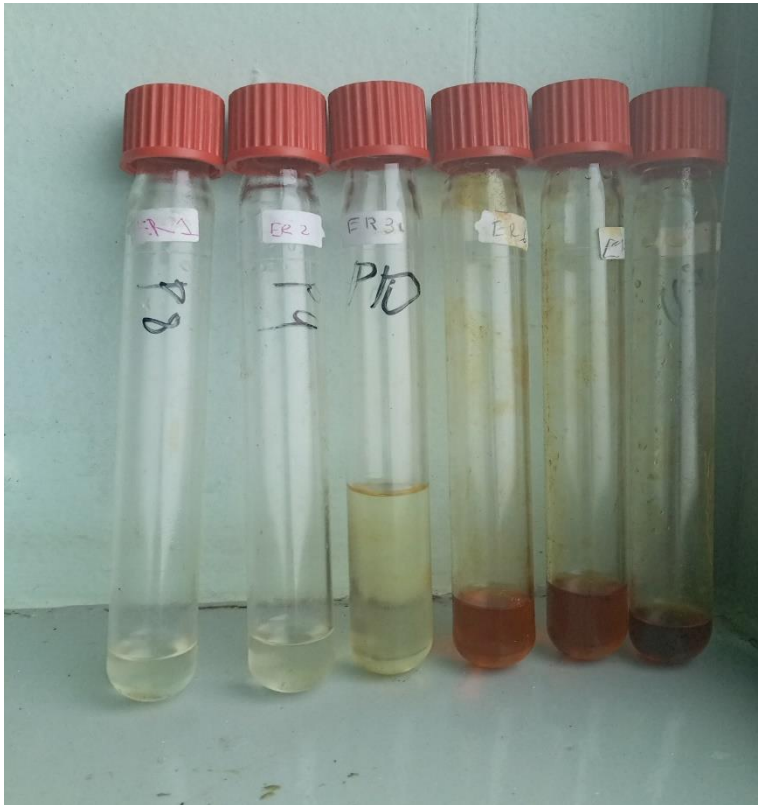


Figure 20: Pictures of the synthesized epoxy resins of both PA (left-first 3 samples) and DDM (right- last three samples) cured coatings.

4.2. FTIR Analysis

After the synthesis of the materials, FTIR was used as a qualitative characterisation to confirm the successful occurrence of the various reactions by identifying functional groups based on the transmittance bands that were identified on the recorded spectrums. Literature served as a reference to identify the correlation of different bands with varying functional groups. OH groups, NH groups including CH and carbonyl groups have characteristic bands and the bands are influenced by the environment where they are located. Thus from FTIR one can draw conclusions about present functional groups with their molecular neighbours including bond structure. FTIR has proved to be successful in analysing PUs based paints and also in tracking ER hardening process (Goldschmidt & Streitberger, 2007). The appearance and disappearance of certain bands in the spectrums as it will be discussed will be a guide in confirming the occurrence of different reactions. The FTIR was done with a PerkinElmer FT-IR C109607 spectrometer with the IR region ranging between 450 and 4000 cm^{-1} .

4.2.1. FTIR analysis of CO and ECO

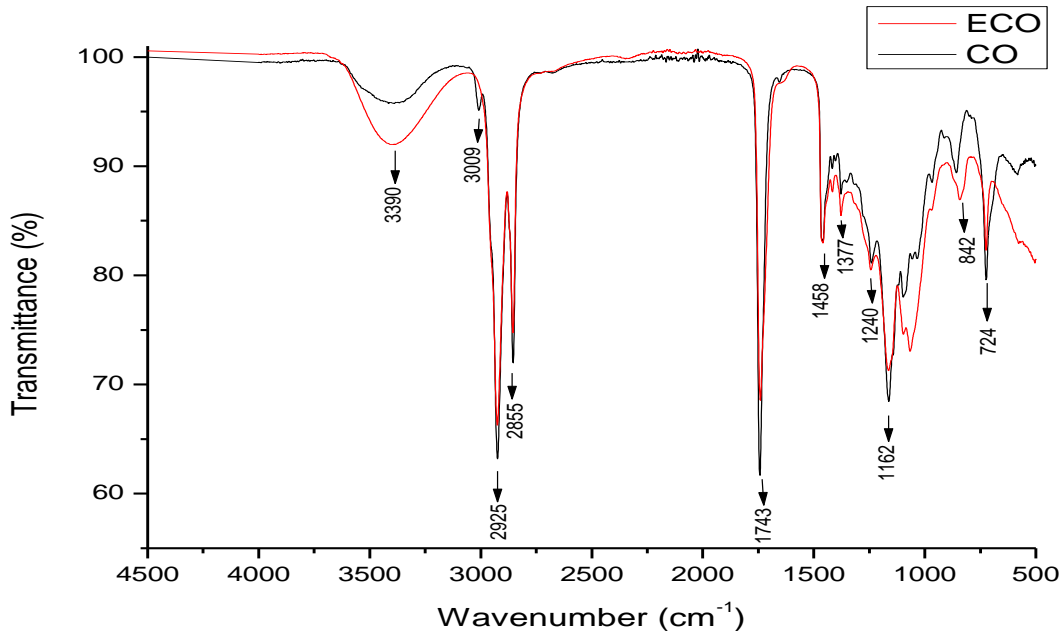


Figure 21: Stacked FTIR spectra for both CO and ECO

The spectrums in Figure 21 are stacked together in-order to compare similar bands in both CO and ECO. The main functional groups that are of interest are the C=C double bonds and the epoxide group. From Figure 21 the band for double bonds can be seen at 3009 cm^{-1} and the epoxide at 842 cm^{-1} . The band for the double bond has completely disappeared on the ECO, which can be seen on the spectrum for CO. During the epoxidation reaction oxygen is added into the C=C double bonds to form a three membered ring of carbon and oxygen. Thus as the epoxidation reaction progresses there will be a disappearance of the C=C double bonds which will be followed by the appearance of the epoxy band in the spectrum which was not present in the CO spectrum. The epoxy group can be located at 823 cm^{-1} and $842/3\text{ cm}^{-1}$ but in the ECO the epoxy functional was located at 842 cm^{-1} and these results correspond to those found by Vlcek & Petrovic, (2006) The ECO spectra show a complete disappearance of the 3009 cm^{-1} band and the spectrum is for the

reaction carried out at 35 °C for 32 hrs at a 4 wt% catalyst loading and 1:2 molar ratio of CO to H_2O_2 which shows a complete conversion of the double bonds to epoxide ring for these reaction conditions. These conditions were determined after optimisation of temperature, reaction time and catalyst amount.

4.2.2. FTIR of RCO

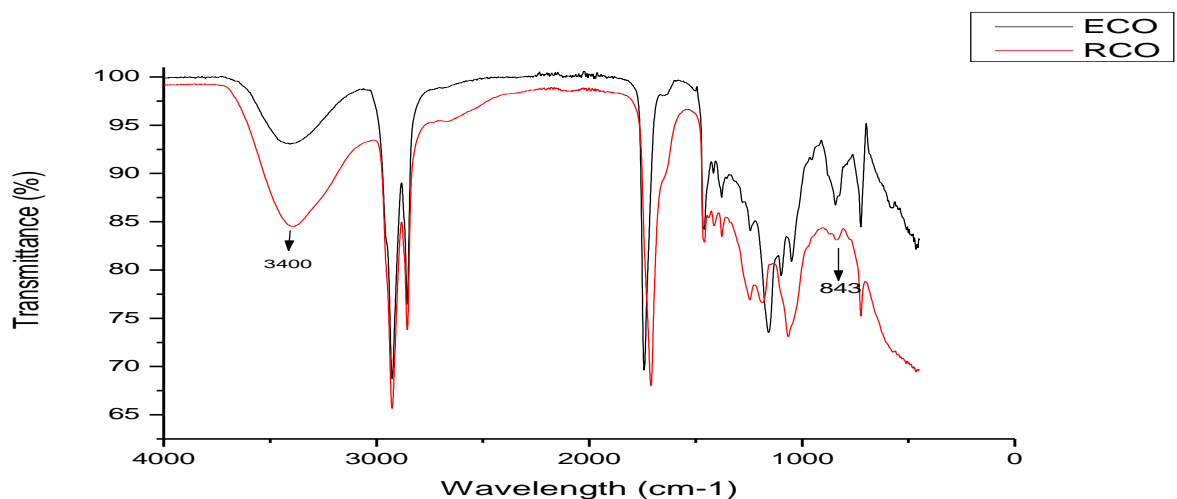


Figure 22: FTIR comparison spectrums of ECO and RCO

After the successful synthesis of ECO, this product was used for the ring opening reaction to produce a polyol. Water was used as a nucleophile during ring opening and the number of OH groups were expected to triple (9OH/mol) from 3OH/mol and thus increasing castor oil functionality and reactivity. During the work up, all the water was removed and the product dried with $MgSO_4$. The peaks that correspond to the OH present in water and the OH attached to the carbon are the same thus the presence of water can mislead in qualitative analysis of the product. The wavelength of 3400 cm^{-1} on the FTIR spectrum correspond to the OH group and the single band at 843 cm^{-1} corresponds to the epoxy group. The spectrums are put together in order to compare the intensity of the peaks of ECO and RCO at 3400 cm^{-1} and 843 cm^{-1} as this serve

as a confirmation of the occurrence of the ring opening reaction. From Figure 22 it can be seen that as the ring opening reaction occurred the oxirane band at 843 cm^{-1} decreased while the band at 3400 cm^{-1} broadened thus increasing in intensity. The same observation was made by Sharma, et al., (2006). The presence of the epoxy group in the RCO although in small quantity as indicated by the decreased intensity of this band shows that the reaction did not reach a full conversion. To study how the conversion is affected by the reaction parameters, the reaction time and catalyst amount were studied as it will be discussed in the $^1\text{H-NMR}$ section.

4.2.3. FTIR for drying oil

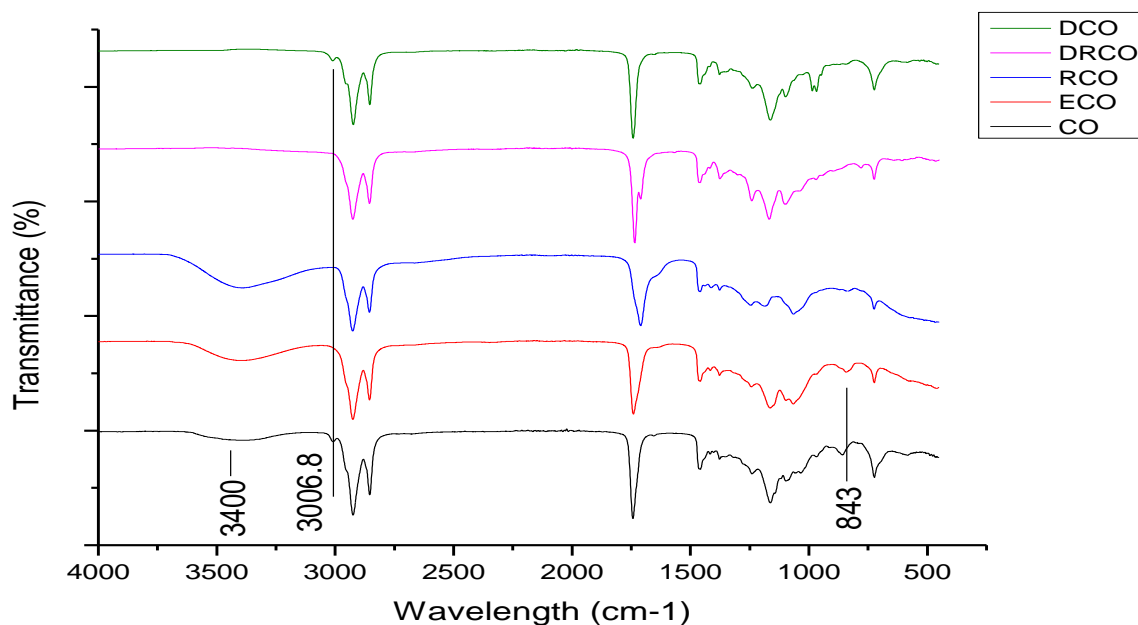


Figure 23: FTIR comparison spectrums of CO, ECO, RCO, DRCO and DCO

The synthesized RCO was used for both dehydration and PUs synthesis. This section discusses the dehydration of RCO and CO to produce a drying oil. The OH group is removed in the form of water during the dehydration reaction thus forming double bonds in return. The number of double bonds were expected to be 9 for DRCO (dehydrated ring opened castor oil) and 6 for DCO, after

the reaction, with some double bonds conjugated in configuration moving from 3 which are present in CO. As it was seen from Figure 23 that the ring opening reaction did not reach full conversion as a result this did have an effect on the dehydration reaction also with regards to the conversion. Both CO and RCO were dehydrated to produce the drying oil for paint production. On the spectra for RCO a band corresponding to the epoxy group (843 cm^{-1}) can still be seen. On the CO spectra, it can be seen that the OH band has completely disappeared with a reappearance of the C=C bonds at 3006.8 cm^{-1} which confirms the occurrence of the dehydration reaction. The spectrum with DRCO, does show the disappearance of the OH group, with a slight reappearance of the C=C double bonds. This observation might be due to the presence of the water within the RCO which remained after the work up of the product as the intensity of the OH group band can account for the water present as well, so the band intensity can be a bit misleading in regards to the extent of the reaction.

4.2.4. Polyurethane synthesis

The polyol obtained from ring opening reaction was used also for synthesizing polyurethanes. Since castor oil contains OH group in its raw state, thus being a natural polyol it was also used to synthesise PUs. During the polyurethane synthesis the OH group present within the polyol reacts with the NCO group of the isocyanate to form urethane linkages (NHCOO). The FTIR spectrums in Figure 24 correspond to CO based PUs. In Figure 24 the emergence of peaks between 1533 and 1534 cm^{-1} corresponds to the bands of the urethane linkage. The absence of 2270 cm^{-1} band which correspond to NCO group on the P17 as a representative sample shows that all the isocyanate disappeared during the poly-addition reaction to form the polyurethane. Similar results were found in the studies performed by Sahoo, et al., (2016), Emrani, et al., (2018) and Macalino,

et al., (2017). Only after the addition of the 2k catalyst is there the appearance of the NCO peak as part of the catalyst. This broad band of the NCO catalyses the drying (curing) process of the paint.

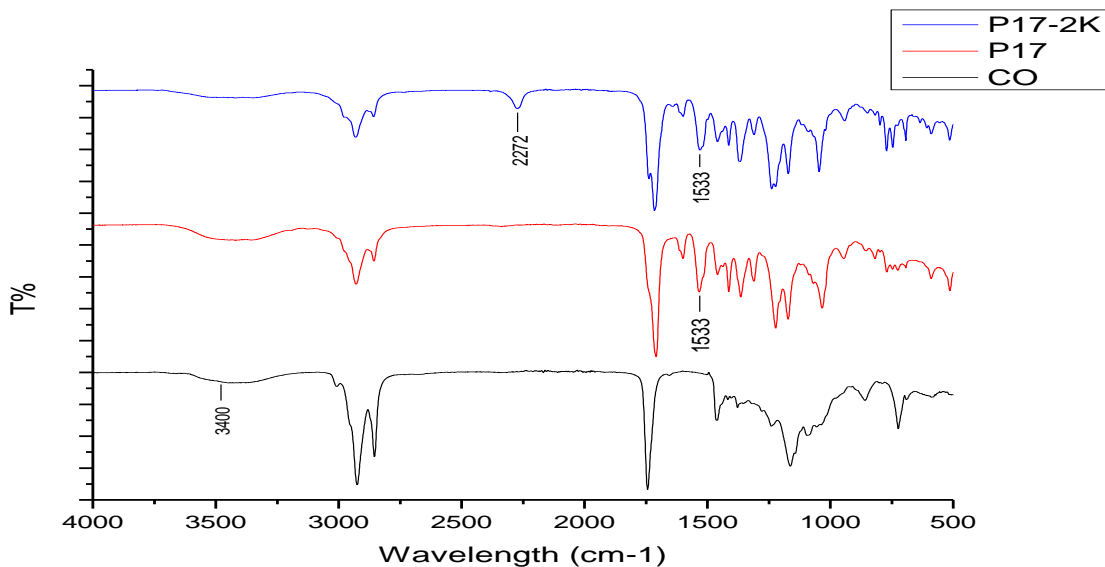


Figure 24: FTIR spectrum of CO and P17 as representative sample for the castor oil based polyurethanes before and after addition of 2k catalyst.

The spectrums represented in Figure 57 in appendix B represent the RCO as a polyol for polyurethane synthesis. Polyol-1 till 3 represent the polyurethanes synthesized using different NCO/OH ratio and the ratio is 0.9, 1.0 and 1.2 respectively. Similar peaks were identified at 1534 cm^{-1} which also correspond to the N-H bond, pointing to the formation of the polyurethane.

4.2.5. Epoxy synthesis

ECO from the epoxidation reaction was used to synthesize ER using PA and DDM as hardener. ER1 and 2 refer to PA based epoxy resins while ER4 and 6 refer to the DDM based epoxy resins. As depicted in Figure 19, the first reaction to occur during the curing process of PA and epoxy resin is the ring opening of the PA forming a monoester. The carboxylic acid which is a resultant product of the ring opening reacts with the epoxy group to form an ester linkage. In the synthesis

of PA-Epoxy resins an initiator was not used but the hydroxyl group present within CO structure served to open the ring. A catalyst was not used, but the reaction was thermally initiated at high temperature (150 °C). FTIR was used to confirm the curing process. Figure 25 is a comparison of FTIR spectrums of ECO, ER2 and PA as the hardener. As the curing process occurs the band at 843 cm^{-1} which correspond to the oxirane ring completely disappeared. There was an increase in the intensity of the carbonyl stretch for triglyceride esters in CO with this band shifting from 1741 cm^{-1} to a lower wavelength of 1717 cm^{-1} as it can be seen in the ER2 spectrum. There was also an appearance of a band at 1160 cm^{-1} which correspond to the ester groups that form by copolymerization during the process. The C=O bands of the PA functionality at 1860 cm^{-1} and 1780 cm^{-1} which can be seen on the PA spectrum have completely disappeared on the ER2 spectrum, which is the spectrum after crosslinking of the PA and epoxy resin. The disappearance of the epoxy band at 843 cm^{-1} and increase in the intensity of the carbonyl stretch of the esters along with the complete consumption of the C=O band of the PA confirms the successful curing of the PA based epoxy resin. This observation on the curing of ECO with an anhydride (PA) was also observed by Pin & Sbirrazzuoli, (2015) when they synthesized a bioresin from epoxidized linseed oil and anhydride.

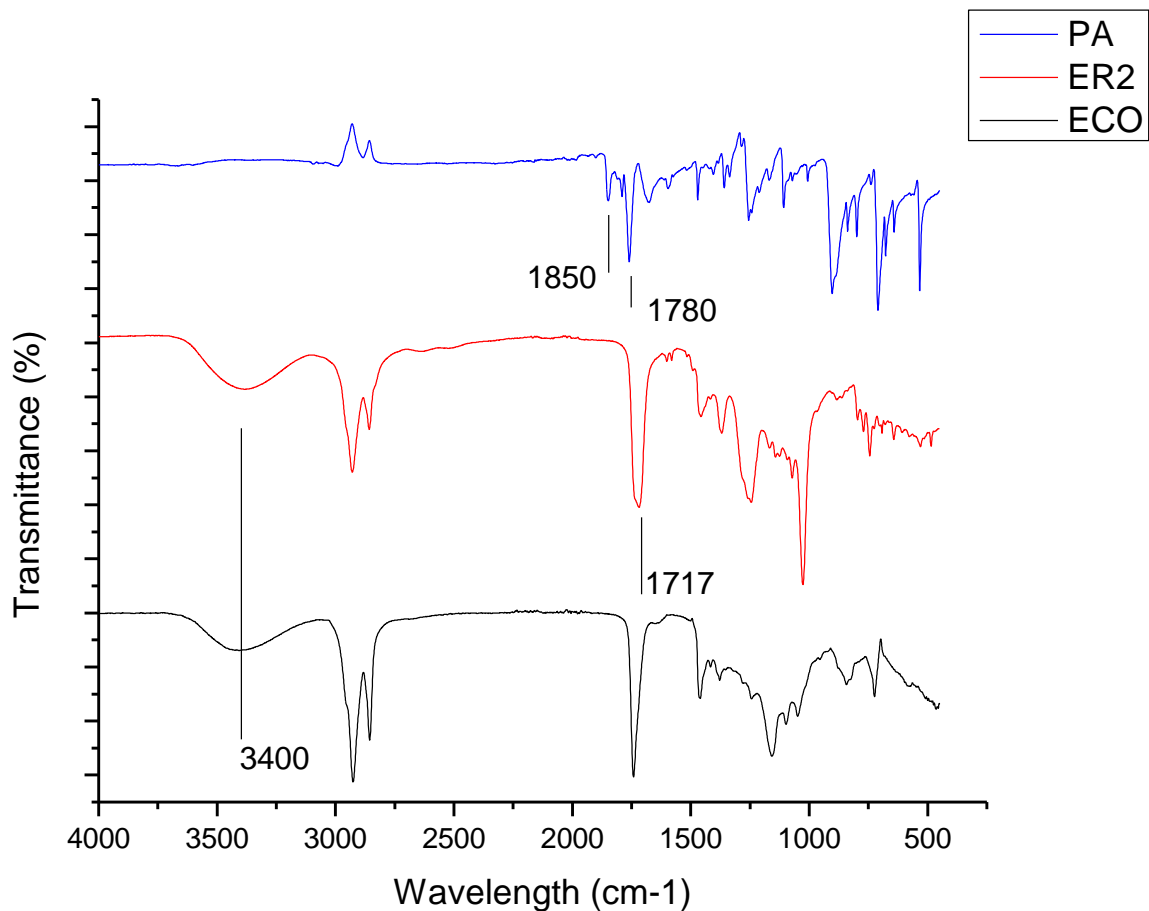


Figure 25: FTIR Spectrum for ECO, ER2 (PA based epoxy resin) and PA

During the curing process of epoxy/DDM the primary amino group reacts with the epoxy group in ECO to form secondary and tertiary amino groups and successive reactions with available epoxy groups leads to a highly branched structure. The main absorptions in the mid-range FTIR are N-H stretching and absorption bands. There is a difference in these bands in relation to the primary or secondary amines. The primary amine stretching bands are found in the range of 3500 and 3300 cm^{-1} as a doublet while the deformation primary amine bands are found in the range of 1650-1500 cm^{-1} (Gonzalez & Baselga, 2012). The secondary amine deformation have less intensity and can be found at a range of 1580-1490 cm^{-1} . Monitoring the epoxy amine reaction is done by

observing the bands of epoxy group at 843 cm^{-1} , primary amines at 3360 cm^{-1} , secondary amines at 1459 cm^{-1} . Figure 26 compares the FTIR spectrums of ECO, ER6 and DDM. It can be seen that the 843 cm^{-1} epoxy band which is prevalent in ECO has completely disappeared in the ER6 spectrum while there is an appearance of bands at 1459 cm^{-1} which correspond to the deformation bands of secondary amine. Stretching bands of primary amine at 3360 cm^{-1} can be seen in both the spectrum of DDM and ER6. The band has decreased substantially in the ER6 spectrum due to the crosslinking reaction of the DDM and ECO. Thus the disappearance of the epoxy group band at 843 cm^{-1} and the appearance of the secondary amines at 1459 cm^{-1} along with the substantial decrease in the primary amines at 3360 cm^{-1} confirms the occurrence of the curing process of the DDM based epoxy resin.

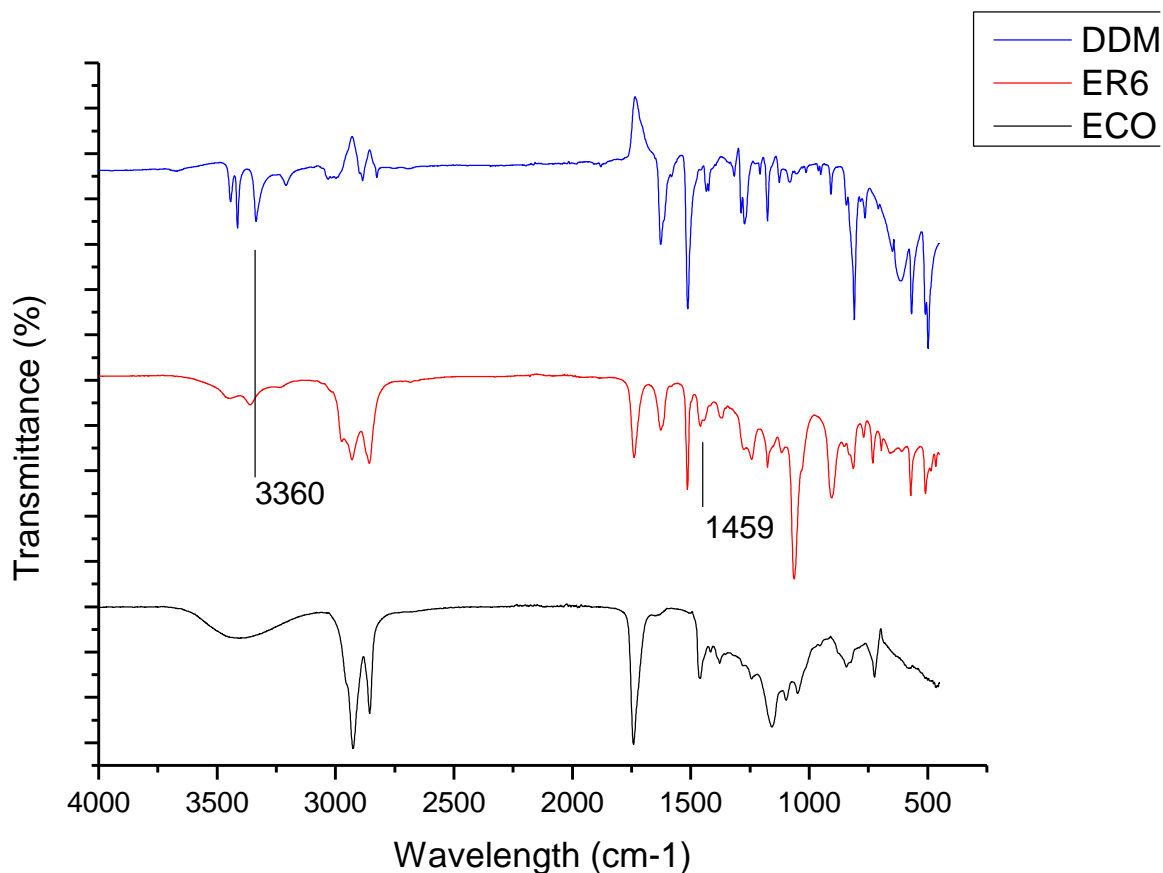


Figure 26: FTIR Spectrums comparing ECO, ER6 (epoxy resin DDM) DDM as hardener

4.3. ^1H NMR Analysis

For the quantitative characterization of the synthesized materials ^1H NMR was used. Depending on the chemical environment of the protons there will be a shift in the resonance frequency (chemical shift) and this phenomenon make ^1H NMR a powerful analytical technique. This shift in frequency is determined according to an internal standard. The integrations of the signals were used for quantitative analysis. From ^1H NMR molecular structures can be determined, as protons can be identified whether they are bonded to an OH group, a C=C unsaturation site, a carboxylic group or just a CH bond. ^1H NMR was used to evaluate the extent of the epoxidation, ring opening and dehydration reaction in terms of conversion. The conversion was calculated by taking the

protons of the glycerol backbone of the oil triglycerides as reference since the modification on castor oil did not involve the ester linkage. This section will discuss the different ^1H NMR spectrums of the synthesized materials.

4.3.1. ^1H NMR analysis of CO and ECO

The Epoxidation reaction was carried out using CALB as a catalyst. The reaction parameters that were varied during this reaction include temperature, reaction time and catalyst amount. The investigation into these parameters was done in order to determine the optimum conditions for the chemo-enzymatic epoxidation of CO. The first parameter that was investigated was the reaction time. Figure 27 shows the chemical structure of castor oil with the functional groups related to the ^1H NMR spectrums when the temperature and catalyst amount was kept constant.

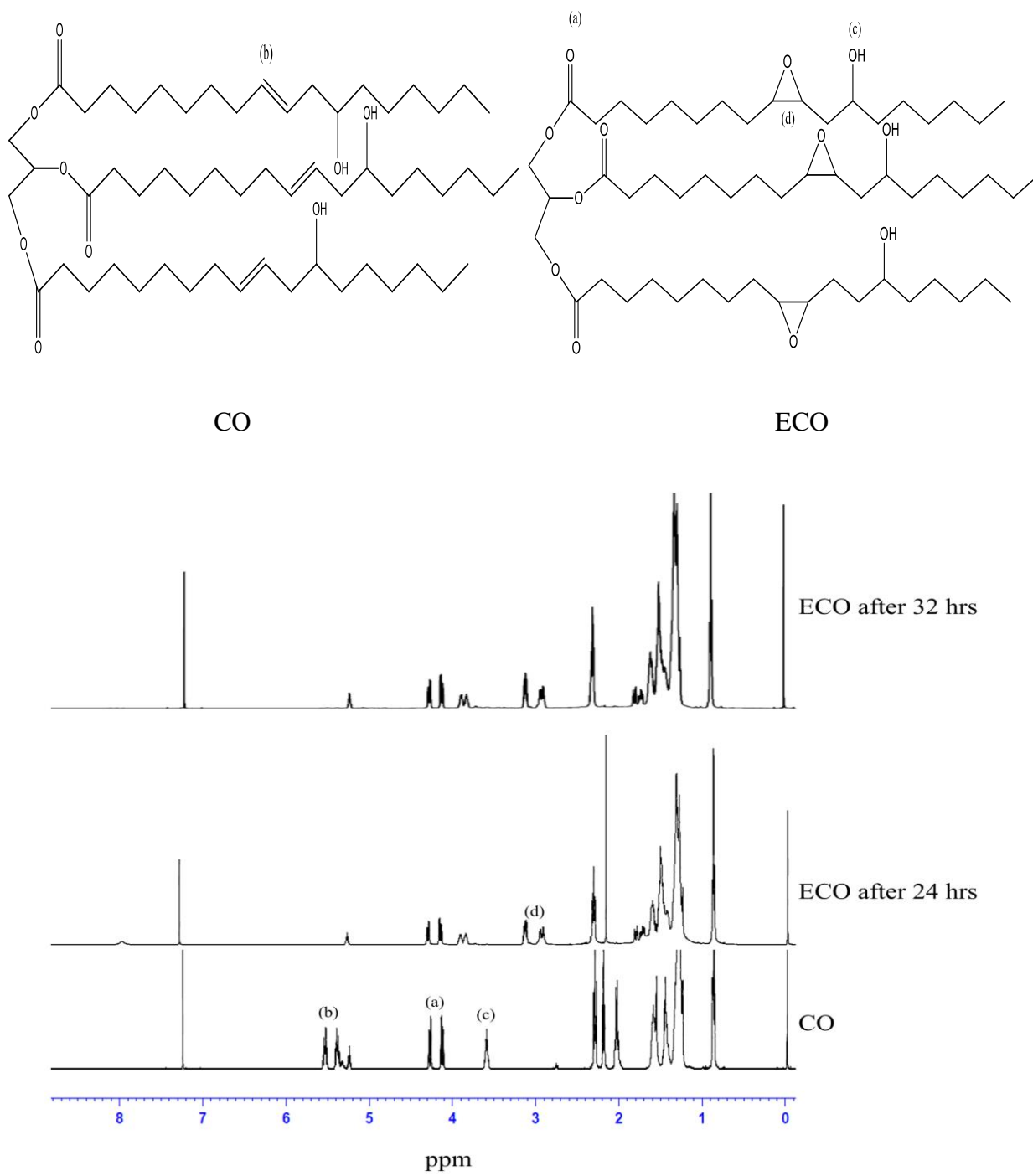


Figure 27: ^1H NMR stacked spectrum of CO and ECO at two reaction times

The conversion was calculated based on the ^1H NMR spectra. The area under each signal is equivalent to a number of hydrogen protons on different functional groups. The integration of signals shows relative numbers of equivalent protons. The signal intensity is proportional to the number of protons present in each of the chemical environments within the molecule. The frequency standard used to measure chemical shift was chloroform-d. The chemical shift at 2.9 – 3.2 ppm refers to protons on the epoxide ring. There are two peaks as the protons are in two different chemical environments. From the ^1H NMR spectrum comparing CO and ECO the double bonds and the epoxide peak can be seen at 5.3 to 5.6 and 2.9 – 3.2 ppm peaks respectively. As the epoxide ring appears, a disappearance of the C=C bonds at the aforementioned chemical shift can be seen.

The effect of the reaction time on the conversion was investigated. The time was varied between 12 and 32 hrs. After 24 hours the conversion was > than 90% but after 32 hrs it was observed that the reaction reached 100% conversion. From ^1H NMR it was observed that after 24 hours although the conversion was high an intermediate could be observed at 7.9 – 8.3 ppm peak but as the time was increased the intermediate converted into an epoxide.

Temperature is an important factor to consider in order to optimize epoxide yield as the enzyme loses activity at high temperatures. The CALB catalyst was found to be stable between 30 and 55 °C . The epoxidation reaction is exothermic but to initiate the reaction a small amount of heat must be supplied hence the temperature chosen for investigation was not at room temperature. The initial temperature investigated was 35 °C as a yield of nearly 100% was obtained from a study conducted by Zhang, et. al (2018) when using CALB immobilised on acrylic resin for soybean oil. Although the catalyst used in this study was immobilized on a different support (immobead 150) this temperature was used as the starting point. The second temperature investigated was 45 °C and the

graph shows the relationship between the temperature, conversion and reaction time. H_2O_2 decomposes at a temperature of $50\text{ }^\circ\text{C}$ and this became the upper limit for temperature investigation. During the reaction H_2O_2 was added dropwise over a period of 20 min so as to limit the amount that comes into direct contact with the enzyme .

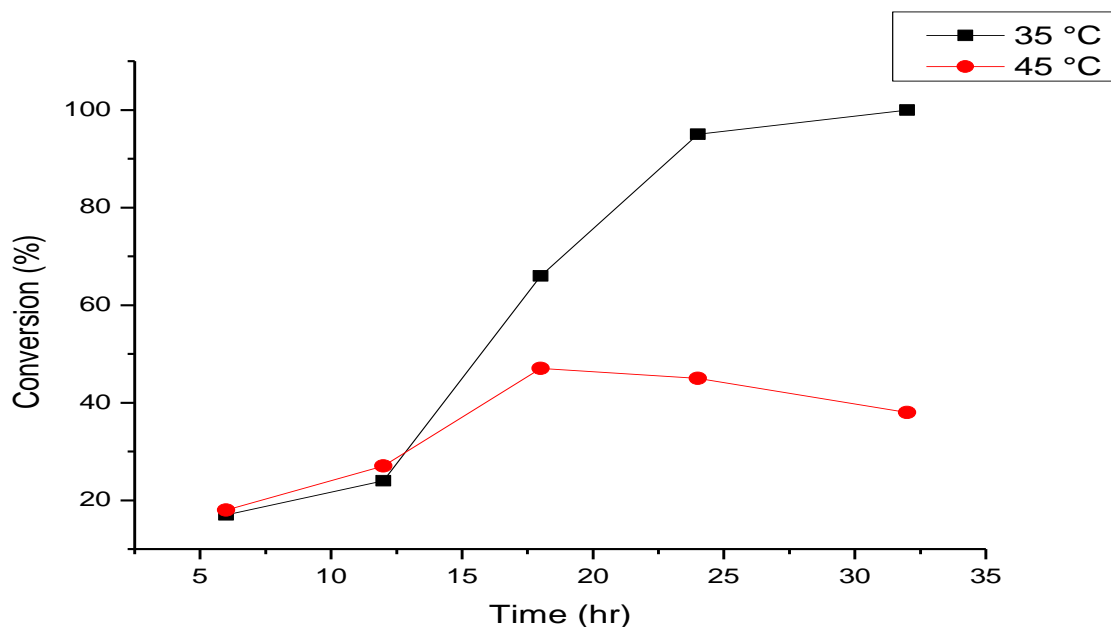


Figure 28: Enzyme-catalyzed epoxidation of castor oil for a time at $35\text{ }^\circ\text{C}$ and $45\text{ }^\circ\text{C}$, 4 wt% (related to castor oil) catalyst loading and 1:2 (Castor oil: H_2O) molar ratio.

From Figure 28 , it can be seen that at $35\text{ }^\circ\text{C}$ the highest conversion is achieved after 32 hrs. although after 24 hrs the conversion is $> 90\%$ from the $^1\text{HNMR}$ spectrum it was evident that an intermediate was identified at 8.1 ppm chemical shift as seen in Figure 27 . As the reaction time was increased the desired conversion of 100% was achieved after 32 hrs. The conversion increased exponentially at $35\text{ }^\circ\text{C}$ but there was a decrease in conversion with time at $45\text{ }^\circ\text{C}$. This behaviour can be attributed to catalyst deactivation by the high temperature and also the presence of a high concentration of H_2O_2 . The reaction was carried out in the absence of a solvent as the solvent

doesn't have a significant effect on the conversion which can be supported by Zhang, et al., (2018). A single reaction was run at 50 °C for 32 hrs and the conversion was < 20 % as such it can be concluded that the optimum reaction temperature is 35°C with castor oil and this also applies to high oleic soybean oil according to the study by Zhang, et al., (2018). The optimum reaction time is 32 hrs with castor oil to get 100% conversion but a time > 24 hrs does give a conversion > 90% but the intermediate must be taken into consideration. The catalyst amount used in this investigation was 4 wt % in relation to the oil.

The catalyst amount also was investigated to determine the effect on conversion. The catalyst amount was varied from 1 to 5 wt%. Conversion increased linearly until it reached the highest conversion of 100% at 5 wt% loading. At 4 wt% the conversion was 98%. The increase in viscosity can be attributed to the addition of oxygen thus increasing the intermolecular forces, molecular weight and polarity of the oil. Figure 29 gives the relationship between the conversion and catalyst amount when the reaction was carried out at 35 °C for 32 hrs.

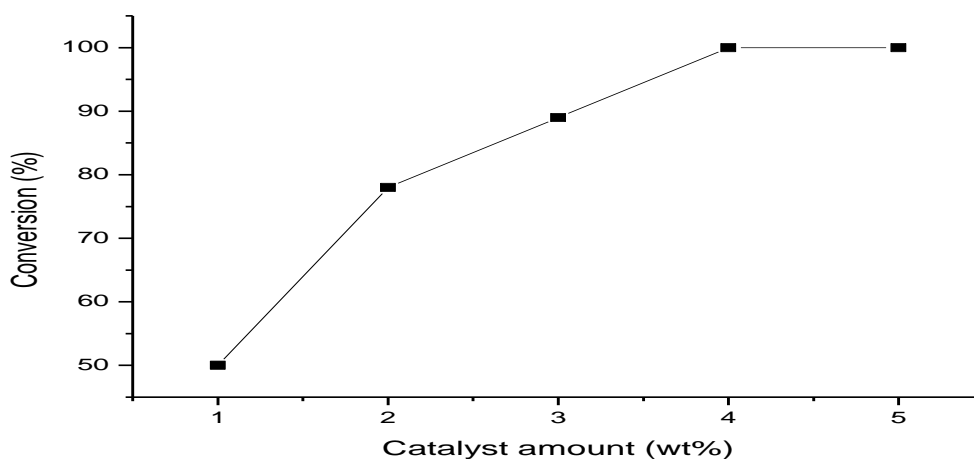


Figure 29: : Enzyme- catalyzed epoxidation at 35 °C , 1:2 (castor oil: H₂O) molar ratio with different catalyst amount.

4.3.2. ¹HNMR spectrums for RCO

The ¹HNMR spectrums on Figure 30 compare the ECO and RCO in relation to the appearance and emergence of new peaks as the ring opening reaction occurred. The peaks at 3.2 and 2.8 ppm correspond to the protons of the epoxy ring while the peaks at 4.0-3.5 ppm correspond to the protons attached to the CHOH group. From Figure 30 it can be seen that the peaks corresponding to the protons of the epoxy ring disappeared and new peaks emerged (RCO spectrum). The peaks at 4.1-4.4 ppm are present in both spectrums and these peaks correspond to the protons of the glycerol structure. Similar peaks were identified by Sharma, et al., (2006) in their study with soybean oil. The retention of these peaks is an indication that during the ring opening with *HClO₄* the hydrolysis of the ester linkage was very minimal. These peaks corresponding to the protons of the glycerol structure were used as a reference to determine the number of other protons for other functional groups. The conversion for the ring opening reaction was found to be 65% for the 1:18:0.2 (castor oil: *H₂O*: *HClO₄*) ratio of reactants. This value slightly varied as the reaction was repeated a couple of times yet the conversion was > 60% not lower. The effect of the reaction time and amount of catalyst (*HClO₄*) on the conversion was also investigated to study the reaction further and the discussion outlines the results. To investigate the effect of the reaction time on conversion, samples were drawn at a time interval of 8 - 48 hrs. Figure 31 shows an increase in conversion as the reaction time was increased but during the experimental work it was found that after 48 hrs the reaction reached an equilibrium and the maximum conversion that could be reached was 70% with all the successive reactions that were done. This can be attributed to the difficulty that is experienced in opening the epoxide ring and also to the fact that the reaction is occurring at 100 °C thus some of the water with the catalyst is lost through evaporation even though a reflux condenser was used. A similar relationship was found between the conversion and catalyst amount.

The amount of catalyst was varied also to evaluate the effect on hydrolysis as a side reaction during the ring opening with a strong acid. The conversion showed similar patterns, there was an increase as the amount of catalyst was increased. The ^1H NMR showed a retention of ester peaks even when the catalyst amount 1:0.3 (mass ratio of oil and catalyst) thus HClO_4 causes minimal hydrolysis during the ring opening. Figure 31 and 32 show the observed results.

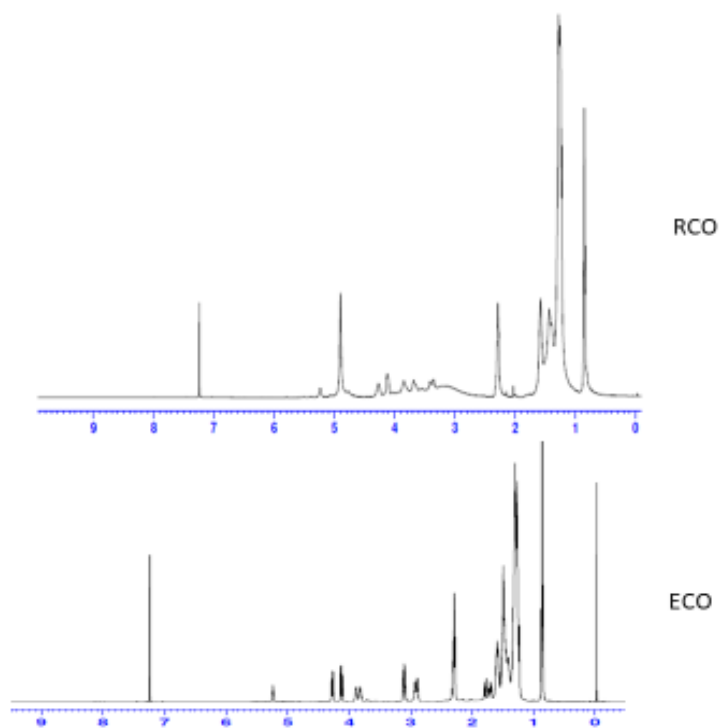


Figure 30: ^1H NMR spectrum of ECO and RCO with the mass ratio of the reactants of 1:18:0.2 (castor oil: H_2O : HClO_4).

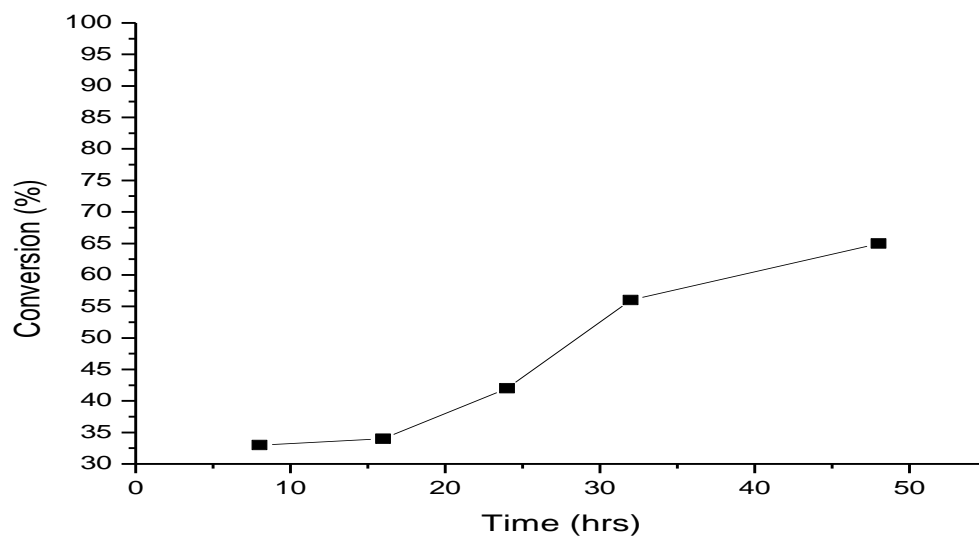


Figure 31: Graph showing the effect of reaction time on conversion when the ratio is 1:18:0.2 for reactants and the temperature is 100 °C.

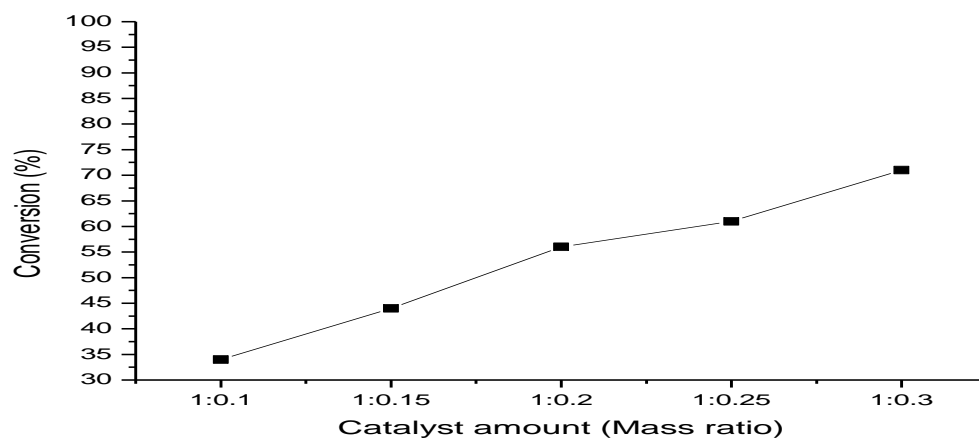


Figure 32: Graph depicting the effect of the amount of HClO_4 as catalyst on the conversion when the reaction conditions are 100 °C temperature and for 48 hrs.

4.3.3. ^1H NMR spectrum for drying oil

The ^1H NMR spectra on Figure 33 were used to confirm the occurrence of the dehydration reaction. Figure 33 compares the ^1H NMR spectra of CO, ECO, RCO, DCO and DRCO. The spectra are stacked together for the purpose of comparing the intensity of peaks and the possibility of similar functional groups still being present in the final drying oil. Comparing CO and DCO, there is a disappearance of the peaks of OH which are found at 4.1 and 3.5 ppm and an increase in the intensity of the C=C peaks at 5.3 and 5.6 ppm. Comparing the ECO, RCO and DRCO: epoxy peaks at 2.3 and 2.9 ppm have disappeared on the RCO, and the OH peaks on the RCO have decreased in the DRCO. The protons of the $-\text{CH}_2 - \text{CH} - \text{CH}_2 -$ of the glycerol backbone were used as reference peaks for calculating the conversion for the DCO and DRCO. The conversion was found to be 43% and 53% respectively when the reaction was done at 240 °C, 0.1 g NaHSO_4 for 120 min. In a study by Mamudu, et al., (2019) when the temperature was 250°C at 1% NaHSO_4 a maximum conversion was reached which gave good drying properties. Temperature was kept in the chosen range to avoid the burning of the oil as well as the reaction time, yet a slight increase in the temperature, catalyst amount and reaction time can improve the conversion significantly.

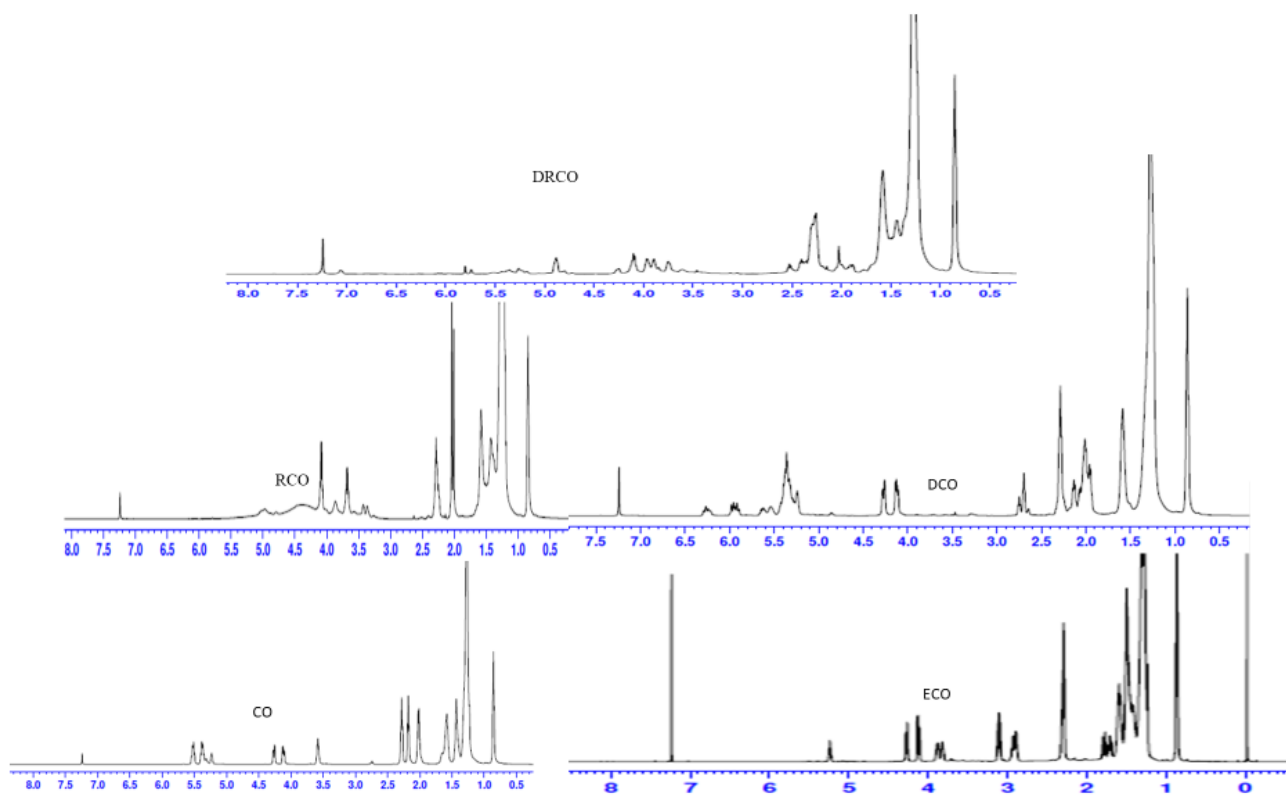


Figure 33: Stacked ^1H NMR spectrums for CO, ECO, RCO, DCO and DRCO

4.4. Rheology studies

The physical behaviour of the paint when placed under stress, during mixing or application undergo some degree of shear thinning. Rheology deals with the changes in viscosity as different levels of force are applied, as temperature is varied, and as solvents and additives come into play. Viscometer readings, although valuable, do not show a full picture and thus for meaningful correlations in coatings, viscosity measurement is done at a wide range of strain rates (Tracton, 2006). Coatings show a significant change in viscosity as different forces are applied as very few liquids are truly Newtonian. More typically, liquids drop in viscosity as shear or work is applied. The phenomenon was identified as shear thinning (Goldschmidt & Streitberger, 2007). The Figures show the relationship between shear stress vs shear rate of the different materials as well as viscosity with shear rate. The graph of the shear stress vs shear rate helps to identify the yield

value of the coating material and from both graphs the viscosity behaviour can be identified, either as Newtonian, Pseudo-plastic, thixotropic or dilatant. Newtonian fluids have an absolute viscosity that is unaltered when stress is applied while pseudo-plastic fluids experiences a drop in viscosity (Tracton, 2006). The yield value is a shear stress that is taken during viscosity measurement with a rheometer at the lowest value of shear. This is the minimum shear required to cause flow. This is an important parameter in understanding behaviour of coatings after being applied on a substrate. Shear stress that acts on the applied coating is very low thus if the yield value is higher than the shear stress or the force of gravity the coating will not level thus it will behave like a solid. If this higher yield value is intrinsic within the coating, then suitable application methods must be considered yet a high yield value makes the coating unusable (Tracton, 2006). Figure 34 is a stress-strain graph for the drying oil and the results show that when stress is applied on the drying oils they approach a Newtonian behaviour with a yield point low that the film levels.

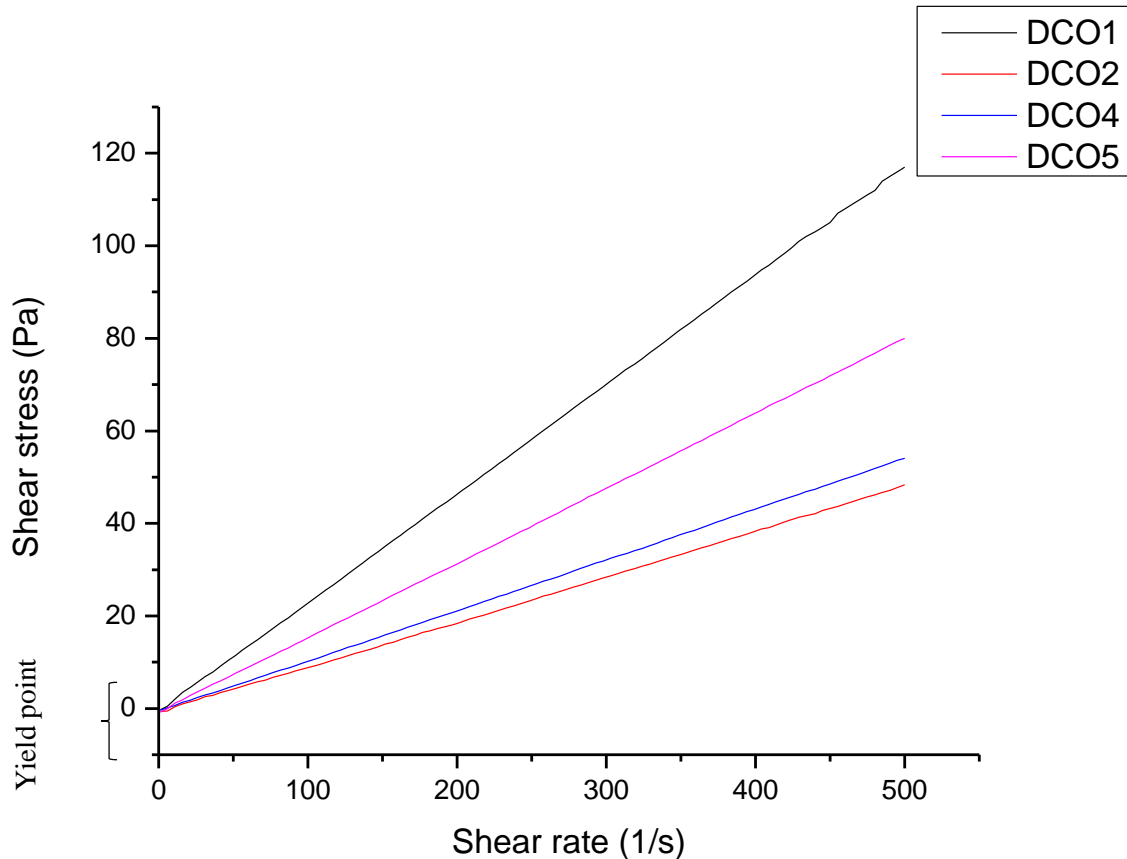


Figure 34: The graph of shear rate vs shear stress for selected samples of the drying oil

The rheology of the polyurethanes based on RCO show a plastic or pseudo-plastic behaviour and also dilatant behaviour, while the polyurethanes based on CO are showing behaviour of a Newtonian fluid. Figure 35 shows the shear stress-shear rate curve also including the yield point. The yield point is of practical value. Dripping is prevented because the yield point exceeds the force of gravity. Low yield point leads to easy flow out but the challenge faced might be of the coating running on surfaces. With pseudo plastic behaviour shear stress causes thinning until a point where there is no longer a change in viscosity.

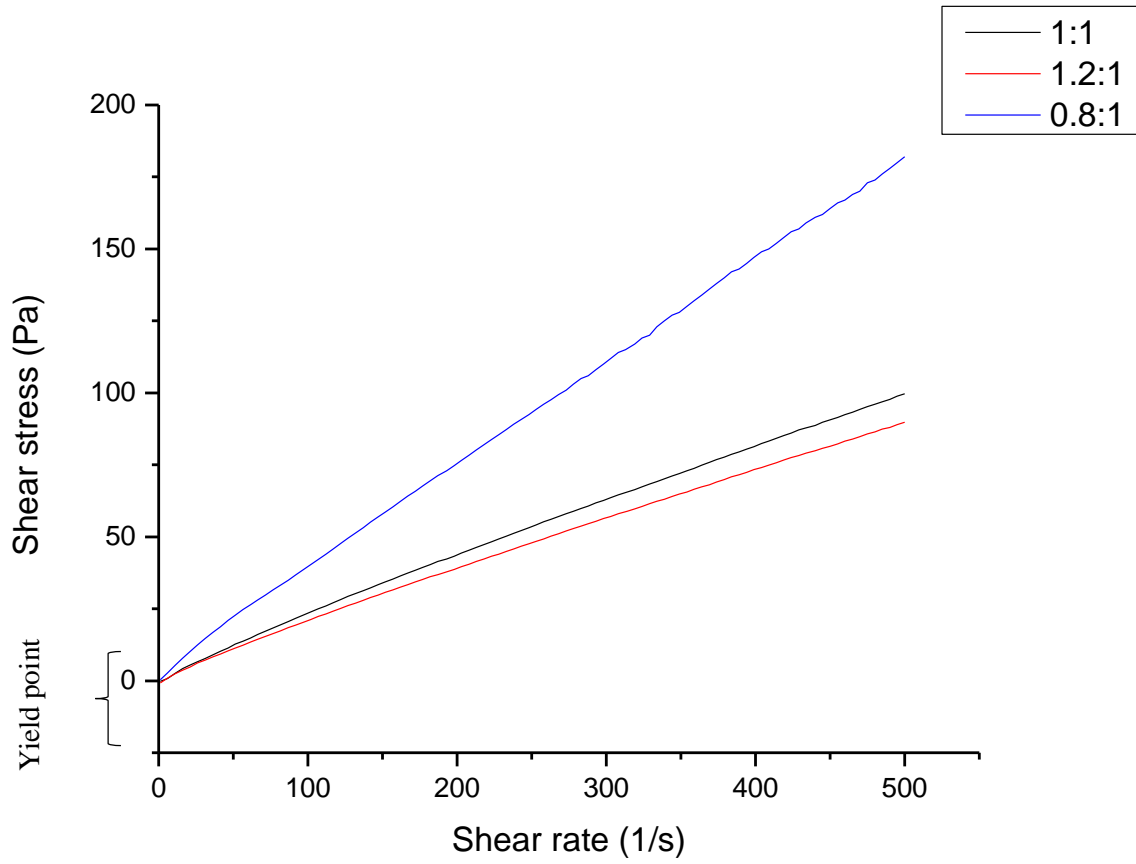


Figure 35: Graph depicting the relationship between the shear rate and shear stress of the CO based polyurethanes.

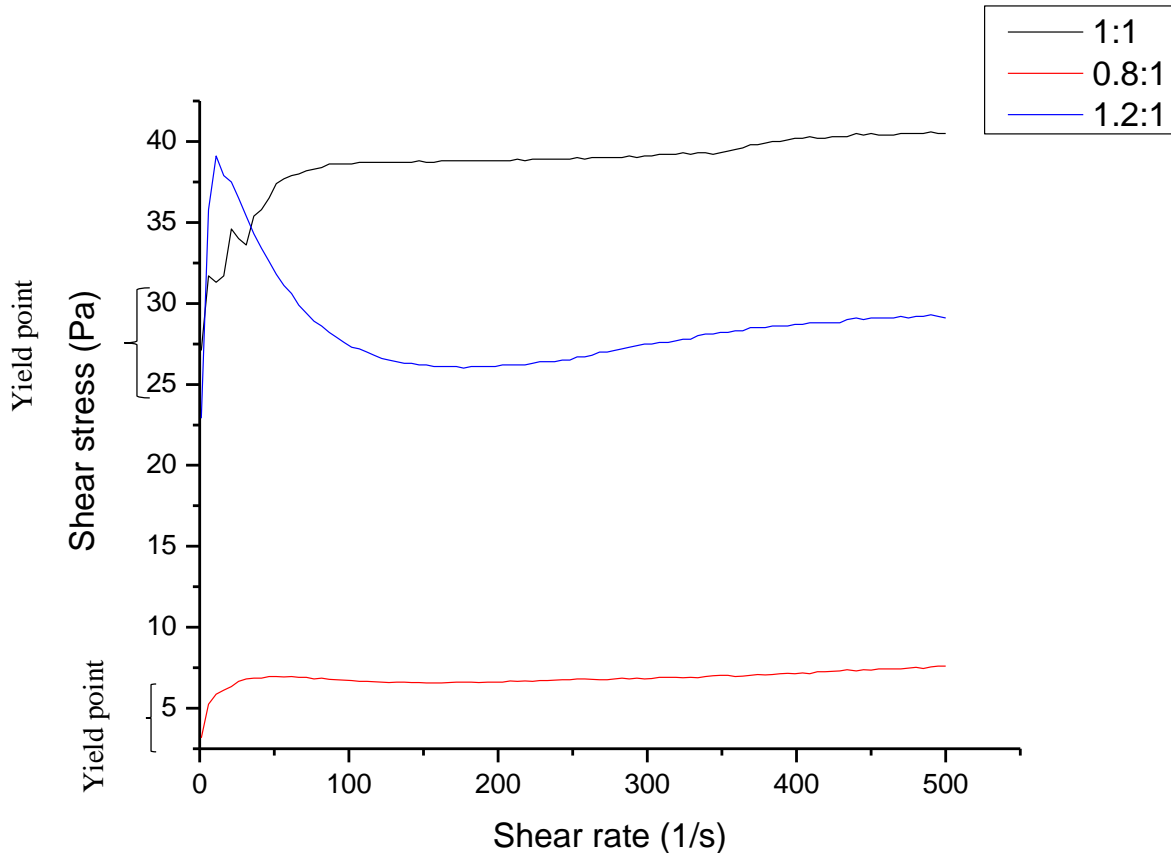


Figure 36: Graph of shear rate with shear stress of polyurethanes based on RCO and MDI and the yield point

Figure 36 shows a graph of shear stress with shear rate of polyurethanes based on RCO and MDI. It can be seen that the yield value when the ratio is 1.2:1 and 1:1 (NCO: OH) is very high and this was observed during application to test for drying, as the coating did not level. Thus for use of RCO for polyurethanes synthesis very low NCO: OH ratio must be used in order to obtain a usable paint. From Figure 36, it can be concluded that 0.8:1 ratio should be taken as the maximum as the yield value was low. The yield value for other coatings studied was found to be low and thus the coatings are usable.

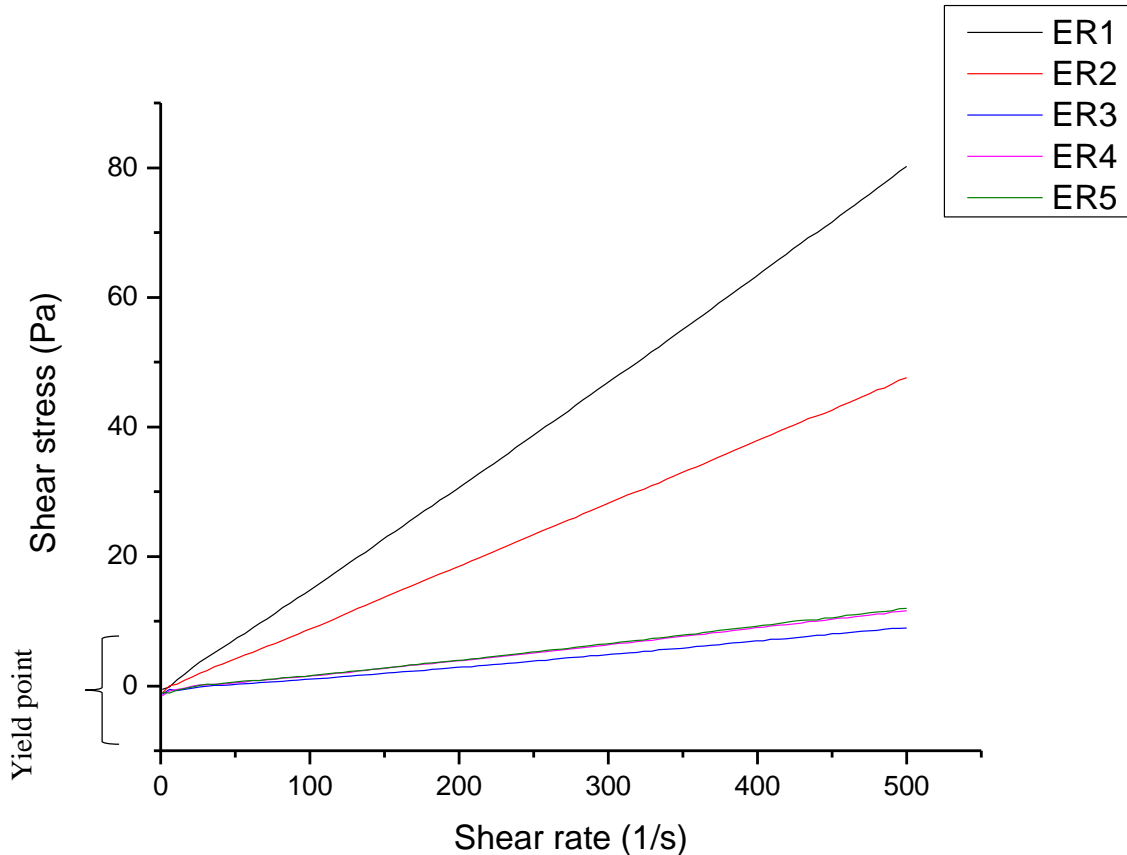


Figure 37: graph illustrating the relationship between increasing shear rate and shear stress of Epoxy resins with PA and DDM as hardener.

Epoxy resins are low viscosity formulations and thus exhibit Newtonian behaviour (Karak, 2012). Figure 37 show that the synthesized Epoxy resins do exhibit this behaviour.

The addition of the thinner within the paint formulation also played a role in reducing viscosity. Figure 38 shows the relationship between shear rate and viscosity. It can be seen from the graph, as the shear rate is increased the viscosity reaches a constant value. This behaviour depicted in Figure 38 is that of a high viscosity Newtonian fluid. The viscosity was regulated by the addition of solvent and thinner, thus the viscosity recorded must be taken with these things in view.

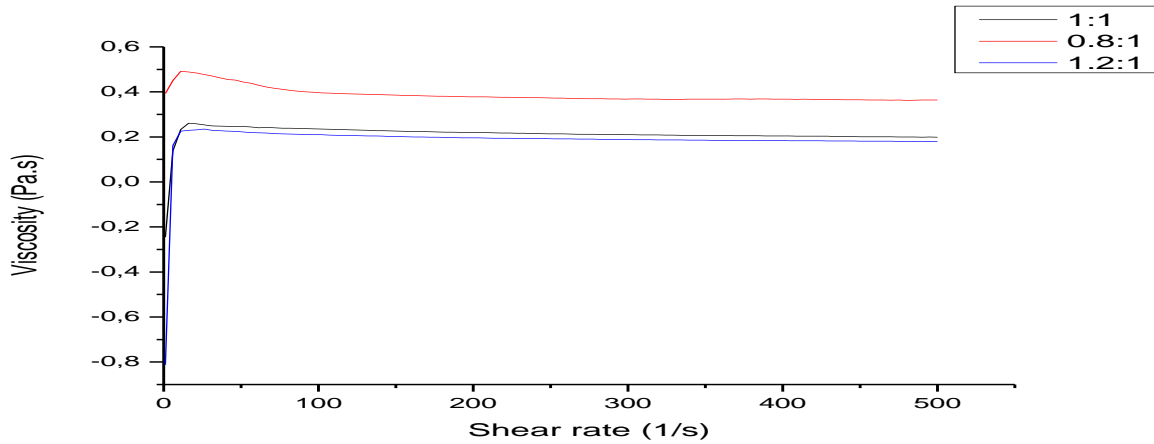


Figure 38: Graph showing the relationship of shear stress and viscosity of CO based polyurethanes at different amounts of MDI.

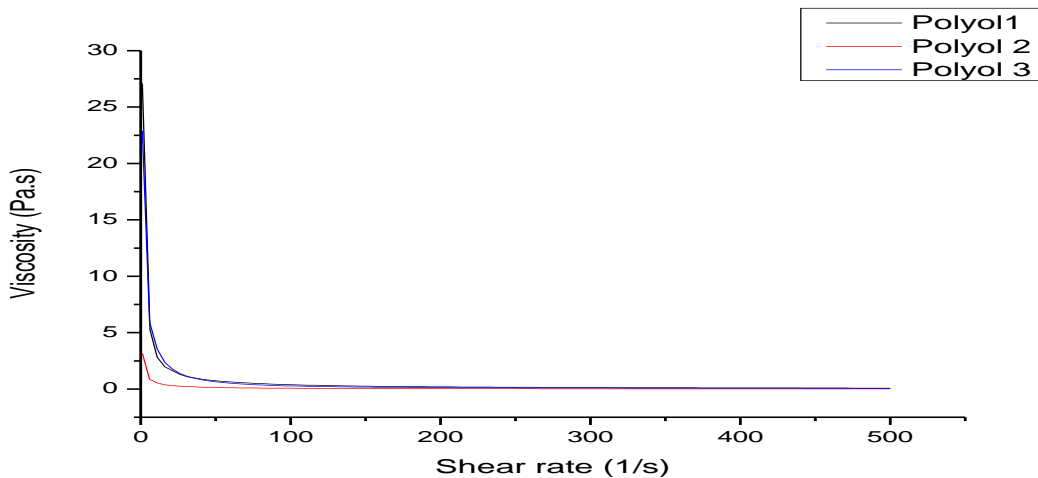


Figure 39: Graph showing the relationship of viscosity with differing shear rate of polyurethane based on RCO with different amounts of MDI.

The viscosity of the RCO based coatings is very high as it can be seen on Figure 39, thus a substantial amount of thinner and solvent would be needed for efficient application of the coating and also to achieve levelling. This high viscosity is because of the increase in the OH groups as this increases hydrogen bonding between the molecules, thus limiting the paint to have a high

resistance to flow. This flow causes the shift of the paint from Newtonian behaviour to Non-Newtonian.

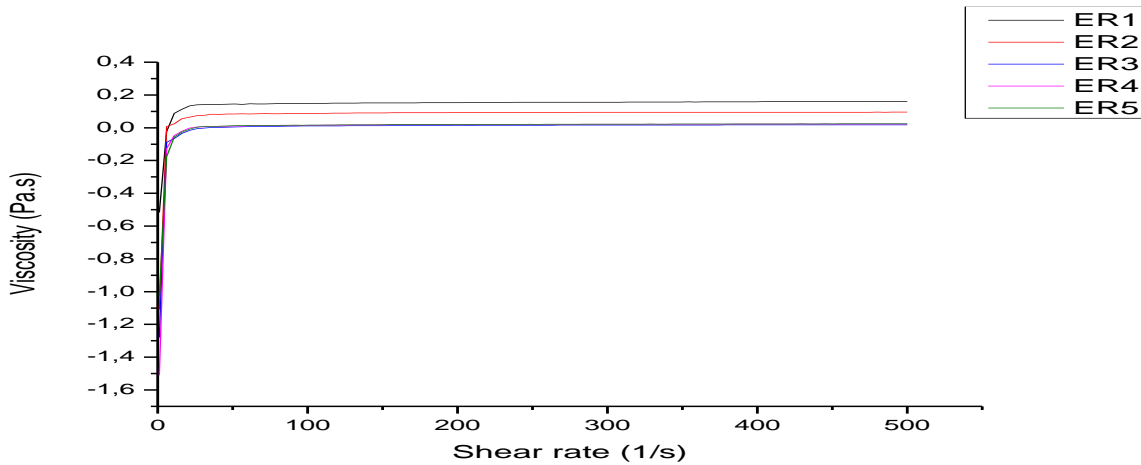


Figure 40: Graph showing the relationship between increasing shear rate with viscosity of Epoxy resin with PA and DDM as hardener.

The ER also displays the same behaviour as the CO based polyurethanes as seen in Figure 40, the viscosity reaches a constant value as the shear rate increases and this is the typical behaviour of a Newtonian liquid.

4.5. Drying time

Curing/drying was carried out at room temperature and the different paints have different curing mechanisms. The drying oil undergoes oxidation while the epoxy and polyurethane coating undergoes curing by both physical drying when the solvent evaporates from the coating and also chemical curing which is poly-addition polymerization causing a crosslinking of the molecules thus resulting in an increase in the molecular weight of the paint. Catalyst can be added to accelerate the rate of cuing/drying. Coatings can undergo a forced curing by the increase of the temperature but for this tests atmospheric conditions were considered. The catalysts used to

accelerate drying was DBTL which was used for the polyurethane coatings and also a 2k fast catalyst which was used for both polyurethanes and epoxy resins. The bar graphs show the curing time for the different paint samples based on drying oil, polyurethanes and epoxy. A building wall was used to test for the drying time of the paint. The various paints with different proportions of the isocyanate, PA/DDM were painted on the wall and the drying time was observed. Figure 52 in appendix A show the painted wall, and Figure 53, 54, 55 and 56 also in appendix A show different polyurethane and epoxy paints respectively after forming a hard film under atmospheric conditions. The pictures show samples for both DBTL and 2k catalyst.

4.5.1. Drying oil

When drying oil is applied on a substrate, it transforms into a hard and elastic film by reaction with atmospheric oxygen through oxidation. As discussed in literature section the primary reaction that occurs is the formation of hydro-peroxides and further decomposition of the peroxides lead to subsequent crosslinking that leads to the formation of the film. The oxygen attaches to the CH bond adjacent to one of the double bonds in case of conjugated double bonds but with isolated double bonds the attachment will be to a CH_2 . Conjugated double bonds are more reactive than isolated double bonds and during the dehydration process both can be found in different proportions. The use of RCO to synthesize a drying oil was for the purpose of improving the possibilities of forming more conjugated double bonds relative to isolated double bonds. This was done in view of improving the drying time.

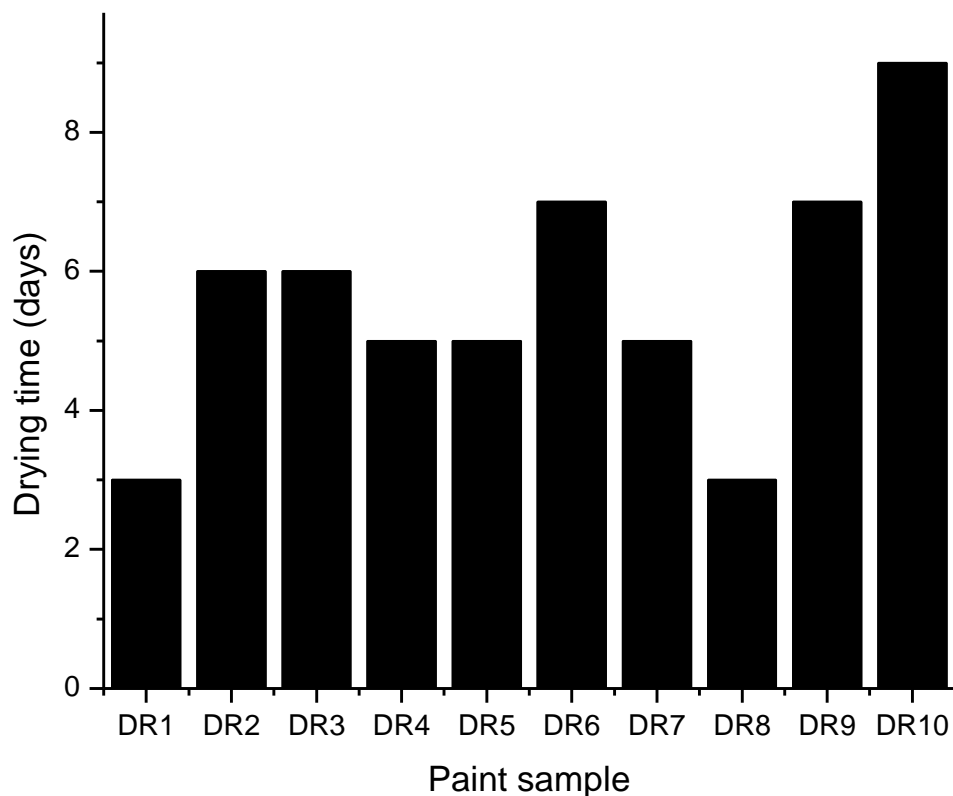


Figure 41: Bar graph comparing the drying time for different paint samples after addition of beeswax, filler and pigment.

From Figure 41, the samples that showed the best drying time was when the temperature was 240 °C, 0.1 g of $NaHSO_4$ and 120 and 90 min of reaction time which is samples DR1 (CO) and DR2 (RCO). The RCO reached a conversion high enough to give good drying properties which can be attributed to the formation of more conjugated double bonds in lower reaction time as compared to CO. The bar graph show that DR1, DR2 and DR7 have good drying times of 2 days for 1 and 2 while 7 has 5 days drying time. DR6, DR9 and DR10 are samples when the reaction conditions were 180 °C, 0.1 g $NaHSO_4$ and reaction time of 120, 90 and 60 min respectively. The drying time is the longest in the bar graph with the maximum of 9 days drying time, these samples are

representative of those of DCO. While samples: DR2, DR3, DR4 and DR5 refer to samples with reaction conditions of 210 °C, 0.1 g $NaHSO_4$ and reaction times of 30, 60.90 and 120 min respectively. The longest drying time for these samples was 6 days. From the observations it can be concluded when the reactions conditions are 240 °C, 0.1 g of $NaHSO_4$ and 120 /90 min then a drying time of 2 days can be obtained which is also a similar drying time obtained by Mamudu, et al, (2019) with a drying time of 2 days for CO when the reaction conditions were 250 °C, 1%, $NaHSO_4$ and 120 min. Although the dehydration reaction reaction showed a low conversion, the good drying time can be associated with the formation of a high proportion of conjugated double bonds. The samples that showed good drying were for DRCO at the aforementioned reaction conditions.

4.5.2. Castor oil/RCO as polyol

The drying time of 1-component polyurethane coatings is affected by atmospheric humidity and temperature, the low humidity and temperature increases the curing time. It was observed that the polyurethanes with a lower NCO: OH ratio start to cure at room temperature but the curing process was slow, thus to obtain a hard film the process lasted up to 7 days for most of the paints. Although, when the ratio was increased the curing to a hard film in ambient conditions was 3 days. It can be concluded that increasing the NCO: OH ratio improves the drying time. The increase in the ratio had a positive impact on chemical resistance of the resins. The downside to this was the fact that the increase in the ratio be it either for the polyurethane/epoxy the resin became more brittle, thus the mechanical strength was compromised as well as the elasticity. The cured resins still did display good hardness as the ratio was increased. Depending on the end application and also the main requirement of the of the paint there is need to consider the effect that increasing the ratio will have on the final coating.

Due to this observation on the drying properties of the paint and also the effect on other properties such as, mechanical strength and elasticity, a commercial hardener was used to better improve the drying properties without compromising the mechanical or elasticity of the paint.

The addition of the chain extender increased the molecular weight of the PUs thus the increase in the crosslink density yet the drying time of 3 days as the lowest for the paints with DBTL was improved further by the addition of 2k catalyst to reduce the drying time. The drying times for different paint samples based on CO based PUs is depicted in Figure 42.

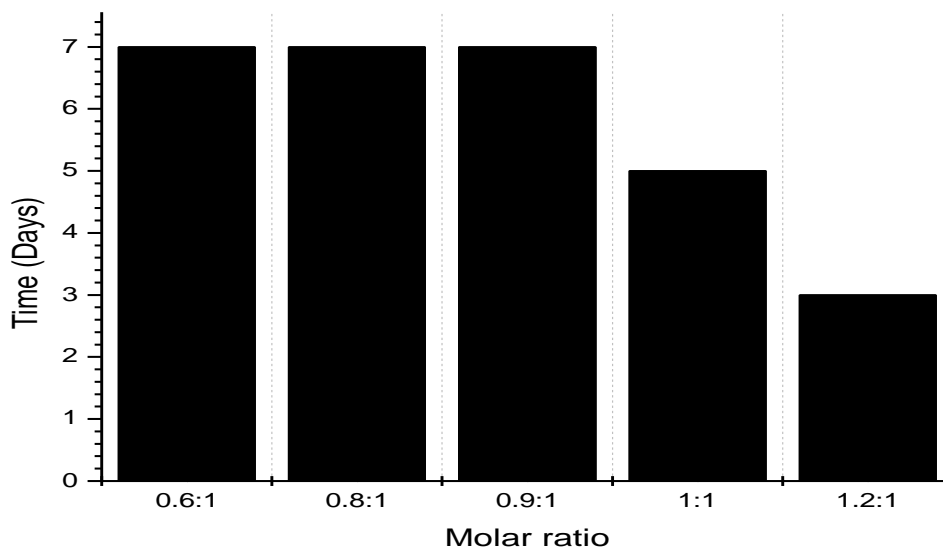


Figure 42: Bar graph comparing the drying time of different polyurethanes when DBTL is used as catalyst.

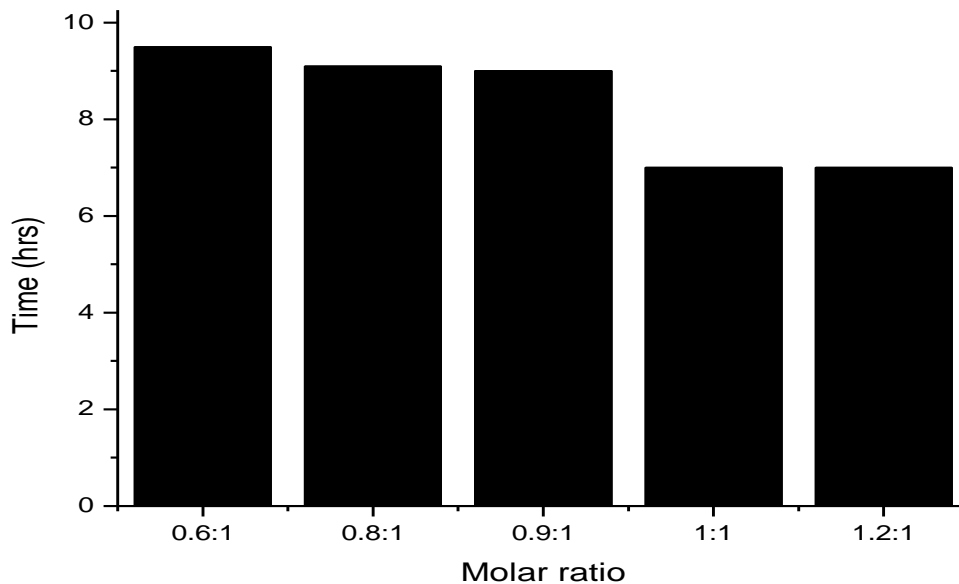


Figure 43: Bar graph comparing the drying time of different polyurethanes when 2k catalyst is used.

The recommended addition ratio of the 2k catalyst is 1-part catalyst to 2-part paint. From Figure 48 it was observed that drying time of the paint was reduced to 6 hours for the 1.2:1 NCO: OH ratio paint sample. Even for the paints that showed a very longest drying times of 7 days with DBTL, with the addition of the 2k catalyst the drying time was reduced to 9 hours. This observation is due to the interaction between the added chain extender and the 2k catalyst thus the crosslinking is accelerated as compared to DBTL catalyst.

To further optimize the ratio was varied from 0.1- 1 parts catalyst with 2-part paint. The drying time ranged from 7 hours to 3 hours touch free time and 15 hours hard dry. Figure 44 depicts the relationship between the mentioned parameters. The resulting paints can find application in automotive industry or for industrial application in general. The addition of the 2k catalyst was to optimize the drying time of the paint so that it can dry very quickly, even at room temperature.

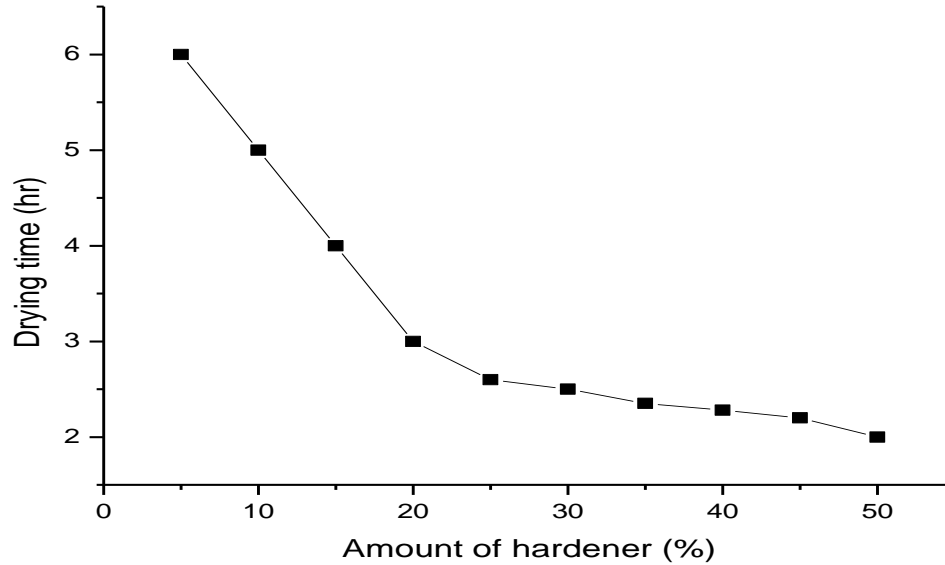


Figure 44: Graph of the drying time when different amount of 2k catalyst is added to a 1:1 ratio castor oil based polyurethane coatings.

Based on the drying time of the synthesized coatings and also for reducing the amount of 2k catalyst, the addition of 2k catalyst in small amounts or quantities does have tremendous effect on the resulting paint. The addition of the 2k catalyst in minute quantities does aid in preserving the integrity of the paint in its bio-based nature. Additives although sometimes added in small concentrations they actually have huge impacts on the coating materials and properties.

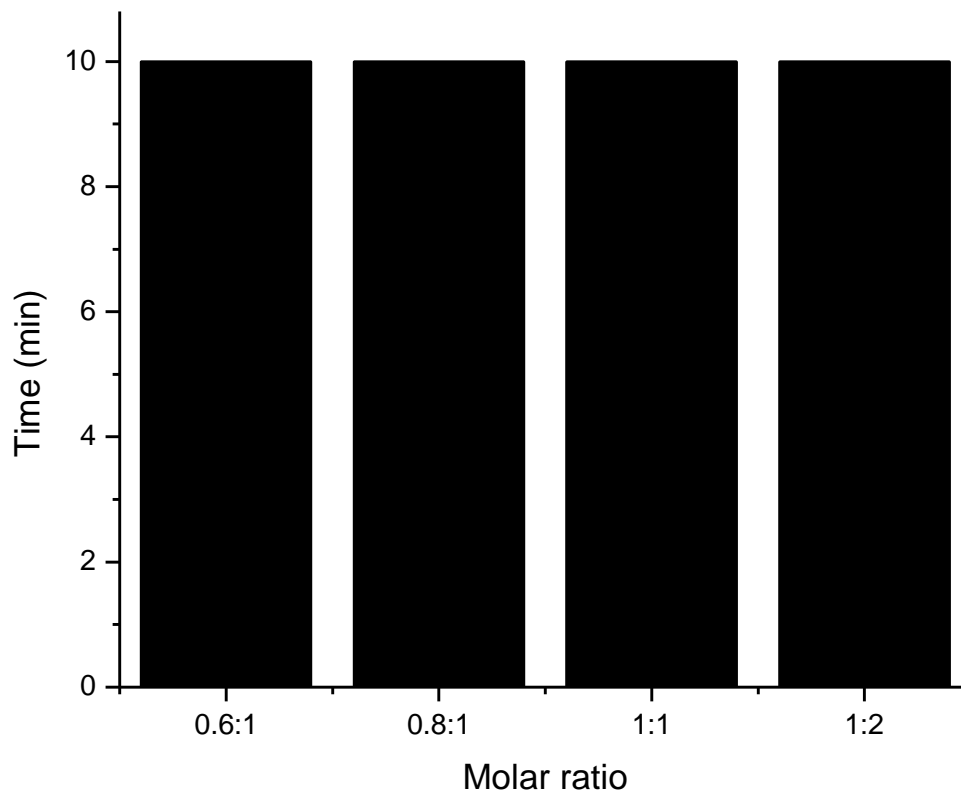


Figure 45: Bar graph comparing the drying time of different RCO based polyurethanes

Figure 45 shows the drying time of RCO based polyurethanes, these paints have a rapid drying of 10 min, such a rapid drying is due to the increased cross link density as the polyol has a high functionality. Yet these coatings lack good elasticity, they formed more of a brittle and rigid film. Thus although the drying seems to be rapid in application. Some additives must be added to further improve the mechanical properties in relation to the elasticity of the paint.

4.5.3. Epoxy resins

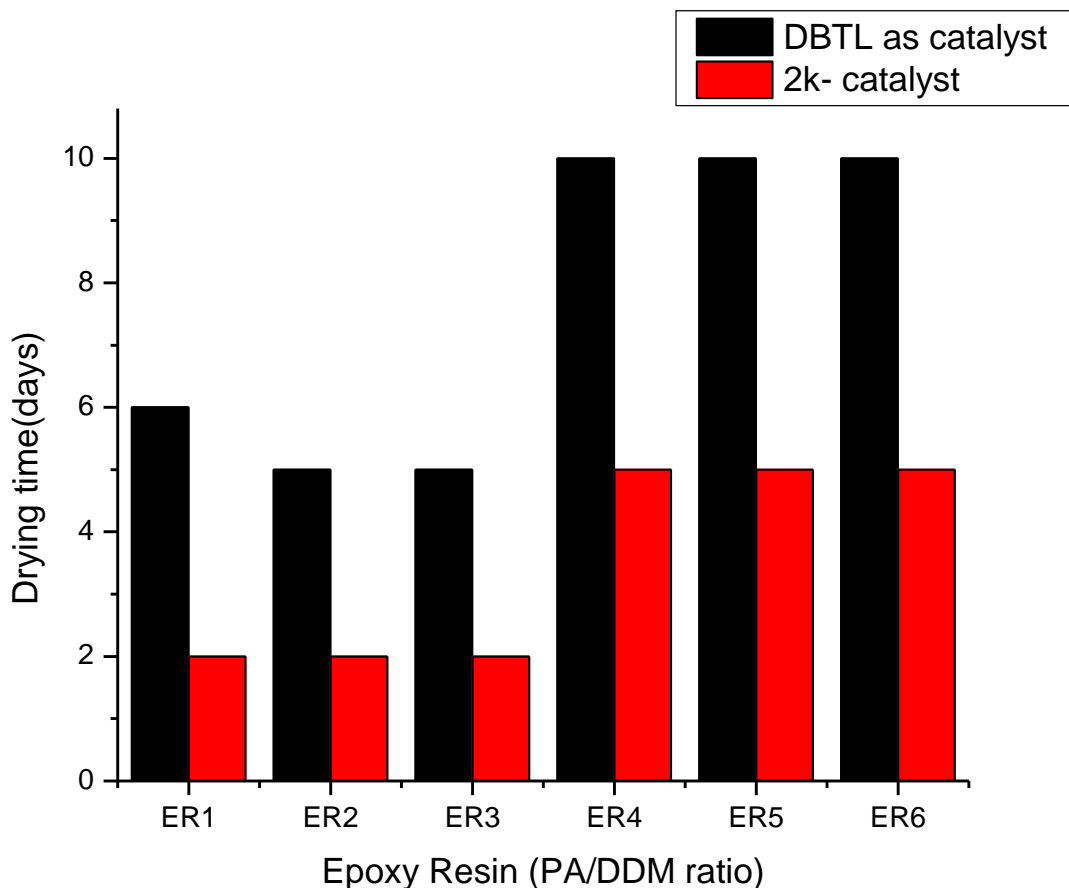


Figure 46: Bar graph comparing the drying time of different ER based paints with PA/DDM as hardener.

During the curing process the epoxy ring being under a lot of strain was easily opened by active hydrogen proton either from an amine (DDM) or carboxylic acid (PA). The synthesized liquid resins were converted into a solid film by the crosslinking of the epoxy and the hardeners. It was observed that the rate of curing/drying was dependant on the molar ratio of hardener to ECO and also on the functionality of ECO and reactivity of the oxirane rings of the ECO since the temperature was kept constant. When the number of epoxy groups is high, having a high reactivity lead to faster cross-linking compared to epoxy resins with lower reactive epoxy groups. The

presence of long and entangled hydrocarbon chains along with epoxy groups not accessible for curing lead to longer drying times of the epoxy resin. ECO may contain hindered oxirane groups that lead slow curing with the hardeners. To accelerate the drying process a drier and 2k additive were added. The amine cured epoxy resins were observed to form a more robust network that had good adhesive characteristics. Increasing the ratio of PA/DDM to ECO had a tremendous effect on the drying time. ER1-ER3 refer to PA based paints and ER4-ER6 refer to DDM based paints in Figure 46. Without a catalyst the drying time was ~ 6 days for the PA based epoxies while ~9 days for the amine epoxies. The addition of the 2k catalyst reduced the drying time to 2days for the PA epoxies and 5 days for DDM epoxies. Although the drying did decrease significantly, the molecular weight is still very low thus there is a need for copolymerization of ECO before epoxy synthesis to increase cross link density.

Chapter 5: Antimicrobial properties of the paint

5.1. Antimicrobial properties

The nanoparticle that was used to impart antimicrobial properties to the different paint formulations was Ag metal. The concentration of Ag NPs added was varied as follows: 0.18, 0.21 and 0.25wt% of the paint formulations. One paint sample was tested when Ag was mixed with TiO_2 , added at 0.21 wt%. Sterile swabs were dipped into broth cultures and used to swab the surfaces of agar plates completely. Each bacteria strain was tested against an undiluted paint sample as the positive control, two diluted paint samples (1/10 and 1/100) and DCO as a negative control. Figure 47 shows the experimental setup for the antimicrobial tests.

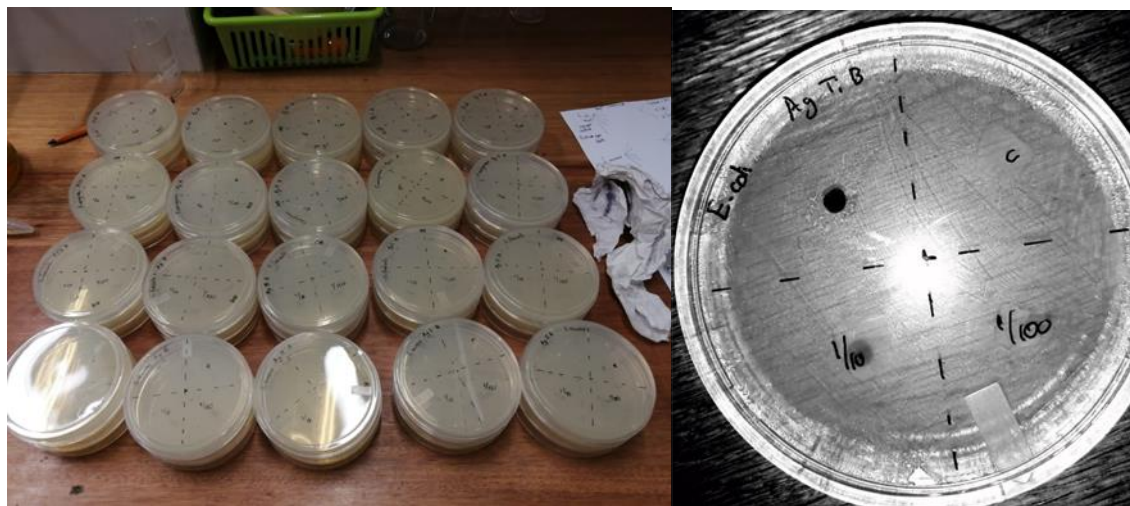


Figure 47: Agar plates before being placed into the incubation room (left) and agar plate spotted with PCO Ag against *Escherichia coli* (right).

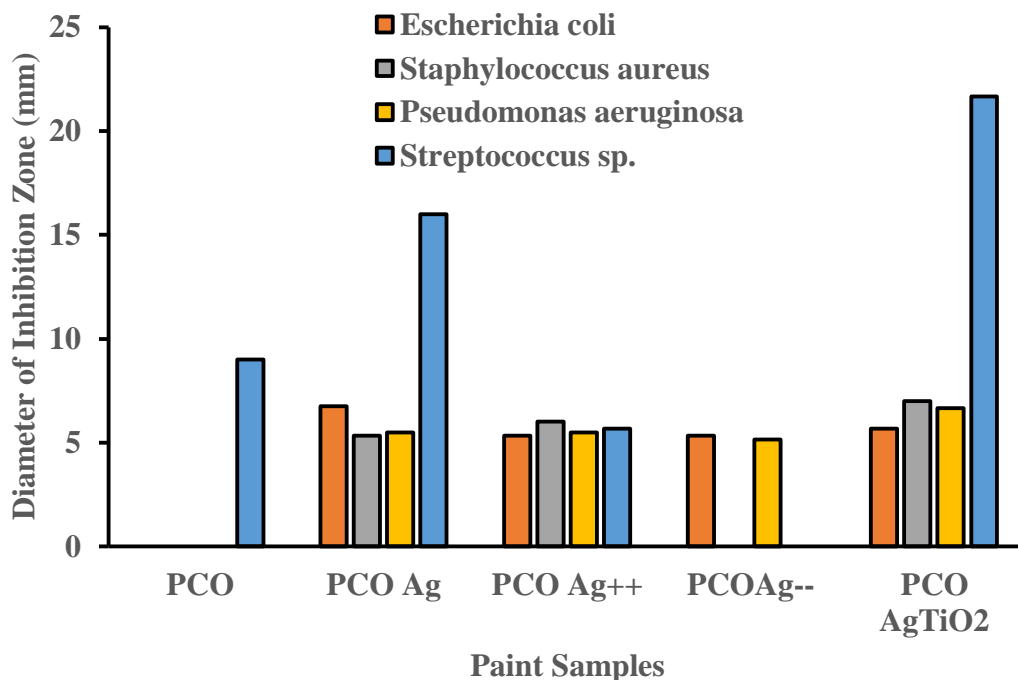


Figure 48: Bar graph showing the inhibition zones for 5 different paint samples exposed to different bacteria.

From Figure 48 it can be seen that the only bacteria that showed susceptibility to the paint samples tested was *Streptococcus sp.* The PCO AgTiO₂ had the highest inhibition zone of 21 mm followed by PCO Ag at 17 mm. This observation is in alignment with literature reviewed by Swaminathan & Sharma, (2018) stating that modified AgNPs have higher growth inhibition towards microbes. *Escherichia coli*, *Pseudomonas aeruginosa*, and *Staphylococcus aureus* showed resistance against the paint samples. For *E.coli*, PCO Ag, PCO Ag++, PCO Ag-- and PCO AgTiO₂ had inhibition zones of 7mm, 5mm, 5mm and 6mm and this pattern was also observed for the other bacteria. PCO Ag-- displayed no inhibition zones for *Staphylococcus aureus* and *Streptococcus sp.* The reason for the absence of inhibition zones for *Escherichia coli*, *Pseudomonas aeruginosa*, and *Staphylococcus aureus* can be attributed to low concentrations of Ag within the paint samples,

thus an increase of this concentration might improve the antimicrobial properties of the samples. The particle size of the Ag and TiO_2 NPs used was 40nm for both as provided commercially. The particle size had the biggest effect in the results obtained, the size of the NPs although in the nanoscale provided a low surface to volume ratio that can lead to low interaction of the NPs with the bacteria. Another factor that may contribute to the trend observed is the agglomeration of the NPs within the paint samples due to the high viscosity of the paint thus hindering a good dispersion during the mixing of the paint formulations.

The differences in the growth inhibition of the NPs studied on both Gram-negative (*Escherichia coli* and *Pseudomonas aeruginosa*) and Gram-positive (*Staphylococcus aureus* and *Streptococcus sp*) bacteria tested can be connected to the differences in the chemical and structural differences in the cell surfaces of the bacteria as cited by Diez-Pascual, (2018). The Gram-negative bacteria outer membrane offers more resistance against substances entering as compared to the Gram-positive hence the high inhibition zones for *Streptococcus sp*. Although *Staphylococcus aureus* is a Gram-positive bacterium, resistance against the NPs can be attributed to the low concentrations of NPs. Thus it can be concluded that *Streptococcus sp* growth inhibition can be obtained at a low concentration of Ag/ AgTiO_2 NPs.

5.2. Anti-radiation properties of the paint

A UV irradiation box fitted with UV lamps was used to expose paint samples to UV radiation. The paint was painted on microscopic slides and placed inside the box for 90 minutes. The paint samples were observed for any changes in gloss under a stereo microscope before UV exposure and after 90 minutes. TiO_2 NPs were added into the paint samples (0.25 wt% of the paint formulation) to give the paint ability to absorb UV radiation. Images from the stereo microscope

were obtained and used to analyse any changes in the paint samples gloss. Figure 49 shows the UV irradiation box for testing the paint for anti-radiation properties.

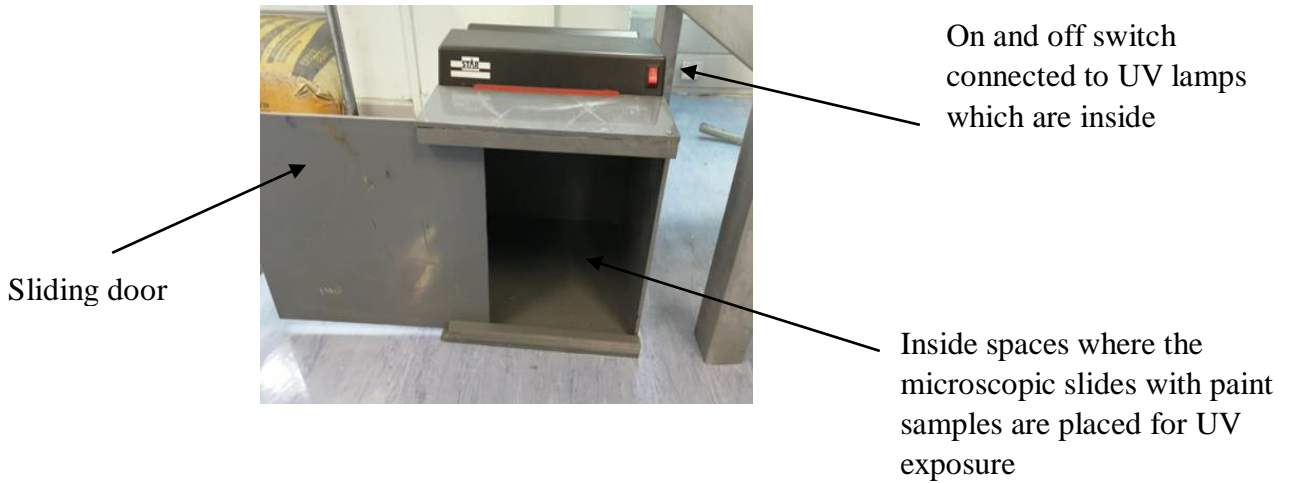


Figure 49: UV irradiation box

Figures 50 and 51 show microscopic images of the paint samples before and after UV irradiation after 90 minutes.

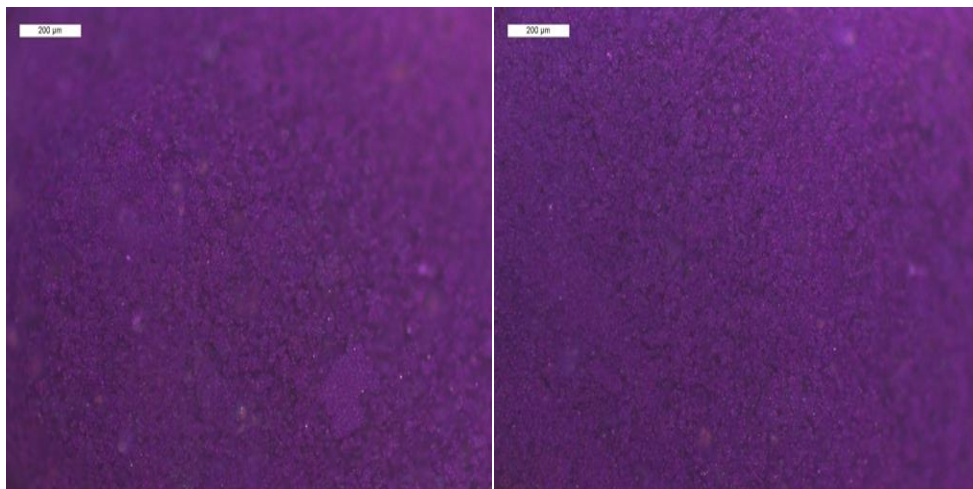


Figure 50: Stereo Microscope Image (200 μ m) for Paint Sample PCO (left) before UV irradiation and (right) 90 minutes after UV irradiation.

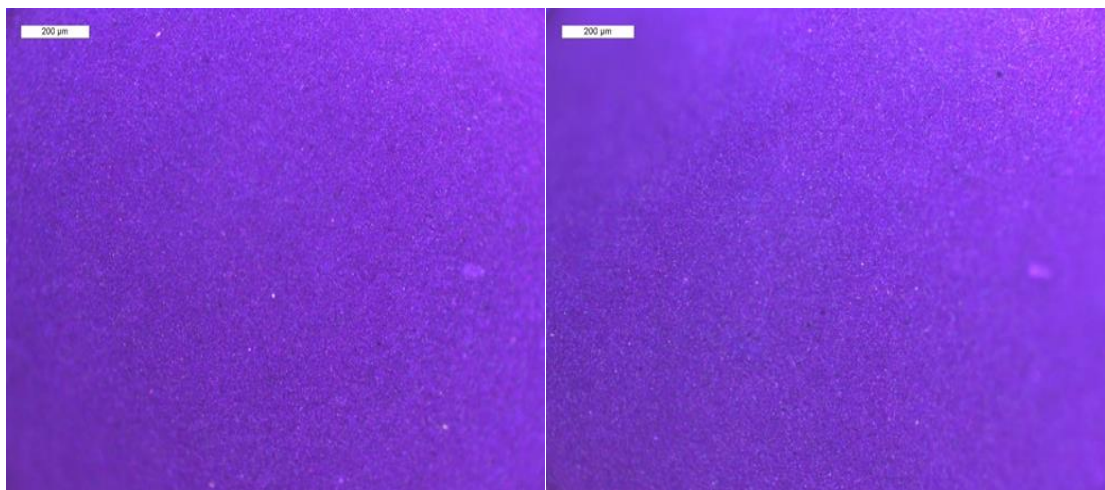


Figure 51: Stereo Microscope Image (200µm) for Paint Sample PCO TiO₂++ (left) before UV irradiation and (right) 90 minutes after UV irradiation.

The stereo microscopic images magnified 200 microns for the paint sample PCO showed some discolouration which is visible in Figure 50 after exposure to UV radiation. This showed that some deterioration was occurring. The paint sample PCO TiO₂++ showed no changes at all after UV irradiation for 90 minutes. This confirmed that the addition of TiO₂ NPs improves the antiradiation properties of the paint sample. The reason for this observation in the paint samples is in agreement with literature. TiO₂ inherently possesses the ability to absorb UV rays and also reflect. Without the addition of these NPs the transmittance of the UV rays is rapid through the PCO (the untreated paint) thus the discolouration within 90 min of exposure. This observation is supported by authors such as Godnjavec et al., (2012), Yang, et al., (2004), Sabzi, et al., (2009) and Godnjavec et al., (2010). The paint formulated can find application in outdoor weather resistant coatings.

Conclusions and Recommendations

Castor oil as a non-edible oil can be used as a substitute for petrochemicals used in the coatings industry. In this study castor oil was modified to produce paints with anti-radiation and antimicrobial properties. Drying oil, polyurethane and epoxy resin were produced as precursors for the production of paint. To increase the functionality of castor oil, chemo-enzymatic epoxidation was done and an epoxide yield of 100% was achieved when CALB was used. After the optimization of the reaction conditions it was found that when the temperature is 35 °C, 4wt% catalyst amount, 1:2 (castor oil: H_2O_2) ratio and 32 hrs reaction time the maximum conversion for castor oil can be achieved. The ECO was then used to synthesize polyol through a ring opening reaction with water as the nucleophile. The catalyst chosen for this reaction was $HClO_4$ as it limits the hydrolysis of the ester linkage during the ring opening reaction. The maximum conversion reached was ~ 70 % at the following reaction conditions: 100 °C temperature 48 hrs reaction time and 1:0.3 mass ratio of oil and $HClO_4$ catalyst amount. The ring opening increases the functionality of castor oil by increasing the number of OH groups. The polyol synthesized was dehydrated to produce a drying oil. The conversion was found to be 43% for CO and 53% RCO respectively when the reaction was done at 240 °C, 0.1 g $NaHSO_4$ for 120 min. The polyol was used to synthesize polyurethanes, which proved not be usable for coatings after the rheology studies were done as the yield value for the coatings was found to be very high thus the coatings have the problem of levelling when applied on a substrate. Polyurethanes were synthesised from CO and these had very good drying time when 2k catalyst was used compared to when only DBTL was used. The drying time reduced from 7 days for some samples to hours. The drying time was measured under atmospheric conditions. Thus the CO based polyurethanes can be used practically when the proper additives are used. The ECO was used to synthesize epoxy based paints. These

paints had a very long drying time of > 7 days even when a 2k catalyst was added, thus the crosslinking density of the resins was very low thus a copolymerization of the ECO is needed in order to increase the molecular weight, leading a higher cross link density. For the testing of antimicrobial and anti-radiation properties Ag and TiO_2 respectively. The paints chosen for testing were the CO based polyurethanes because of the good drying time and also the paints based on the drying oil. It was found that that *Streptococcus sp* growth inhibition can be obtained at a low concentration of Ag/Ag TiO_2 NPs within the paints. The reason for the absence of inhibition zones for *Escherichia coli*, *Pseudomonas aeruginosa*, and *Staphylococcus aureus* can be attributed to low concentrations of Ag within the paint samples, thus an increase of this concentration might improve the antimicrobial properties of the samples. For the anti-radiation properties it was found that paint sample PCO TiO_2 showed no changes at all after UV irradiation for 90 minutes. This confirmed that the addition of TiO_2 NPs improves the antiradiation properties of the paint sample. Thus the paints could be used for outdoor weathering resistant coatings.

After this study it can be recommended that:

- The synthesis of the CO based epoxy paints be done with copolymerisation of ECO to increase the molecular weight thus increasing the crosslinking density to improve the drying time of the oil.
- One should explore the reaction conditions for the dehydration of CO and RCO in-order to further optimize the conversion of the reaction.
- Try alternative route to reduce reaction time for epoxidation and ring opening reactions
- With the RCO based polyurethanes, a plasticiser may added to make them usable as coatings.
- For future work, we suggest the use of a bio-isocyanate for polyurethane synthesis.

- The anti-radiation properties of the paints can be further investigated for X-rays and γ – *rays* radiation attenuation properties.
- Other additives may be evaluated to further improve the antimicrobial and anti-radiation properties of the paints.
- A study on the cost effectiveness of the final coatings should be done.

References

Abdelfattah, M. S. H., Abu-Elgazeed, O. S. M., Mawla, E. A. E. & Abdelazeem, M. A., 2018. On Biodiesels from castor oil using catalytic pyrolysis. *Energy*, Volume 143, pp. 950-960.

Abdullah, Z. T. & Muhammed, S. B., 2021. The impacts of Oil Price on Exchange rate: Evidence from Iraq. *Black Sea Journal of Managemet and Marketing* , 2(3), pp. 1- 11.

Achaya, K., 1971. Chemical Derivatives of Castor Oil. *Journal of the American Oil Chemist's Society*, Volume 48.

Aloui, F. et al., 2007. Inorganic UV absorbers for the photostabilisation of Wood-clearcoating systems: Comparison with Organic UV absorbers. *Applied Surface Science*, Volume 253, pp. 3737-3745.

Alwaseem, H., Donahue, C. J. & Marincean, S., 2014. Catalytic Transfer Hydrogenation of Castor oil. *Journal of Chemical Education*, Volume 91, pp. 575-578.

Ayanlade, A. et al., 2020. When Climate Turns Nasty, What Are Recent and Future Implications? Ecological and Human Health Review of Climate Change Impacts. *Current Climate Change Reports*, Volume 6, pp. 55-65.

Bajwa, A. S., Sathaye, S., Kulkami, V. M. & Patwardhan, A. V., 2016. Chemoenzymatic epoxidation of karanja oil: an alternative to chemical epoxidation?. *Asia-Pacific Journal of Chemical Engineering*, pp. 314-322.

Bechtold, A. et al., 2020. Synthesis and applications of Silver nanoparticles as biocidal agent in polyurethane coating. *J.Coat.Technol.Res*, 17(3), pp. 613 - 620.

Belgacem, M. N. & Gandini, A., 2008. *Monomers, Polymers and Composites from Renewable Resources*. Oxford: Elsevier .

Bhowmick, D. & Sarma, S., 1977. Dehydration of Castor Oil. *Ind. Eng. Chem. Prod. Res. Dev*, 16(1).

Biermann, U. et al., 2000. New synthesis with oils and Fats as Renewable Raw Materials for the Chemical Industry. *Angew. Chem. Int. Ed.*, Volume 39, pp. 2206-2224.

Boda, M., Bhasagi, P., Sawande, A. & Andodgi, 2015. Analysis of Kinematic Viscosity for Liquids by Varying Temperature. *International Journal of Innovative Reserach in Science, Engineering and Technology*, 4(4), pp. 1951-1954.

Bryan, E., 1993. *Chemistry and Technology of Epoxy Resins*. Dordrecht, UK: Springer Science + Business Media.

Carlsson, A. S. et al., 2011. Replacing fossil Oil with Fresh Oil- with what and for what?. *Eur.J. Lipid Sci. Technol*, Volume 113, pp. 812-831.

Carter, R. J. & Bristow, M., 1952. United States Patent Office, Patent No. 2598108.

Cayli, G., Gurbuz, D. & Cinarli, A., 2019. Characterization and Polymerization of Epoxidized Methacrylated Castor Oil. *European Journal of Lipid Science and technology*, 121(1700189).

Chen, G.-L., Chen, G.-B., Li, Y.-H. & Wu, W.-T., 2014. A study of thermal pyrolysis of Castor meal using the Taguchi method. *Energy*, Volume 71, pp. 62-70.

Chong, C. L., 2012. Measurement and Maintenance of Palm Oil Quality. In: *Palm Oil: Production, Processing, Characterization and Uses*. s.l.:Elsevier Inc, pp. 431-470.

Cirule, D. et al., 2021. Enhancing Thermally Modified Wood Stability against Discoloration. *Coatings*, 11(1), p. 81.

Cristea, M. V., Riedl, B. & Blanchet, P., 2010. Enhancing the Performance of Exterior Waterborne coatings for wood by Inorganic nanosized UV absorbers. *Progress in Organic Coatings*, Volume 69, pp. 432-441.

Cunningham, M. F. et al., 2019. Future green Chemistry and Sustainability needs in Polymeric Coatings. *Green Chem*, Volume 21, pp. 4919-4926.

de Cassia de Souza Schneider, R., Lara, L. R. S., Kaercher, J. A. & Schneider, M., 2013. Environmental Impact of Castor oil Catalytic transfer Hydrogenation. *Clean Techn Environ Policy*, Volume 15, pp. 977-985.

de Souza, V. H. R., Silva, S. A., Ramos, L. P. & Zawadzki, S. F., 2012. Synthesis and Characterization of Polyols Derived from Corn oil by Epoxidation and Ozonolysis. *Journal of the American Oil Chemists' Society*, Volume 89, pp. 1723-1731.

De, B., Gupta, K., Mandal, M. & Karak, N., 2014. Biodegradable Hyperbranched Epoxy from Castor oil-based hyperbranched Polyester Polyol. *American Chemical Society Sustainable Chemical Engineering*, Volume 2, pp. 445-453.

Del Rio, E. et al., 2011. Shape Memory Polyurethanes from Renewable Polyols obtained by ATMET Polymerization of Glyceryl Triundec-10-enoate and 10-undecenol. *Macromolecular Chemistry and Physics*, Volume 212, pp. 1392-1399.

Desroches, M. et al., 2012. From Vegetable Oils to Polyurethanes: Synthetic Routes to Polyols and Main Industrial Products. *Polymer Reviews*, Volume 52, pp. 38-79.

- Diamante, L. M. & Lan, T., 2014. Absolute Viscosities of Vegetable Oils at Different Temperatures and Shear Rate Range of 64.5 to 4835 s⁻¹. *Journal of Food processing* , pp. 1-6.
- Diez-Pascual, A. M., 2018. Antimicrobial Coatings Based on Linseed oil/TiO₂ Nanocomposites. In: *Handbook of Antimicrobial Coatings*. Amsterdam: Elsevier, pp. 412-434.
- Diez-Pascual, A. M., 2018. Antimicrobial Coatings Based on Linseed Oil/TiO₂ Nanocomposites. In: *Handbook of Antimicrobial Coatings* . Amsterdam : Elsevier , pp. 411-431.
- Dijkstra, A. J., 2012. Kinetics and Mechanism of the Hydrogenation Process- the state of the art. *Eur.J.Lipid.Technol*, Volume 114, pp. 985-998.
- Ding, J.-F.et al., 2018. Dehydration of Castor Oil over a NaHSO₄/MCM-41 Catalyst Prepared by Supercritical Impregnation. *Chem.Eng.Technol*, 41(11), pp. 2186-2195.
- Douka, A., Vouyiouka, S., Papaspyridi, L.-M. & Papaspyrides, C. D., 2018. A review on Enzymatic Polymerization to produce Polycondensation Polymers: The case of aliphatic polyesters, polyamides and polyesteramides. *Progress in Polymer Science*, Volume 79, pp. 1-25.
- Duleba, J., Czirson, K., Siodmiak, T. & Marszatt, M. P., 2019. Lipase B from *Candida antarctica*- the wide applicable biocatalyst in obtaining pharmaceutical compounds. *Medical Research Journal*, 4(3), pp. 174-177.
- Dyer, J. M., Stymne, S., Green, A. G. & Carlsson, A. S., 2008. High-Value oils from plants. *The plant Journal*, Volume 54, pp. 640-655.
- Ebata, H., Toshima, K. & Matsumura, S., 2007. Lipase-Catalyzed Synthesis and Curing of High-Molecular Weight Polyricinoleate. *Macromolecular Bioscience*, Volume 7, pp. 798-803.

- Elango, R. K. et al., 2019. Transesterification of castor oil for biodiesel production: Process Optimization and Characterization. *Microchemical Journal*, Volume 145, pp. 1162-1168.
- Elmas, T., 2016. Development of a novel radiation shielding Material. *International Journal of Advances in Science Engineering and Technology*, 2 May.4(2).
- Emrani, J. et al., 2018. Synthesis and Characterization of Bio-Based Polyurethane Polymers. *American Journal of Engineering and Applied Sciences* , 11(4), pp. 1298-1309.
- EN ISO 6860, 2006. *Paints and Varnishes- Bend test (Conical Mandrel)*, s.l.: s.n.
- Erhan, S. Z., 2005. *Industrial Uses of Vegetable Oils*. Champaign, Illinois : AOCS Press.
- Esen, H. & Cayli, G., 2016. Epoxidation and Polymerization of acrylated Castor oil. *European Journal of Lipid Science and Technology*, Volume 118, pp. 959-966.
- Esmaili, J. & Rahimpour, F., 2017. Regeneration of spent Nickel Catalyst from hydrogenation Process of edible oils: Heat Treatment with Hydrogen Injection. *International Journal of Hydrogen Energy*, Volume 42, pp. 24197-24204.
- European Standard [DIN EN ISO 4624], 2003. *Paints, Varnishes and Plastics* , Brussels: s.n.
- Evans, B. R., Lian, J. & Ji, W., 2018. Evaluation of shielding performance for newly developed composite materials. *Annals of Nuclear Energy*, Volume 116, pp. 1-9.
- Fadhil, A. B., Al-Tikrity, E. T. & Albadree, M. A., 2017. Biodiesel production from mixed non edible oils, Castor seed oil and Waste Fish oil. *Fuel*, Volume 210, pp. 721-728.
- Fakhruddin, K. S. et al., 2020. Clinical efficacy and the antimicrobial potential of Silver formulations in arresting dental caries: a systematic review. *BMC Oral Health*, 20(160), pp. 1-13.

Fan, X., Burton, R. & Yongchang, Z., 2010. Glycerol (Byproduct of Biodiesel Production) as a source for Fuels and Chemicals: Mini Review. *The Open Fuels & Energy Science Journal*, Volume 3, pp. 17-22.

Giakoumis, E. G., 2018. Analysis of 22 Vegetable oils' physico-chemical properties and fatty acid composition on a statistical basis, and correlation with the degree of unsaturation. *Renewable Energy*, Volume 126, pp. 403-419.

Gibson, G., 2017. Epoxy Resins. In: *Brydson's Plastics Materials (8th Edition)*. s.l.:Elsevier, pp. 773-797.

Gilbert, E., 1941. *The Unique Chemistry of Castor Oil*.

Godnjavec, J., Znoj, B., Venturini, P. & Znidarsic, A., 2010. The application of rutile nanocrystalline Titanium Dioxide as UV absorber. *Informacije MIDEA*, Volume 40, pp. 6-9.

Godnjavec, J. et al., 2012. Stabilization of rutile TiO₂ Nanoparticles with GLYMO in Polyacrylic clear coating. *Materials and Technology*, Volume 46, pp. 19-24.

Goldschmidt, A. & Streitberger, H.-J., 2007. *BASF Handbook on Basics of Coating Technology*. Germany: Vincentz Network .

Goldschmidt, A. & Streitberger, H.-J., 2007. *Basics of Coating Technology*. Munster/Germany: BASF Coatings.

Gonzalez, M. G., Cabanelas, J. C. & Baselga, J., 2012. Applications of FTIR on epoxy resins-identification, monitoring the curing process, phase separation and water uptake . In: *Infrared Spectroscopy- Materials Science, Engineering and Technology*. Rijeka, Croatia: InTech, pp. 261-284.

- Gonzalez, M. G. C. J. C. & Baselga, J., 2012. Applications of FTIR on Epoxy Resins- Identification, Monitoring the Curing process, Phase Separation and Water Uptake. In: *Infrared Spectroscopy-Materials Science, Engineering and Technology*. s.l.:Intechopen, pp. 261-284.
- Guner, F. S., 1997. Castor oil dehydration Kinetics. *JAOCS*, 74(4).
- Guner, F. S., Yagcl, Y. & Erciges, A., 2006. Polymers from triglyceride oils. *Progress in Polymer Science*, Volume 31, pp. 633-670.
- Gunstone, F. D., 2002. *Vegetable Oils in Food Technology: Composition, Properties and Uses*. Oxford: Blackwell Publishing .
- Gunstone, F. D., 2004. *The Chemistry of Oils and Fats: Source, Composition, Properties and Uses*. Oxford: Blackwell Publishing .
- Guo, A. & Petrovic, Z., 2005. Vegetable Oil-Based Polyols. In: *Industrial Uses of Vegetable Oils*. Champaign, Illinois : AOCS Press, pp. 116-136.
- Hablot, E., Zheng, D., Bouquey, M. & Averous, L., 2008. Polyurethanes Based on Castor Oil: Kinetics, Chemical, Mechanical and Thermal Properties. *Macromolecular Materials and Engineering*, Volume 293, pp. 922-929.
- He, D. & Liu, L., 2019. Analytical Aspects of Rice Bran Oil. In: *Rice Bran and Rice Bran Oil: Chemistry, Processing and Utilization* . s.l.:Elsevier , pp. 169-181.
- Hernandez, E., Mosiewicki, M. A. & Marcovich, N. E., 2020. Bio-Based Polymers Obtained from Modified Fatty Acids and Soybean Oil with Tailorable Physical and Mechanical Performance. *European Journal of Lipid Science and Technology*, 122(10), pp. 1-12.

Hill, K., 2000. Fats and Oils as Oleochemical raw materials. *Pure and Applied Chemistry*, 72(7), pp. 1255-1264.

Hlaing, N. N. & Oo, M. M., 2008. Manufacture of Alkyd Resin from castor oil. *World Academy of Science, Engineering and Technology*, Volume 48.

Hochmannova, L. & Vytrasova, J., 2010. Photocatalytic and antimicrobial effects of interior paints. *Progress in Organic Coatings*, Volume 67, pp. 1-5.

Huang, M.-T. & Zhai, P.-M., 2021. Achieving Paris Agreement temperature goals requires carbon neutrality by middle century with far-reaching transitions in the whole society. *Advances in Climate Change Research*, Volume 12, pp. 281-286.

International Organisation for Standardization [ISO], 2006. *Paints and Varnishes- Cross-cut test (ISO 2409)*, Switzerland: s.n.

Ionescu, M., 2005. *Chemistry and Technology of Polyols for Polyurethanes*. Shawbury: Rapra Technology.

Ionescu, M. et al., 2016. Highly functional polyols from castor oil for rigid polyurethanes. *European Polymer Journal*, Volume 84, pp. 736-749.

Jenkin, N., Molebatsi, P., Ramsarup, P. & Dr Rosenberg, E., 2016. *Green Skills in the South African Surface Coatings Sector: A focus on paint*, s.l.: s.n.

Jian-Fei, D. et al., 2018. Dehydration of Castor Oil over a NaHSO₄/MCM-41 catalyst prepared by supercritical Impregnation. *Chemical Engineering Technology*, 41(11), pp. 2186-2195.

Jirous-Rajkovic, V. & Mikleic, J., 2021. Enhancing Weathering Resistance of Wood - A Review. *Polymers*, 13(2), p. 1980.

Jones, F. N., Nichols, M. E. & Pappas, S. P., 2017. *Organic Coatings: Science and Technology*. USA: John Wiley & Sons, Inc.

Kansara, K. S. S., Parmar, R. & Patel, N., 2004. High Solids Polyurethane Coatings from Castor Oil based Polyester Polyols. *International Journal of Polymeric Materials*, Volume 53, pp. 283-293.

Karak, N., 2012. Vegetable oil-based epoxies. In: *Vegetable Oil-Based Polymers: Properties, Processing and Applications*. s.l.:Woodhead Publishing Limited , pp. 180-207.

Karmakar, G. et al., 2021. A Short Review on Polymeric Biomaterials as Additives for Lubricants. *Polymers*, Volume 13, p. 1333.

Keera, S., El Sabagh, S. & Taman, A., 2018. Castor Oil biodiesel Production and Optimization. *Egyptian Journal of Petroleum*.

Kemp, W., 1986. *NMR IN CHEMISTRY: A Multinuclear Introduction*. London: THE MACMILLAN PRESS LTD.

Khiratkar, A. G. et al., 2018. Transesterification of Castor Oil using benzimidazolium based Bronsted acid ionic liquid catalyst. *Fuel*, Volume 231, pp. 458-467.

Kim, J. S. et al., 2007. Antimicrobial effects of Silver nanoparticles. *Nanomedicine: Nanotechnology, Biology, and Medicine*, Volume 3, pp. 95-101.

Kirk-Othmer, 2004. *Kirk-Othmer Encyclopedia of Chemical Technology*. s.l.:John Wiley & Sons.

Klaas, M. R. g. & Warwel, S., 1999. Complete and Partial epoxidation of plant oils by lipase-catalyzed perhydrolysis. *Industrial Crops and Products*, Volume 9, pp. 125-132.

Komorowska-Durka, M., Dimitrakis, G., Bogdal, D. & Stankiewics, A. S. G. D., 2015. A Concise review on microwave-assisted polycondensation reactions and curing of polycondensation polymers with focus on the effect of process conditions. *Chemical Engineering Journal*, Volume 264, pp. 633-644.

Krstic, J. et al., 2015. Influence of Ni/SiO₂ activity on the reaction pathway in Sunflower oil hydrogenation. *Chemical Engineering Research and Design*, Volume 100, pp. 72-80.

Kundurur, K. R., Basu, A., Zoda, M. H. & Domb, A. J., 2015. Castor Oil-Based Biodegradable Polyesters. *Biomacromolecules*, Volume 16, pp. 2572-2587.

Lafarga, T., BObo, G. & Aguilo-Aguayo, I., 2021. *Oil and Oilseed Processing Opportunities and Challenges*. USA: John Wiley & Sons Ltd.

Lebarbe, T., 2014. Synthesis of novel "green" polyesters from plant oils: application to the rubber-toughening of poly (L-lactide).

Lee, J. H., Kim, S. H. & Oh, K. W., 2021. Bio-Based Polyurethane Foams with Castor Oil Based Multifunctional Polyols for Improved Compressive Properties. *Polymers* , 13(4), p. 576.

Liang, D. et al., 2019. Tunable thermo-physical performance of castor oil-based polyurethanes with tailored release of coated fertilizers. *Journal of Cleaner Production*, Volume 210, pp. 1207-1215.

Liang, H. et al., 2018. Castor oil-based Cationic waterborne polyurethane dispersions: Storage stability, thermo-physical properties and antibacterial properties. *Industrial Crops and Products*, Volume 117, pp. 169-178.

- Liang, H. et al., 2018. Aqueous anionic polyurethane dispersions from castor oil. *Industrial Crops & Products*, Volume 122, pp. 182-189.
- Li, R. et al., 2017. Gamma ray shielding property, shielding mechanism and predicting model of continuous basalt fiber reinforced polymer matrix composite containing functional fiber. *Materials and Design*, Volume 124, pp. 121-130.
- Liu, C., Li, J., Lei, W. & Zhou, Y., 2014. Development of biobased unsaturated polyester resin containing highly functionalized castor oil. *Industrial Crops and Products*, Volume 52, pp. 329-337.
- Liu, Y. & Mecking, S., 2019. A synthetic Polyester from Plant Oil Feedstock by Functionalizing Polymerization. *Angewandte Chemie*, Volume 131, pp. 3384-3388.
- Lligas, G., Ronda, J. c., Galia, M. & Cadiz, V., 2013. Renewable Polymeric Materials from Vegetable Oils: a perspective. *Materials Today*, 16(9).
- Macalino, A., Salen, V., Reyes & LQ, 2017. Castor Oil Based Polyurethane: Synthesis and Characterization. *Materials Science and Engineering* , Volume 229.
- Madbouly, S. A., Zhang, C. & Kessler, M. R., 2016. *Bio-Based Plant Oil Polymers and Composites*. Amsterdam: Elsevier Inc.
- Mahltig, B., 2018. Metal Pigments as Antimicrobial Agent and Coating Additives. In: *Handbook of Antimicrobial Coatings*. Amsterdam : Elsevier, pp. 283-298.
- Mahltig, B. et al., 2005. Optimized UV protecting Coatings by combination of Organic and Inorganic UV absorbers. *Thin Solid Films*, Volume 485, pp. 108-114.

Mamudu, A. O. et al., 2019. Effects of Sodium Bisulphate Catalyst on the Dehydration of Castor Oil for the paint Industry. *International Journal of Mechanical Engineering and Technology*, 10(03), pp. 353-363.

Manawwer, A. et al., 2014. Vegetable oil based eco-friendly coating materials: A review Article. *Arabian Journal of Chemistry*, Volume 7, pp. 469-479.

Mannari, V. & Patel, C. J., 2015. *Understanding Coatings Raw Materials*. Hanover: Vincentz Network .

Martinelli, M. et al., 2005. Castor oil Hydrogenation by a Catalytic Hydrogen Transfer System using Limonene as Hydrogen Donor. *JAACS*, 82(4).

Martino, L. et al., 2014. Bio-based polyamide 11: Synthesis, rheology and solid-state properties of star structures. *European Polymer Journal*, Volume 59, pp. 69-77.

Matyjaszewski, K. & Davis, T. P., 2002. *Handbook of Radical Polymerization*. Hoboken : John Wiley & Sons.

Meier, M. A., Metger, J. O. & Schubert, U. S., 2007. Plant oil renewable resources as green alternatives in polymer science. *Chemical Society Reviews*, Volume 36, pp. 1788-1802.

Mensah, A. J. A. M. & Brien, P., 2018. Castor oil: A suitable green source of capping agent for nanoparticle synthesis and facile surface functionalization. *Royal Society Open Science*, Volume 5, p. 180824.

Mensah, M., Awudza, J. & O'Brien, P., 2018. Castor oil: a suitable green source of capping agent for the nanoparticle syntheses and facile surface functionalization. *Royal society open science*, 5(180824).

- Metzger, J. O., 2009. Fats and Oils as renewable feedstock for Chemistry. *European Journal of Lipid Science Technology*, Volume 111, pp. 865-876.
- Miao, S., Wang, P., Su, Z. & Zhang, S., 2014. Vegetable-oil-based polymers as future polymeric biomaterials. *Acta Biomaterialia*, Volume 10, pp. 1692-1704.
- Mischke, P., 2010. *Film Formation in Modern Paint Systems*. Hannover: Vincentz Network .
- Moghadam, P. N., Yarmohamadi, M., Hasanzadeh, R. & Nuri, S., 2016. Preparation of Polyurethane wood adhesives by polyols formulated with polyester polyols based on Castor oil. *International Journal of Adhesion & adhesives*, Volume 68, pp. 273-282.
- Moreno, A. et al., 2018. Linear and branched acetal polymers from castor oil via acetal metathesis polymerization. *European Polymer Journal*, Volume 108, pp. 348 - 356.
- Mortley, A., Bonin, H. & Bui, V., 2007. Synthesis and Properties of radiation modified thermally cured Castor oil based Polyurethanes. *Nuclear Instruments and Methods in Physics Research B*, Volume 265, pp. 98-103.
- Mubofu, E., 2016. Castor oil as a potential renewable resource for the production of functional materials. *Sustainable Chemical Processes*, 4(11).
- Muller, B., 2010. *Understanding Additives*. Hannover: Vincentz Network .
- Muller, B. & Poth, U., 2011. *Coatings Formulation*. 2nd Revised Edition ed. Hannover: Vincentz Network .
- Mutlu, H. & Meier, M. A. R., 2010. Castor oil as a renewable resource for the chemical industry. *Eur. J. Lipid Sci. Technol.*, Volume 112, pp. 10-30.

Naughton, F. C., 1974. Production, Chemistry, and Commercial Applications of Various Chemicals from castor oil. *Journal of the American Oil Chemists' Society*, Volume 51.

Navas, M. B. et al., 2018. Transesterification of Soybean and Castor oil with methanol and butanol using heterogenous basic catalysts to obtain biodiesel. *Chemical Engineering Science*, Volume 187, pp. 444-454.

Negrell, C. et al., 2016. Self-extinguishing bio-based Polyamides. *Polymer Degradation and Stability*, Volume 134, pp. 10-18.

Nekhavambe, E., Mukaya, H. E. & Nkazi, D. B., 2019. Development of Castor Oil-based Polymers: review. *Journal of Advanced Manufacturing and Processing*.

Nezihe, A., Elif, D., Ozlem, Y. & Tuncer, E. A., 2011. Microwave Heating Application to Produce Dehydrated Castor oil. *Ind.Eng.Chem.Res*, Volume 50, pp. 398-403.

Nikolic, G. et al., 2010. Fast Fourier Transform IR Characterization of Epoxy GY systems Crosslinked with Aliphatic and Cycloaliphatic EH polyamine Adducts. *Sensors*, Volume 10, pp. 684-696.

Noreen, A. et al., 2016. Bio-based polyurethane: An efficient and environmentally friendly coating systems: A review. *Progress in Organic Coatings*, Volume 91, pp. 25-32.

Odian, G., 2004. *Principles of Polymerization*. New Jersey: John Wiley & sons.

O'Donnel, J. H., 1989. Radiation Chemistry of polymers. *American Chemical Society* .

Ozdemir, T. & Yilmaz, S. N., 2018. Mixed radiation shielding via 3-layered polydimethylsiloxane rubber composite containing hexagonal boron nitride, boron oxide, bismuth oxide for each layer. *Radiation Physics and Chemistry*, Volume 152, pp. 17-22.

Palanichamy, S. & Subramanian, G., 2017. Antifouling properties of marine bacteriocin incorporated epoxy based paint. *Progress in Organic Coatings*, Volume 103, pp. 33-39.

Paluvai, N. R., Mohanty, S. & Nayak, S. K., 2015. Fabrication and Evaluation of acrylated epoxidized Castor oil-Toughened Diglycidyl Ether of Bisphenol A Nanocomposites. *The Canadian Journal of Chemical Engineering*, Volume 93, pp. 2107-2116.

Paluvai, N. R., Smita, M. & Nayak, S., 2015. Mechanical and thermal properties of Sisal fiber reinforced acrylated epoxidized castor oil toughened diglycidyl ether of bisphenol A epoxy nanocomposites. *Journal of Reinforced Plastics and Composites*, 34(18), pp. 1476-1490.

Paraskar, P. M., Prabhudesai, M. S., Hatkar, V. M. & Kulkarni, R. D., 2021. Vegetable Oil based Polyurethane Coatings- A Sustainable approach: A review. *Progress in Organic Coatings*, Volume 156, p. 106267.

Patle, D. S. et al., 2018. Ultrasonication - Assisted and Benzimidazolium - Based Bronsted Acid Ionic Liquid- Catalyzed Transesterification of Castor Oil. *ACS Omega*, Volume 3, pp. 15455-15463.

Patterson, H., 2011. Quality and Control. In: *Hydrogenation of Fats and Oils: Theory and Practice* . s.l.:Elsevier , pp. 329-350.

Perin, G. et al., 2008. Transesterification of Castor Oil assisted by microwave irradiation. *Fuel*, Volume 87, pp. 2838-2841.

Pin, J.-M. & Sbirrazzuoli, N. M. A., 2015. From Epoxidized Linseed oil to Bioresin: An overall Approach of Epoxy/Anhydride Cross-Linking. *ChemSusChem*, Volume 8, pp. 1232-1243.

Pradhan, S., Pandey, P., Mohanty, S. & Nayak, S. R., 2016. Insight on the Chemistry of Epoxy and its Curing for Coating Applications: A Detailed Investigation and Future Perspectives. *Polymer-Plastics Technology and Engineering*, 55(8), pp. 862 - 877.

Pramanik, S., Sagar, K., Konwar, B. K. & Karak, N., 2012. Synthesis, Characterization and Properties of a Castor oil modified biodegradable poly(ester amide) resin. *Progress in Organic Coatings*, Volume 75, pp. 569-578.

Ramezani, K., Rowshanzamir, S. & Eikani, M., 2010. Castor oil Transesterification reaction: A kinetic Study and Optimization of parameters. *Energy*, Volume 35, pp. 4142-4148.

Rojas, M. F. et al., 2017. New biocomposites based on Castor oil polyurethane foams and ionic liquids for CO₂ capture. *Fluid Phase Equilibria*, Volume 452, pp. 103-112.

Roudsari, G. M., Mohanty, A. K. & Misra, M., 2017. Green Approaches to Engineer Tough Biobased Epoxies: A Review. *ACS Sustainable Chemistry & Engineering*, Volume 5, pp. 9528-9541.

Ruiz, L. et al., 2019. Synthesis of acid degradable oxidation responsive poly(β -thioetherester)s from castor oil. *European polymer Journal*, Volume 110, pp. 183-191.

Sabzi, M., Mirabedini, S., Zohuriaan-Mehr, J. & Atai, M., 2009. Surface modification of TiO₂ nano-particles with Silane coupling agent and Investigation of its effect on the properties of polyurethane composite coating. *Progress in Organic Coatings*, Volume 65, pp. 222-228.

Sahoo, S., Kalita, H., Mohanty, S. & Nayak, S. K., 2016. Synthesis of Vegetable Oil-Based Polyurethane: A Study on Curing Kinetics Behaviour. *International Journal of Chemical Kinetics*, Volume 48, pp. 622-634.

Salihu, B. Z., Gana, A. K. & Apuyor, B. O., 2014. Castor Oil plant (*Ricinus Communis L.*) : Botany, ecology and uses. *International Journal of Science and Research*, 3(5), pp. 1333-1341.

Salimon, J., Salih, N. & Yousif, E., 2012. Industrial Development and Applications of Plant Oils and their biobased Oleochemicals. *Arabian Journal of Chemistry*, Volume 5, pp. 135-145.

Sanchez M, J. F., Boldrini, D. E., Tonetto, G. M. & Damiani, D. E., 2011. Palladium Catalyst on anodized aluminum monoliths for the partial hydrogenation of vegetable oil. *Chemical Engineering Journal*, Volume 167, pp. 355-361.

Sankaranarayanan, S. & Srinivasan, K., 2015. Preparation of functionalized Castor oil derivatives with tunable physical properties using heterogenous acid and base catalyst. *Royal Society of Chemistry*, Volume 5, pp. 50289-50297.

Sanyang, M. L. & Jawaid, M., 2019. *Biobased Polymers and Nanocomposites: Preparation, Processing, Properties & Performance*. Switzerland: Springer Nature.

Sathiskumar, P. & Gridhar, M., 2011. Synthesis, Characterization, degradation of biodegradable Castor oil based polyesters. *Polymer Degradation and Stability*, Volume 96, pp. 1695-1704.

Scholz, V. & da Silva, J. N., 2008. Prospects and risks of the use of Castor oil as a Fuel. *Biomass and Bioenergy*, Volume 32, pp. 95-100.

Scrimgeour, C., 2005. Chemistry of Fatty Acids. In: *Bailey's Industrial Oil and Fat Products* . s.l.:John Wiley & Sons, Inc, pp. 1- 44.

Severino, L. S. et al., 2012. A review on the challenges for increased production of castor. *Agronomy Journal*, 104(4).

Shahzad, U., 2015. The Need For Renewable Energy Sources. *International Journal of Information Technology and Electrical Engineering* .

Shaik, A., Baidya, K., Nehete, K. & Shyamroy, S., 2019. Synthesis and Characterization of Castor-oil based branched polyols from renewable resources and their Polyurethane-Urea Coatings. *J.Coat.Technol.Res.*, 16(2), pp. 387- 400.

Shaik, M. R., Alam, M. & Alandis, N. M., 2015. Development of Castor Oil Based Poly (urethane-esteramide) / TiO₂ Nanocomposites as Anticorrosive and Antimicrobial Coatings. *Journal of Nanomaterials* , pp. 1-10.

Shao, C.-H.et al., 2014. Monitoring of radiation dose rates around a clinical nuclear medicine site. *Radiation Physics and Chemistry*, Volume 104, pp. 124-128.

Sharma, B. K., Adhvaryu, A., Liu, Z. & Erhan, S. Z., 2006. Chemical Modification of Vegetable oils for Lubricant Applications. *JAOCs*, 83(2), pp. 130-136.

Sharma, C. et al., 2016. A Pre-Polyaddition mediation of Castor Oil for polyurethane formation. *Journal of Applied Polymer Science*.

Sharma, V. & Kundu, P., 2008. Condensation Polymers from natural oils. *Progress in Polymer Science*, Volume 33, pp. 1199-1215.

Silva, A. L. & Bordado, J. C., 2004. Recent Developments in Polyurethane Catalysis: Catalytic Mechanisms Review. *Catalysis Reviews*, 46(1), pp. 31-51.

Singh, A., Tiwari, A., Bajpai, J. & Bajpai, A. K., 2018. Polymer-Based Antimicrobial Coatings as Potential Biomaterials from Action to Application . In: *Handbook of Antimicrobial Coatings* . Amsterdam : Elsevier , pp. 27-61.

Snezana Sinadinovic-Fiser, Milovan Jankovic, Olga Borota, 2012. Epoxidation of castor oil with peracetic acid formed in situ in the presence of an ion exchange resin. *Chemical Engineering and Processing*, Volume 62, pp. 106-113.

Soliman, H., Elsayed, A. & Dyaa, A., 2018. Antimicrobial activity of Silver nanoparticles biosynthesized by *Rhodotorula* Sp. Strain ATL72. *Egyptian Journal of Basic and Applied Sciences*, Volume 5, pp. 228-233.

Sondi, I. & Salopek-Sondi, B., 2004. Silver nanoparticles as antimicrobial agent: a case study on *E. Coli* as a model for Gram-negative bacteria. *Journal of Colloid and Interface Science*, Volume 275, pp. 177-182.

Swaminathan, M. & Sharma, N. K., 2018. Antimicrobial Activity of Engineered Nanoparticles Used as Coating agents. In: *Handbook of Ecomaterials*. Switzerland: Springer International Publishing , pp. 1-16.

Swamy, K. B., Siddaramaiah & Somashekah, R., 2003. Structure-Property relationship of Castor Oil based diol chain extended polyurethane (PUs). *Journal Of Materials Science*, Volume 38, pp. 451-460.

Tallent, W. & Sumrell, G., 1974. Production, Chemistry and Commercial Applications of Various Chemicals from Castor Oil. *Journal of the American Oil Chemists' Society*, Volume 51.

Tammekivi, E., Vahur, S., Vilbaste, M. & Leito, I., 2021. Quantitative GC-MS Analysis of Artificially Aged Paints with Variable Pigment and Linseed Oil Ratios. *Molecules* , 26(8), p. 2218.

Tayde, S., Thorat, P. & Sonawane, A., 2017. Synthesis of Polyurethane Coating using Castor oil as a bio-polyol and its Characterization. *International Journal of Scientific Development and Research*, 2(4), pp. 254 - 264.

Tenorio-Alfonso, A., Pizarro, M., Sanchez, M. & France, J., 2018. Assessing the rheological properties and adhesion performance on different substrates of a novel green polyurethane based on Castor oil and cellulose acetate: A comparison with commercial adhesives. *International Journal of Adhesion and Adhesives*, Volume 82, pp. 21-26.

Tesser, R. et al., 2020. Oleochemistry Products . In: *Industrial Oil Plant*. Singapore: Springer, pp. 201-268.

Thakur, S. & Karak, N., 2013. Castor oil-based hyperbranched polyurethane as advanced surface coating materials. *Progress in Organic Coatings*, Volume 76, pp. 157-164.

Tiwari, A. & Chaturvedi, A., 2018. Antimicrobial Coatings- Technology Advancement or Scientific Myth . In: *Handbook of Antimicrobial Coatings* . Amsterdam : Elsevier , pp. 1-5.

Tomvall, U., Orellana-Coca, C., Hatti-Kaul, R. & Adlercreutz, D., 2007. Stability of immobilized *Candida antarctica* lipase B during Chemo-enzymatic epoxidation of fatty acids. *Enzyme and Microbial Technology*, Volume 40, pp. 447-451.

Tondi, G. & Schnabel, T., 2020. Bio-Based Polymers for Engineered Green Materials. *Polymers*, 12(775), pp. 1- 4.

Torato, G. et al., 2014. Synthesis of Castor oil-derived Polyesters with antimicrobial activity. *European Polymer Journal*, Volume 56, pp. 174-184.

Tracton, A. A., 2006. *Coatings Technology Handbook*. New York: Taylor & Francis Group, LLC.

Trovati, G. et al., 2019. Production and Characterization of Polyurethane Castor oil (*Ricinus Communis*) foam for nautal. *Polymer Testing*, Volume 73, pp. 87-93.

Tumosa, C. S. & Mecklenburg, M. F., 2012. Oil Paints: The Chemistry of Drying Oils and the Potential for Solvent Disruption. *Smithsonian Contributions to Museum Conservation*, Volume 3, pp. 52-58.

Van De Mark, M. R. & Sandefur, K., 2005. Vegetable Oils in Paint and Coatings. *Inform*, 16(8).

Vasilev, K., 2019. Nanoengineered Antibacterial Coatings and Materials: A Perspective. *Coatings*, 9(654), pp. 1-12.

Vlcek, T. & Petrovic, Z. S., 2006. Optimization of the Chemoenzymatic Epoxidation of Soybean Oil. *JAOCs*, 83(3), pp. 247-252.

Wang, X. et al., 2019. Synthesis and Properties of Castor oil-based waterborne polyurethane/Sodium alginate composites with tunable properties. *Carbohydrate Polymers*, Volume 208, pp. 391-397.

Wigg, D., 2007. Radiation: Facts , Fallacies and Phobias. *Australasian Radiology*, Volume 51, pp. 21-25.

Winklaar, A., 2009. *Coatings Basics*. Hannover: Vincentz Network .

Wool, R. P. & Sun, X. S., 2005. *Bio-based polymers and composites*. s.l.:Elsevier.

Wool, R. P. & Sun, X. S., 2005. *Bio-based Polymers and Composites*. s.l.:Elsevier Science & Technology.

Xing, J. et al., 2021. Preparation of Efficient Ultraviolet-Protective Transparent Coating by Using a Titanium-containing Hybrid Oligomer. *ACS Appl.Mater.Interfaces*, 13(4), pp. 5592-5601.

- Xu, H. et al., 2020. Plasticization Effect of Bio-Based Plasticizers from Soybean Oil for Tire Tread Rubber. *Polymers*, 12(3), p. 623.
- Yang, F., Hanna, M. A. & Sun, R., 2012. Value- Added uses for Crude Glycerol- a Product of biodiesel production. *Biotechnology for Fuels*, 5(13).
- Yang, H., Zhu, S. & Pan, N., 2004. Studying the Mechanisms of Titanium Dioxide as Ultraviolet-Blocking Additive for Films and Fabrics by an Improved Scheme. *Journal of Applied Polymer Science*, Volume 92, pp. 3201-3210.
- Yokozawa, T. & Yokoyama, A., 2007. Chain-growth polymerization: The living polymerization process in polycondensation. *Progress in Polymer Science*, Volume 32, pp. 147-172.
- Zhang, C., Garrison, T. F., Madbouly, S. A. & Kessler, M. R., 2017. Recent Advances in Vegetable oil-based Polymers and their Composites. *Progress in Polymer Science*, Volume 71, pp. 91-143.
- Zhang, C., Garrison, T. F., Madbouly, S. A. & Kessler, M. R., 2017. Recent Advances in Vegetable oil-based polymers and their composites. *Progression in Polymer Science*, Volume 71, pp. 91-143.
- Zhang, C. & Kessler, M. R., 2016. *Bio-Based Plant Oil Polymers and Composites*. Amsterdam: Elsevier Inc.
- Zhang, X., Burchell, J. & Mosier, N. S., 2018. Enzymatic Epoxidation of High Oleic Soybean Oil. *ACS Sustainable Chem. Eng*, Volume 6, pp. 8578-8583.
- Zhang, X. et al., 2017. Enhancing the neutron shielding ability of polyethylene composites with an alternating multi-layered structure. *Composites Science and Technology*, Volume 150, pp. 16-23.

Appendix

Appendix A: Coatings based on drying oil, polyurethane and epoxy resins after being painted on a wall to cure under atmospheric conditions



Figure 52: Picture of different samples painted on a wall to test for the drying time under atmospheric conditions.

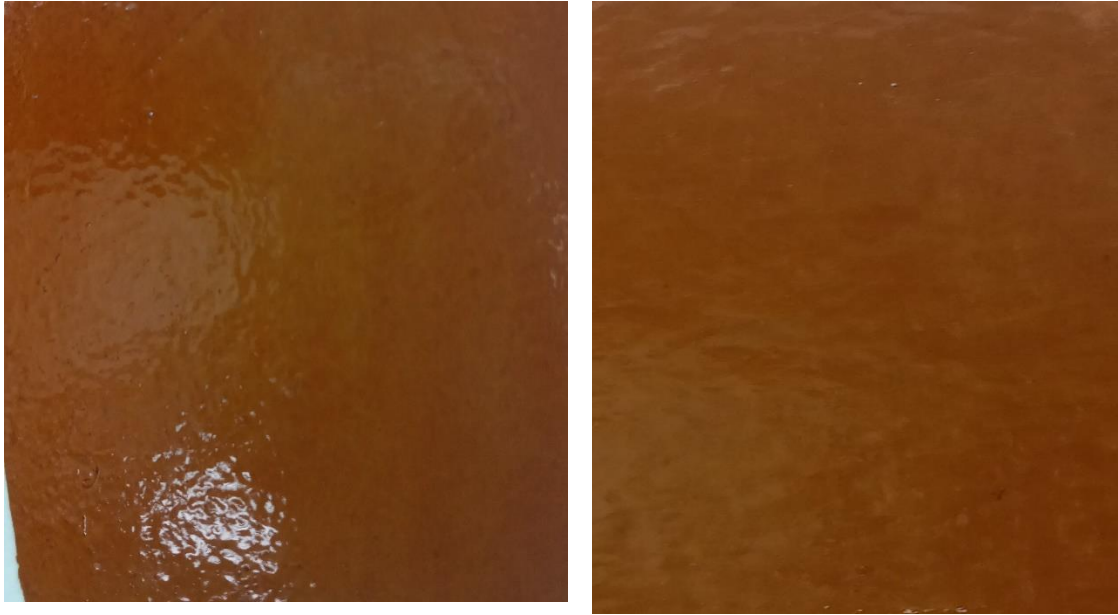


Figure 53: Epoxy paints with DDM as the hardener after film formation



Figure 54: Polyurethanes based on CO and MDI without pigment after film formation

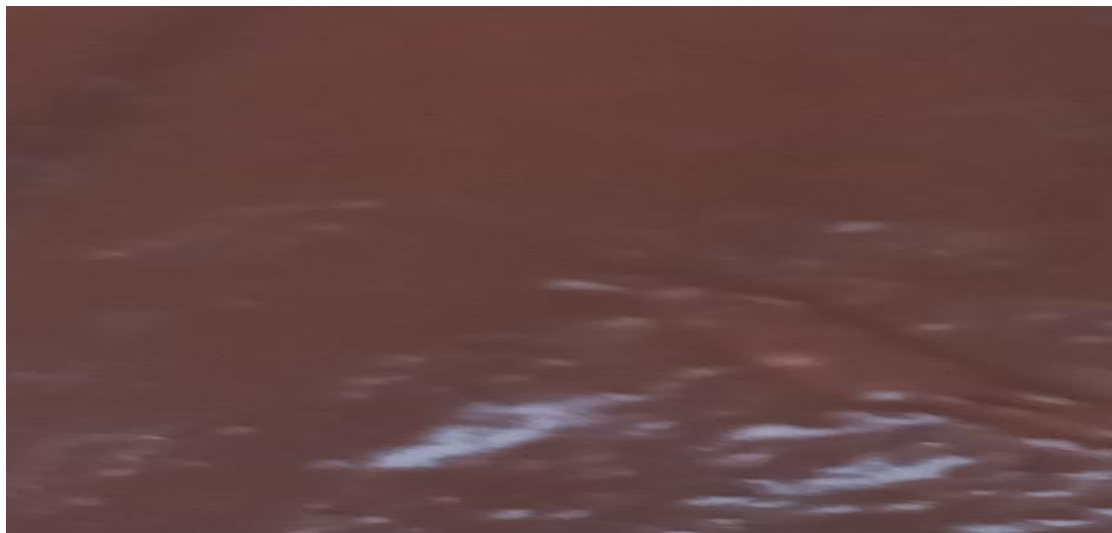
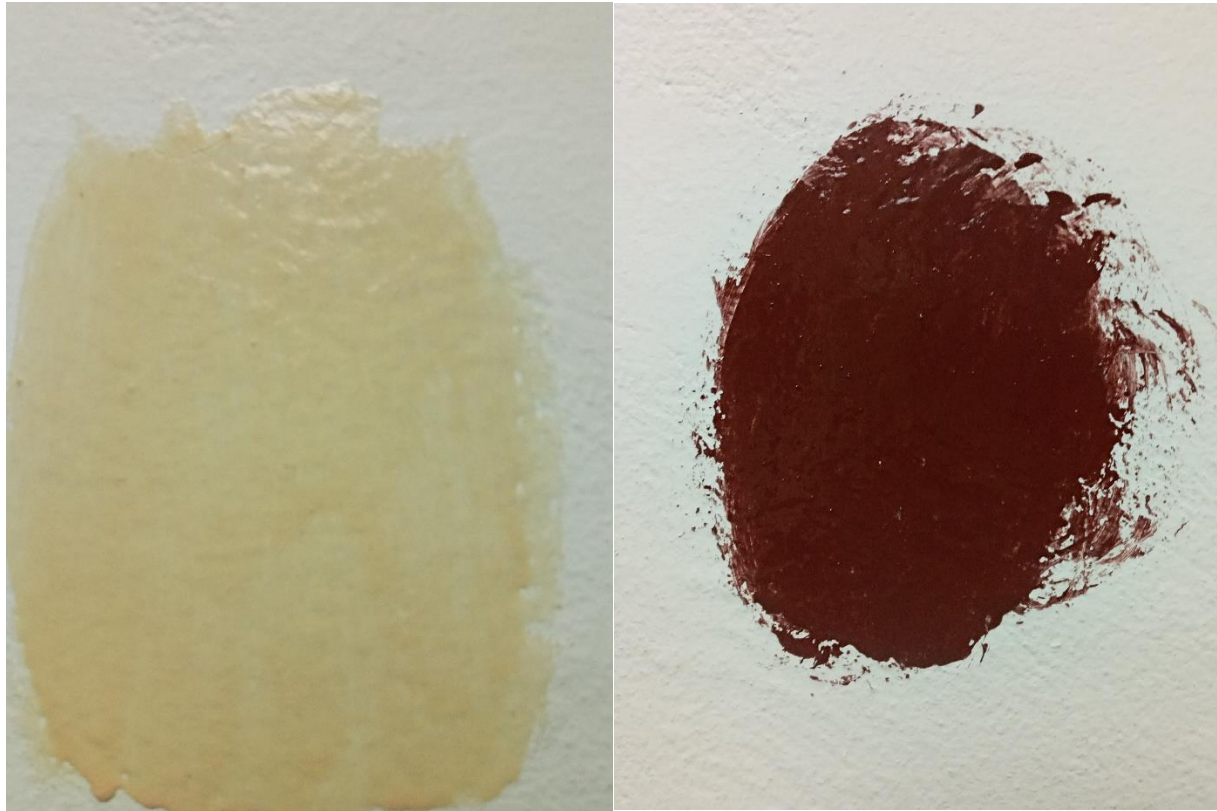


Figure 55: PUs based on CO with Bismuth oxide pigment (top left) and Iron oxide (top right and bottom middle) after film formation.



Figure 56: Epoxy resins with PA as hardener after film formation

Appendix B: FTIR Spectra

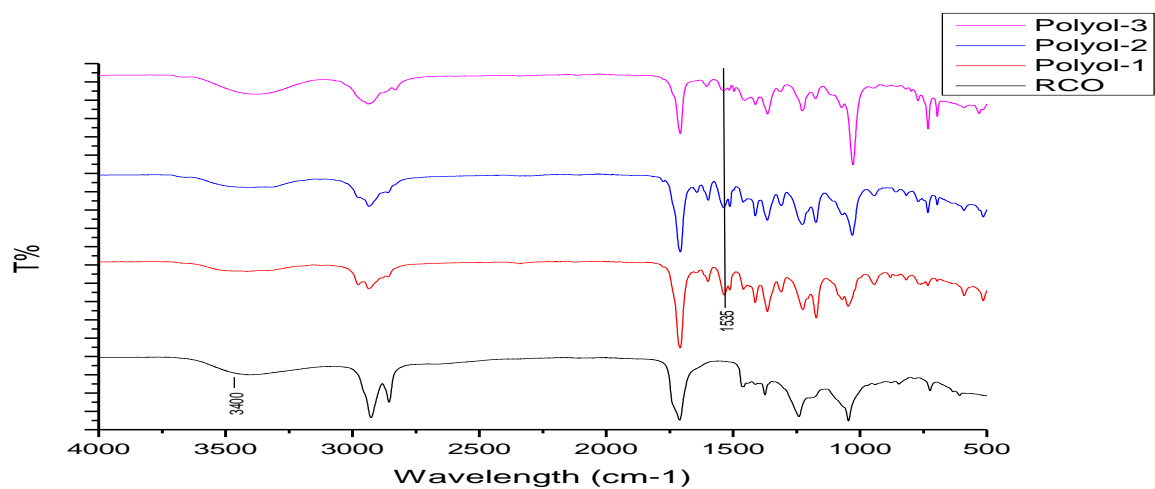


Figure 57: Stacked FTIR spectrums of RCO and RCO based polyurethanes synthesized using different amounts of MDI.

Appendix C: Pictures of reaction Set up and Equipment used



Figure 58: Epoxidation reaction set-up



Figure 59: Ring opening reaction set-up

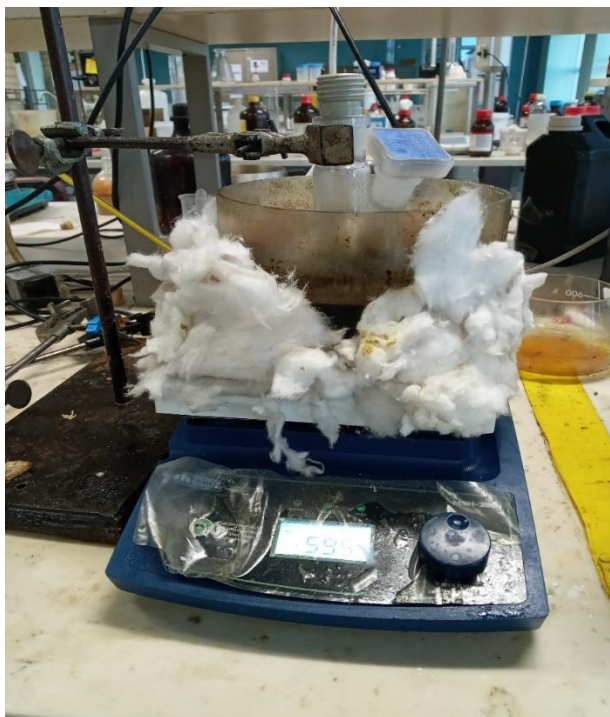


Figure 60: The experimental setup for polyurethane synthesis.

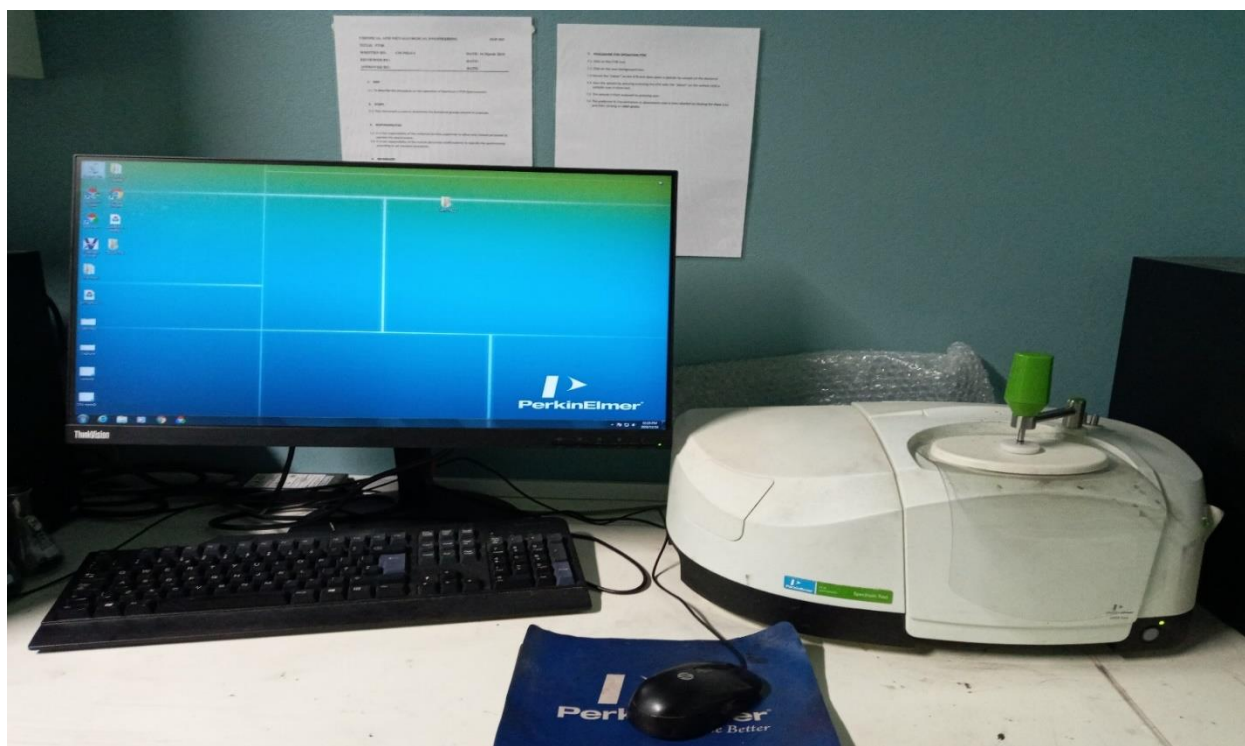


Figure 61: Fourier Transform Infrared Spectroscopy (FTIR) equipment



Figure 62: Magnetic Nuclear Resonance equipment

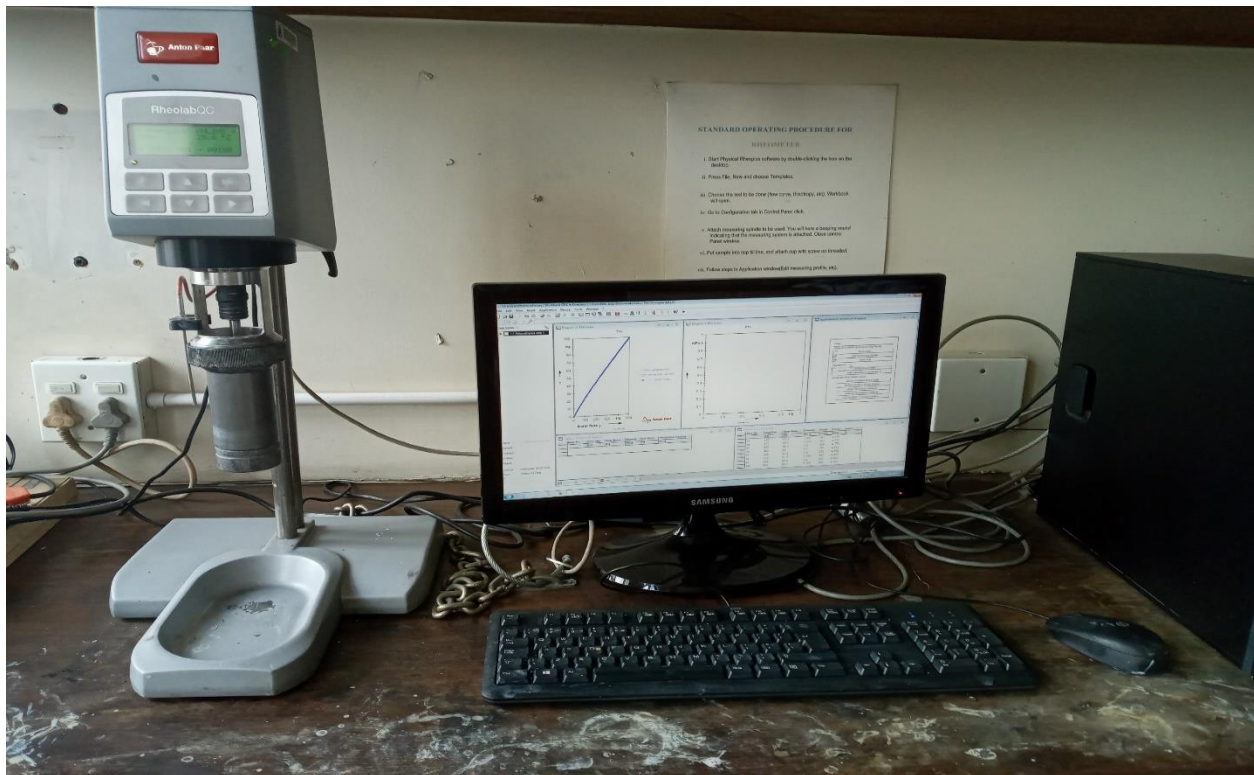


Figure 63: Rheometer equipment